LA TROBE UNIVERSITY

# Atomic Engineering of Diamond Surfaces with Group IV Elements

*Author:*
Michael Jeffrey SEAR

*Supervisors:*
Professor Chris PAKES
Doctor Alastair STACEY

*A thesis submitted in fulfillment of the requirements for the degree of Doctor of Philosophy*

*in the*

Department of Chemistry and Physics
School of Molecular Sciences

January 1, 2019

# Declaration of Authorship

I, Michael Jeffrey SEAR, declare that this thesis titled, "Atomic Engineering of Diamond Surfaces with Group IV Elements" and the work presented in it are my own. I confirm that:

- This work was done wholly or mainly while in candidature for a research degree at this University.
- Where any part of this thesis has previously been submitted for a degree or any other qualification at this University or any other institution, this has been clearly stated.
- Where I have consulted the published work of others, this is always clearly attributed.
- Where I have quoted from the work of others, the source is always given. With the exception of such quotations, this thesis is entirely my own work.
- I have acknowledged all main sources of help.
- Where the thesis is based on work done by myself jointly with others, I have made clear exactly what was done by others and what I have contributed myself.

Signed: 

Date:

LA TROBE UNIVERSITY

# *Abstract*

Department of Chemistry and Physics
School of Molecular Sciences

Doctor of Philosophy

**Atomic Engineering of Diamond Surfaces with Group IV Elements**

by Michael Jeffrey SEAR

This thesis presents investigations into chemical modification of diamond (100) surfaces, primarily using silicon and germanium. The goal of these studies was to show that the novel diamond terminations which can be formed using these elements may be useful as future device platforms, since they are stable, tuneable by further chemical modification, and usable with existing diamond device functionality via surface transfer doping.

Diamond is desirable as a device material due to its bulk properties which make it exemplary for high power and high frequency electronics. Diamond surfaces have been explored for a range of electronic device applications for which silicon is not a suitable substrate material. Many of these applications exploit the large variation in surface electronic structure which is accessible by a change in the chemical termination of the surface. While hydrogen and oxygen terminations of diamond have been well explored, and several other chemical species have been shown to bond, there remains a broad set of functions which are not well serviced by these existing structures. Silicon and germanium share a valence with carbon and adopt the same crystal structure in their bulk forms; by bonding these elements to diamond surfaces, novel terminations were developed which may provide new functionality for surface-chemistry based devices.

I show that it is possible to form an ordered (3x1) symmetry termination of diamond with germanium; that the oxygen modified silicon termination is susceptible to the formation of a hole accumulation layer when dosed with a molecular adlayer; that the germanium termination may be modified with oxygen; that both Group IV terminations are stable to very high temperature, and finally that the silicon termination of the diamond (100) surface may be further functionalized with fluorine.

# Contents

# List of Figures

# List of Abbreviations

| | |
|---|---|
| **2D/3D** | Two **d**imensional/Three **d**imensional |
| **AS** | **A**ustralian **S**ynchrotron |
| **CBM/VBM** | **C**onduction **B**and **M**inimum / **V**alence **Band M**aximum |
| **CPD** | **C**ontact **P**otential **D**ifference |
| **CVD** | **C**hemical **V**apour **D**eposition |
| **EF** | **F**ermi Level |
| (**I**)MFP | (**I**nelastic) **M**ean **F**ree **P**ath |
| **KP** | **K**elvin **P**robe |
| **LEED L**ow | **E**nergy **E**lectron **D**iffraction |
| **ML** | Monolayer |
| (**N/P**)**EA** | (**N**egative/**P**ositive) **E**lectron **A**ffinity |
| **NV** | **N**itrogen **V**acancy Centre |
| **SXR** | **S**oft **X**-**R**ay spectroscopy beamline |
| **UHV** | **U**ltra **H**igh **V**acuum |
| **XPS** | **X**-ray **P**hotoelectron **S**pectroscopy |
| | |
| **XTD** | **X** **t**erminated **d**iamond, X = H, O, N, F, Cl, Si, Ge, SiO, SiF |
| **GIV**, **GIVTD**, **GIVTF** | **G**roup **IV**, **G**roup **IV** **t**erminated **d**iamond, **G**roup **IV** **t**ermination **f**amily |

# Chapter 1

# Introduction

Developments in modern electronics have been the driving force in the advancement of a vast range of fields including everything from stock market prediction and financial planning, to finite element modelling of materials for Formula 1 racing cars.

To date, all major forms of electronics which are in widespread use have been based on the silicon-on-insulator architecture, and increases in speed, processing power and compactness have come from improvements in the fabrication and design of silicon based transistors. Processing power has been observed to double approximately every two years, a behaviour which is described by Moore's Law. This trend, however, is predicted to slow in the near future, as transistor size reaches the minimum limit imposed by the physical size of atoms. In anticipation of this size limit, and in hopes of circumventing it, many contemporary research efforts are focused instead on the development of other material systems for producing improved transistor properties. The materials which are under exploration in this field include III-V semiconductor systems, SiGe alloys, and relevant to this thesis: diamond.

Diamond is an elemental Group IV semiconductor, like silicon and germanium, which is comprised entirely of tetrahedrally coordinated carbon. The diamond crystal structure may be represented by two intersecting face-centred cubic crystals, with a carbon-carbon bond length of 1.55.

While Si and Ge share the same structure, diamond is distinguished from the others in its Group by a number of features. It possesses unparalleled physical strength and hardness, being one of the hardest materials known. It has, also, incredibly high thermal conductivity, $\kappa = 24$ W/(cm.K), 16 times higher than silicon. Diamond is called a wide-bandgap semiconductor, with a 5.47 eV indirect band gap, and an electric breakdown field of 10 MV/cm.

These features all contribute to the identification of diamond as the ideal possible material for high power and high frequency electronics, and the only material which can compete with or exceed silicon carbide for these purposes. SiC is identified as a promising candidate for power electronics for the same reasons as diamond: high breakdown field, high thermal conductivity, large band gap... but in all of these features it is exceeded by diamond. The obvious downside of diamond, compared

FIGURE 1.1

to silicon, is the higher cost, and the large difficulty in producing pure, flat, single crystal samples.

Silicon wafers may be prepared by the Czochralski process, in which a large cylindrical slug of silicon is drawn out of melt, using a seed crystal. This process yields large diameter (up to and including 450mm), atomically pure, single crystals which can be easily sliced into wafers for further processing. Additionally, after decades of use, the process has been optimized to be as cheap and efficient as possible. In contrast, it is only in the last two decades that the laboratory production of single crystal diamond by chemical vapour deposition (CVD) has been successfully achieved with regularity, and production of electronic grade single crystals is still limited to 10mm square samples at the largest. The difficulty, in particular, of producing conductive and atomically flat diamond samples has meant that studies which rely on high quality surfaces have been relatively rare.

A unique limitation in diamond is the difficulty which is found in doping the crystal. While potential dopant atoms include nitrogen, phosphorus and lithium, the only useful dopant currently in use is boron. This is because phosphorus and lithium resist inclusion during growth, and the nitrogen acceptor level is too deep in the band gap. Furthermore, diamond is only the most stable allotrope of carbon at extremely high pressures; at atmospheric pressure, sufficient heating causes diamond to overcome an activation barrier and relax into graphite, which does not possess the remarkable physical properties which are desirable in diamond. This effectively procludes the post-growth insertion of dopant atoms by ion beam implantation, as it is difficult to heal the resulting damage, as can be done with silicon or germanium by annealing. Boron, on the other hand, can be incorporated into diamond during CVD growth, by the addition of borane gas, $B_2H_6$(g), into the feed. These doping difficulties limit the use of diamond to unipolar p-type conductive devices.

In addition to the bulk properties which make diamond so desirable as a substrate, the diamond surface is also of independent interest for device and electronic research and applications. To a large degree this interest stems from the fact that the surface is highly tunable. That is to say, the electronic and chemical properties of diamond surfaces can be controlled and changed by a change in its terminating chemical species. Exploitation of this phenomenon, by creating and characterizing new chemical terminations of the (100) diamond surface, is the subject of this thesis.

It is worth discussing in more depth what I mean by 'tunable'. Figure 1.1 shows three possibilities for the band alignment of the diamond surface: hydrogen terminated, unterminated, and oxygen terminated. On each of these surfaces, the bulk band gap remains the same, as it is a property of the material, but the relationship between the conduction band minimum and the vacuum level changes. In the case

of hydrogen terminated diamond, the conduction band actually moves *above* the vacuum level. This condition, known as negative electron affinity (NEA), is otherwise only seen in highly engineered systems, such as cesium oxide on gallium arsenide. In the case of HTD, it occurs as a consequence of the small dimensions of the diamond surface, and the resulting high areal density of hydrogen on the surface. Hydrogen has a lower electronegativity than carbon, thus the surface dipole for HTD acts as an accelerating potential for electrons leaving the surface. A feature of the NEA is that there is no barrier to emission for electrons excited to the conduction band; this means that hydrogen terminated diamond is an extremely efficient photocathode. [1] This fact has led to several studies optimizing the negative electron affinity by the exploration of a number of metal oxide surface terminations (discussed in Chapter 3).

The negative electron affinity of the hydrogen terminated surface presents a solution to the doping problem mentioned above. It has been shown, initially by Maier *et al.* [2] and subsequently by many others, that when in the presence of a layer of water, the chemical potential for the reduction of water is below the level of the surface valence band maximum. This allows the spontaneous transfer of electrons from the diamond to the water layer, and a resulting formation of a near-surface hole accumulation layer. This is the origin of the surface conductivity seen on hydrogen terminated diamond, which would otherwise be insulating.

The fact that this only occurs on hydrogen terminated diamond, and not oxygen terminated diamond, has allowed for the fabrication of electronic devices on the diamond surface which have regions of conductivity and insulation defined by surface termination. [3]

The development of new diamond terminations is motivated by the hope to either improve the functionality of the diamond system, for example by amplifying the electron emission effect of the NEA, or find other variations of the surface conductivity device model; or the hope of adding functionality from other systems to the highly desirable bulk properties of diamond, such as by providing a biochemical bonding platform by amine termination.

Recent work by members of our research group has produced an entirely new type of diamond surface termination, which has not been reported in any other work; this is the silicon terminated diamond. [4] This new termination is interesting for a number of reasons: it is formed without the harsh chemical treatments which are common with other diamond terminations (this is discussed in Chapter 3), suggesting that it maintains the atomically flat topography created by hydrogen termination; it is the only diamond termination other than hydrogen which uses an element with lower electronegativity than carbon, and thus possesses a negative electron affinity; and, possibly most interestingly, it is believed to be comprised of silicon atoms with two dangling bonds, allowing it to be further functionalized.

This thesis aims to demonstrate several ways that the recently developed silicon terminated diamond can be adapted for

# Chapter 2

# Experimental Techniques

This section describes the operation and principles

## 2.1 X-ray photoelectron spectroscopy

The basis of x-ray photoelectron spectroscopy (XPS) is the physical process of photoemission: the ejection of an electron from a material as a result of the adsorption of a photon with sufficient energy. The core working principle of the technique is the measurement of the intensity of electrons emitted from a sample as a function of kinetic energy.

It was conceived, as an analytical technique, under the name ESCA: electron spectroscopy for chemical analysis, so called by Kai Siegbahn in his description in 1967. [5] This name was chosen to highlight the fact that it allows for the extraction of not just elemental, but actual chemical information from the sample. That is to say, high resolution measurement of the kinetic energy of the electrons from a material yields information about the local electrostatic potential environment from which they originated; a property which is most strongly affected by chemical bonding. His work in developing ESCA (XPS) resulted in Siegbahn receiving the Nobel Prize in 1981. The photoemission effect itself was described by Einstein in 1905 resulting in him earning the Nobel Prize in Physics in 1921. [6, 7]

The XPS technique consists of three principal components: the x-ray source, the analyzer, and the detector. These interact with the photoelectric effect in the following way: x-rays generated by the source are incident upon a sample, which undergoes photoemission as those x-rays are absorbed by electrons within the sample. Electrons which are emitted possess a range of energies (described in more detail below) and thus must be discriminated for the purpose of quantification; this is performed by the electron optics which comprise the analyzer. Finally, the electrons which are selected by the analyzer are then measured by the detector.

### 2.1.1 Synchrotron Radiation

In the context of this thesis, the x-ray source is synchrotron radiation; light generated by the radial acceleration of high energy electrons. A full treatment of the synchrotron effect is easily the subject of books, e.g. Wiedemann [8], but the salient

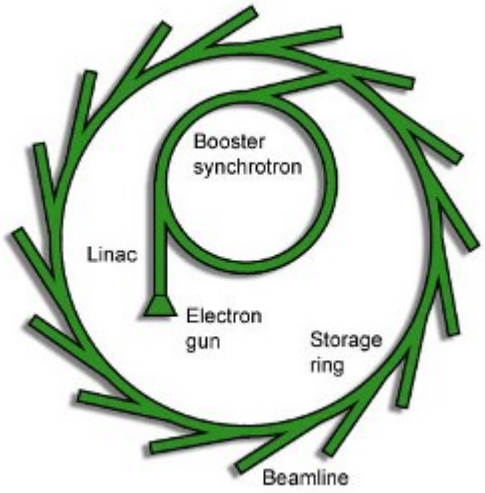


FIGURE 2.1: Schematic of the general structure of a modern synchrotron, showing the linear accelerator, booster ring, storage ring and beamlines. Taken from the Diamond website [9]

points of the mechanism will be covered here, in order to elucidate the origin of the tunable photon energy which is exploited in our studies to maximize surface sensitivity.

It is a consequence of the conservation of energy that charged particles emit light when decelerated or deflected. Synchrotron radiation is the result of the specific case whereby a charged particle—usually an electron, and in the discussion henceforth an electron because it is both easier to type, and the type of particle used in the Australian Synchrotron—is radially accelerated around a curve, while maintaining a constant speed. In the reference frame which moves with the accelerated particle, the electron's velocity is zero, and the radiated power of photon emission is dependent on the angle, relative to the direction of acceleration, with the relationship:

$$P \propto cos(\theta^2). \tag{2.1}$$

This symmetric distribution, when transformed into the frame of the laboratory in which the electron is moving with a constant, relativistic, speed, results in the observed emission as a high intensity, narrow cone, with opening angle proportional to $1/\gamma$, where $\gamma$ is the relativistic Lorentz factor. A schematic of these relative distributions is shown in Figure 2.2. The characteristic features of synchrotron radiation are its high brilliance, high flux, and broad energy spectrum, with a peak in intensity proportional to the square of the Lorentz factor, and to the strength of the magnetic field with which it is accelerated. The frequency of the peak intensity of radiation is given by:

$$\nu_{peak} = 0.29 \cdot \frac{3e}{2m_e c} \cdot \gamma^2 B \tag{2.2}$$

As the electron optics within a synchrotron ring are designed to work with a particular electron energy (i.e. velocity, i.e. Lorentz factor), control of the peak of the

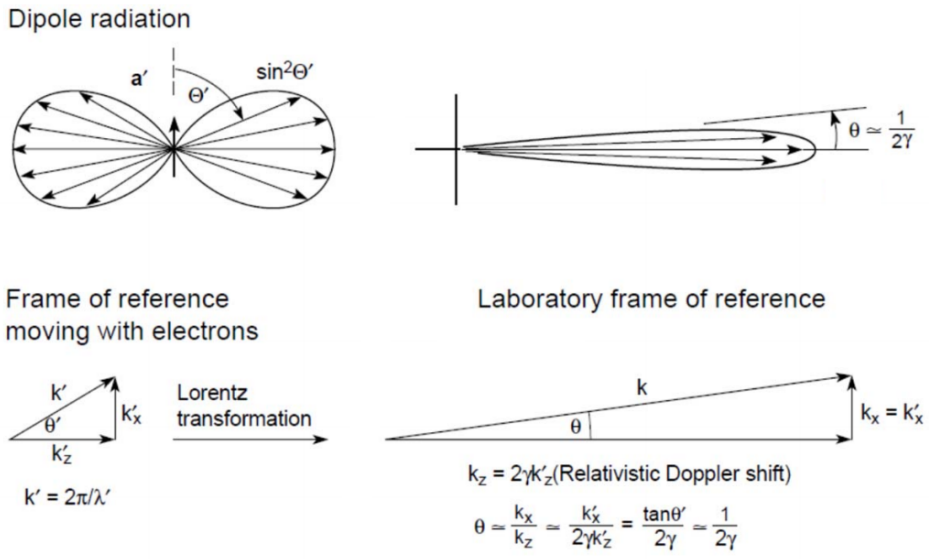


FIGURE 2.2: The angular distributions of photons emitted from an accelerated charge in the particle reference frame (left) and the laboratory frame (right). From [10]

generated radiation is typically done by altering the strength of the magnetic field, *B*.

The first generation of synchrotron facilities used the parasitic lost light caused by the acceleration of particles in accelerator rings. In contrast, modern synchrotron facilities are entirely dedicated to the production of useful light for a range of analytical techniques, including XPS. As such, they are typically comprised of several stages, designed to maximize the useful lifetime of energetic electrons. In the case of the Australian Synchrotron (AS), which was used in all the studies described in Chapters 4-7, the major sections are (i) the linear accelerator (linac), used to introduce electrons with an initial energy, (ii) the booster ring, which accelerates the electrons to the working energy, (iii) the storage ring in which the electrons are maintained at a stable energy by regular RF booster cavities, and (iv) insertion devices, which use the energetic electrons to generate synchrotron light. [11]

Within the AS linear accelerator, electrons are produced in the electron gun in vacuum, by thermionic emission from a cathode filament. By the application of a radio frequency to the electron gun, the electrons are emitted within packets of charge, called bunches, separated by time. From the gun, these electron bunches are accelerated into the linac by a high potential gradient. RF cavities are used to restrict the bunches in space, so that they can be further accelerated to 00 MeV, and passed into the booster ring. [11]

The booster ring is the smaller of the two ring sections which comprise the AS. It requires electrons to be grou nto bunches, so that they can be accelerated by a single RF cavity operating at 500 MHz, while they are guided by a set of 60 steering and focussing magnets, which keep the bunches on the correct path and shape. By the end of this process, the electrons are at the working energy of 3 GeV, and are

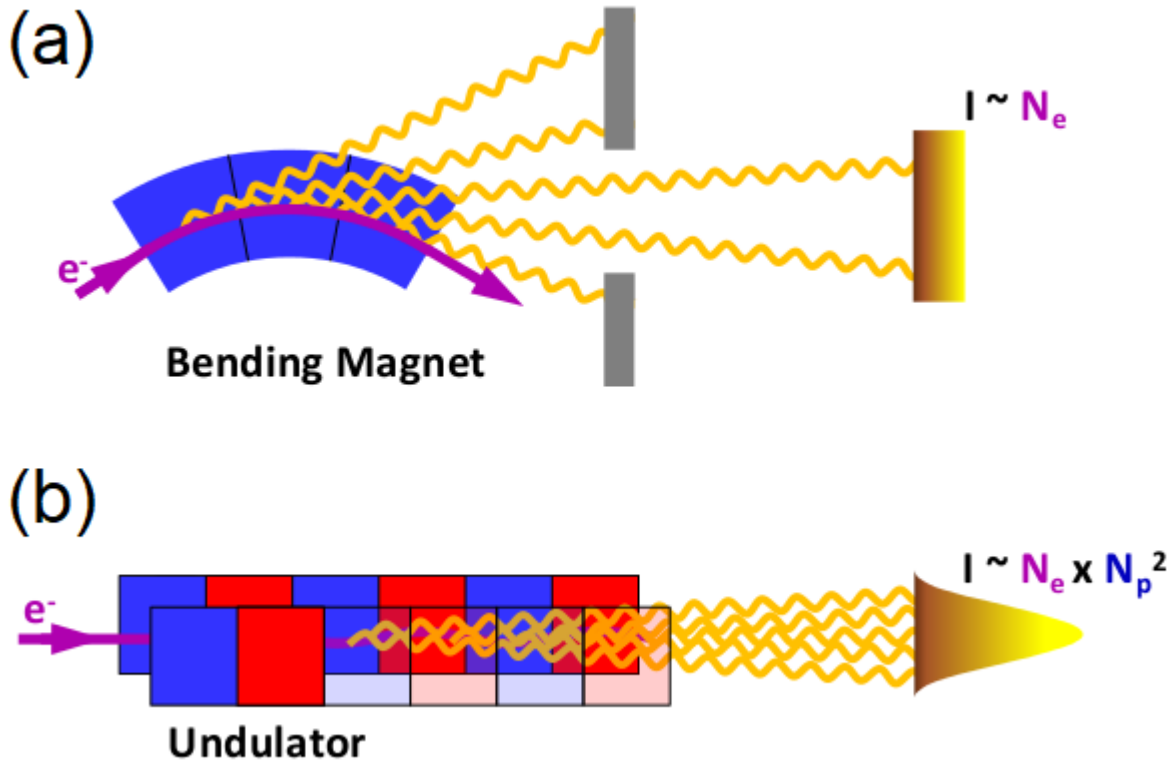


FIGURE 2.3: Bending magnet radiation (a) sweeps through a large angle, while undulator radiation (b) is confined to a smaller cone as a result of the electron path sweeping back and forth. Adapted from [12]

passed from the booster ring to the storage ring, where they are maintained at that energy by four more 500 MHz RF cavities. [11]

The storage ring at the Australian Synchrotron is comprised of 14 sectors, each containing an arc and a straight section. The arc sections each contain two bending magnets; these magnets redirect electrons around the ring, and generate synchrotron light with a broad spectrum of energies. The straight sections are designed to accommodate other instruments called insertion devices, which also generate light, with a different intensity vs. energy distribution. The Soft X-Ray spectroscopy beamline (SXR) which was used throughout this thesis uses such an insertion device, called an undulator. [11]

As stated above, synchrotron radiation occurs when electrons at relativistic velocities are deflected by a magnetic field. Qualitatively, photons are emitted in a forward-focussed cone about the original trajectory of the particle, which is stretched in one dimension as the path of the particle sweeps through an angle. A schematic diagram of this effect is shown in Figure 2.3 (a). The principle of an undulator is to use a series of opposite alignment magnets to oscillate electrons along a sinusoidal pattern, with the spacing of the magnets designed such that the generated photons

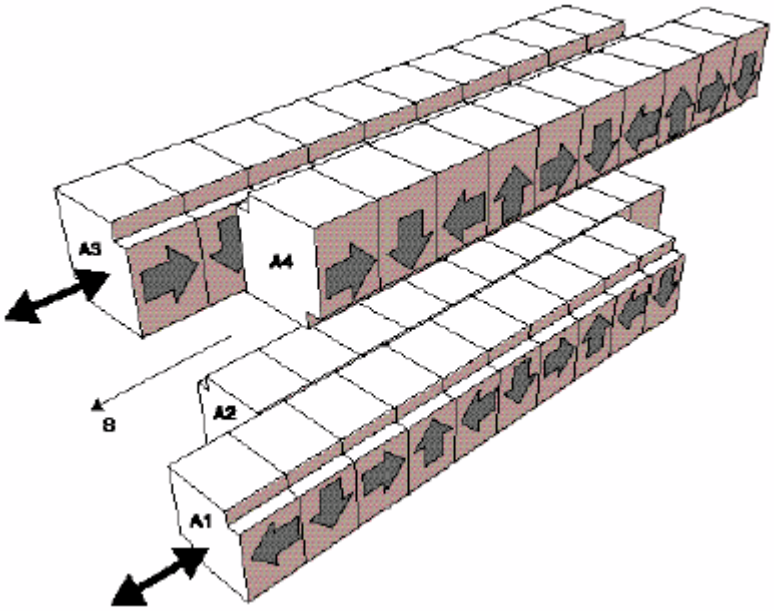


FIGURE 2.4: The four girder arrangement which comprises the APPLE II style undulator. From [13]

are emitted in phase, greatly amplifying the resulting flux at particular resonant energies. The interference effect which amplifies the emission intensity also causes the spatial distribution of emitted photons to be more tightly controlled; this can be seen in Figure 2.3 (b).

Light emitted in this case will be polarized. The SXR beamline insertion device is an APPLE II type undulator, pictured in Figure 2.4. In this design, the undulator is constructed with 4 independent magnetic arrays, so that the polarization can be precisely chosen as linear, circular or elliptical. The linear polarization mode was used in all studies within this thesis, but it is not otherwise important for understanding this work. Controlling the separation of the poles of the undulator also allows the peak intensity of the output to be shifted in energy. Combined with a monochromator to precisely select the desired photon energy; this is the origin of the tunable x-ray energies which are used in this thesis, with the SXR beamline having access to a 90 eV to 2500 eV energy range. This generated photon beam is passed through a series of x-ray optics to shape the beam to a small point, whereupon it is incident on the sample.

### 2.1.2 Photoexcitation

A representative schematic of the band structure of a semiconductor is shown in Figure 2.5. It is important, for the discussion of photoelectron spectroscopy, to be precise about the definition of the various energies which are referred to within this thesis. Throughout the studies which are discussed in this thesis, energies are referred to as 'Binding energy', or $E_B$. This should be understood to be the energy

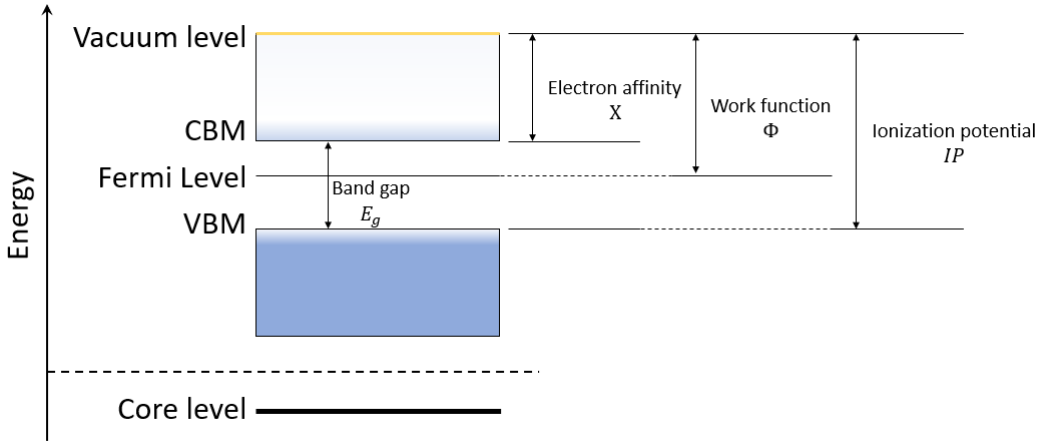


FIGURE 2.5: Schematic of the band structure of a semiconductor, showing graphical definitions of the important energies.

relative to the sample Fermi level, and thus separated from the vacuum level by a further (sample) work function, $\phi$.

The band structure shows the distribution of initial states from which electrons can be excited by photoabsorption. The signal measured by XPS can be connected to this distribution by considering a series of steps; formally, the physical model which is used is called the Three Step Model of photoemission. These steps are (i) photoexcitation from a bound state, (ii) transport through the material to the material-vacuum interface, and (iii) transition through the interface to a free electron final state. After emission, the electrons may be collected by electrostatic lenses, and passed to the analyser.

Electrons in a material occupy one of the states which lie below the Fermi level, either within the valence band, or in a deeper core level. XPS is typically used to probe core levels. When an incident photon is absorbed by an electron, assuming the energy is sufficient to do so, the electron is promoted to the continuum of states above the vacuum level, resulting in a kinetic energy $E_K$, which is equal to the photon energy less the binding energy and work function.

$$E_K = \hbar\omega - E_B - \phi_S \tag{2.3}$$

As this can occur for all electrons with energy less than the photon energy, photoabsorption leads to the generation of a set of excited states which replicates the distribution of initial states, with an energy offset of $\hbar\omega$. See Figure 2.6 (a).

While the excited electron is in transit to the vacuum interface, it is possible for it to inelastically scatter from other particles, and thus lose energy. This means that the electrons which reach the interface will possess a range of energies from their initial excited range, down to zero kinetic energy, and each core level peak contributes an associated step in the background signal. See Figure 2.6 (b)

In order to account for the step in signal around a core level due to inelastically

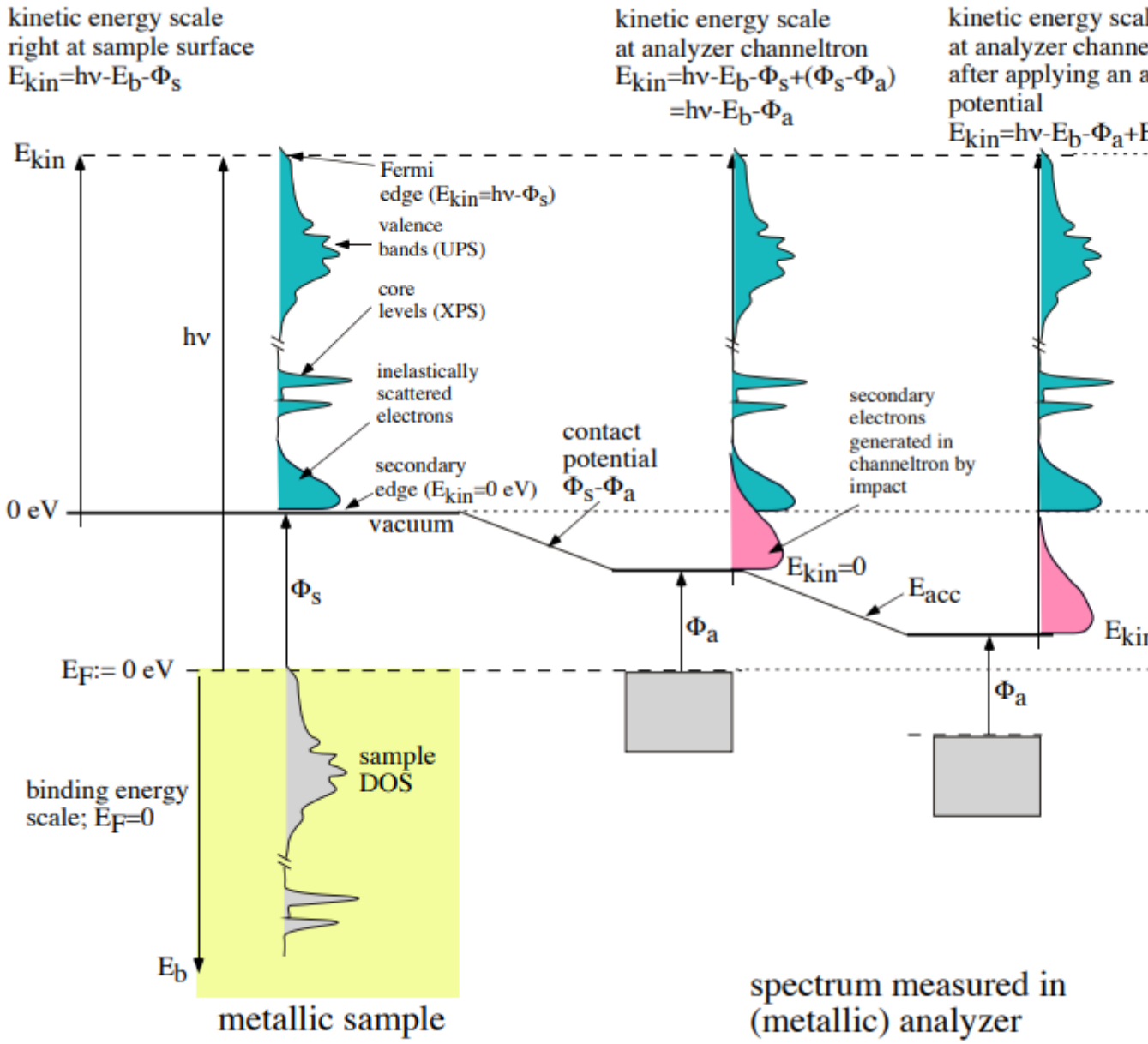


FIGURE 2.6: Figure. From [14]

FIGURE 2.7: Demonstration of the Shirley background shape, from [16]

FIGURE 2.8: Caption

scattered electrons, each core level spectrum has a background subtracted prior to component decomposition. This is necessary to derive meaningful information from the peak when comparing component intensities and positions. There are several models which can be used for the shape of this inelastic background, but the most commonly used background in literature is the shape devised by Shirley. [15]

The Shirley method sets an energy window around the peak ($E_{high}$ to $E_{low}$), positioned at the higher and lower plateaus. Shirley takes the assumption that all photoelectrons from the peak region have equal probability of energy loss through scattering. Thus, the background contribution is proportional to intensity, for each point in the region. The shape of the background may be found by an iterative process where the *S*ubstracted spectrum for iteration $N$ is equal to the *I*nitial spectrum minus a scaled integral of the $(N-1)$ iteration. Using the *I*nitial spectrum as the zeroth iteration, the scaling factor $k$ is found by setting the post-peak energy to 0. This process is described by the formula:

$$S_N(E) = I(E) - k\int_{E_{low}}^{E_{high}} S_{N-1}(\varepsilon)\cdot d\varepsilon \tag{2.4}$$

The Shirley method of background subtraction has been employed for all photoelectron spectra reported throughout this thesis, and an example of a C1s core level, showing the Shirley background, can be seen in Figure 2.7

The mean distance through which an electron travels before losing energy through scattering is the inelastic mean free path, $\lambda$, which varies strongly with the electron kinetic energy. An interesting feature of $\lambda$ is the observation that it appears to have a minimum at around $E_K = 50eV$, independent of the material in which the electron is travelling. This is called the "universal curve", and is a key reason for using a synchrotron source for surface modification studies. Figure 2.8 shows the observed mean free paths for a range of materials and energies. By tuning the photon energy such that the mean free path is at or near the minimum (around 50-70 eV), we can gain the maximum available surface sensitivity, and this is a primary advantage of the use of a tunable photon energy synchrotron x-ray source.

Once outside the material, electrons experience an accelerating (or sometimes retarding) electric field, due to the difference in work function between the sample and the electron analyser. This is because the sample and analyser are in electric contact for XPS, thus the two share a Fermi level, and the difference in work functions is represented by a linear decrease in the vacuum level, as shown in Figure 2.6 (c). This means that the kinetic energy measured by the analyser must be corrected by

this same amount:

$$E_{K(sample)} = E_{K(analyser)} + \phi_S - \phi_A \tag{2.5}$$

This means that to determine the true binding energy position of a component, the work function of the analyser must be measured. In practice, this is done by calibrating the measured position of the gold 4f peak, or the Fermi edge of a metal sample, to their reference positions, respectively 84.0 eV, and 0.0eV.

### 2.1.3 Detection

Electrons ejected from the material will have, as stated above, a range of kinetic energies which are the result of the photon energy and the energy levels of the material. In order to produce a photoemission intensity vs energy spectrum, these electrons must be dispersed based on their kinetic energies. The device which performs this dispersion is the photoelectron analyser.

The precise manufacture and design of modern electron analysers is extremely complex, and has been optimized to achieve the maximum possible signal to noise ratio and energy resolution. Modern analysers may be paired with 2D detectors to gain the ability to simulatenously measure a range of energies ('snapshot mode'), or produce an image of the sample. In the case of the SXR beamline of the AS, the detector is a relatively simple channel electron multiplier detector which is optimized for high energy resolution.

The most common kind of electron analyser used in XPS, and the type used in all studies in this thesis, is the hemispherical analyser. This analyser is so-named because it is comprised of a pair of concentric hemispheres which are held at a potential difference. Electrons are guided and focussed by the electrostatic acceptance lens of the analyser, and enter with a particular kinetic energy. The acceptance lens, and an aperture, limit the spatial and angular range which the hemisphere accepts. The voltages on the inner and outer shells ar

When entering the hemispherical analyser, the path of the electrons is deflected by the electric field within. By tuning the bias voltage between the inner and outer shells, only electrons with a particular kinetic energy range are able to pass through the analyser without impacting the sides. This is depicted schematically in Figure ?? In this figure, the energy labelled $E_0$ is the kinetic energy for which the photoelectron intensity is being measured. If electrons entering the analyser have $E < E_0$, the hit the inner hemisphere, and likewise with the outer hemisphere for $E > E_0$. The range of energies which are close enough to $E_0$ to pass through is called the pass energy $E_p$. The complete energy resolution of the analyser is given by the entrance slit width $W$, the radius of the analyser $R$, and the acceptance angle $\alpha$, as follows:

$$\Delta E = E_p\left(\frac{W}{2R} + \frac{\alpha^2}{2}\right). \tag{2.6}$$

The SXR beamline uses a SPECS PHOIBOS 150 hemispherical analyser with a channeltron detector. The analyser entrance slit width dimensions are 7mm×20mm. The carbon core level is always recorded with a photon energy of 350 eV, and a pass energy of 5 eV, resulting in an electron kinetic energy of around 66 eV, and an instrumental resolution of 144.1 meV for this core level.[17]

### 2.1.4 Core level fitting

After calibrating the energy position of spectra using a gold reference, and subtracting a background by the Shirley method, photoelectron core level spectra may be decomposed into a set of contributing peaks which represent distinct electronic environments, usually due to chemical bonding. An example of a C1s core level is shown in Figure

The shifts in binding energy due to local environment, in XPS, are typically on the order of 1 eV. In the spectrum shown in Figure a fluorine terminated diamond sample is shown to possess four peak

The lineshape used to fit photoelectron spectra is a symmetric curve that is a convolution of a Gaussian and a Lorentzian lineshape. These elements represent, respectively, instrumental broadening due to the photon energy resolution of the source and the energy resolution analyser, and intrinsic broadening due to the lifetime of the core hole induced by photoemission.

*Spin-orbit splitti

### 2.1.5 Coverage

## 2.2 Low energy electron diffraction

While the main technique used for analysis in this thesis is x-ray photoelectron spectroscopy, that only provides direct information of the chemical environment of the surface atoms. In order to get a fuller understanding of their nature, low energy electron diffraction (LEED) has been used to characterize the physical structure of the diamond surface modifications which are explored in Chapters 4 to 7.

Low energy electron diffraction, as the name suggests, is a technique which uses the diffraction of low kinetic energy (30-300 eV) electrons to probe the physical symmetry of ordered crystalline surfaces and surface adlayers. The surface sensitivity of LEED, as with XPS, stems from the low penetration/escape depth of low kinetic energy electrons within solids, and thus, as with XPS, it must be operated in ultrahigh vacuum.

In function, a collimated beam of electrons is impinged upon a sample surface at normal incidence, and the reflected electron signal is collected by a two dimensional detector. In most cases, and in particular the case of the LEED system used in this thesis, the detector is a circular section of a sphere, coated with a phosphorescent coating, such that the spots which are illuminated by the backscattered electrons

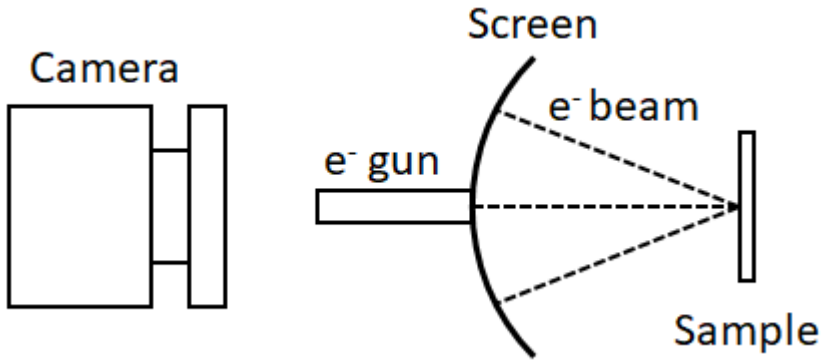


FIGURE 2.9: Simplified schematic of the elements of a low energy electron diffraction system.

glow, and the signal is recorded by a camera inline with the screen and electron gun. This geometry is depicted schematically in Figure 2.9

The condition for constructive interference for waves reflecting from a crystalline surface is the Bragg equation:

$$n\lambda = d\sin(\theta) \tag{2.7}$$

where $n$ is an integer corresponding to the (1st, 2nd... nth) order of the reflection, and $\theta$ is the angle between incident and reflected beams. In order for this equation to be satisfied, the de Broglie wavelength of the incident electrons must be on the order of the crystal cell dimensions. The de Broglie relation, for a free electron, is given by:

$$\lambda_{e^-} = \frac{h}{p} = \frac{h}{\sqrt{2mE_k}} = \frac{h}{\sqrt{2meV}} \tag{2.8}$$

for the Planck constant, $h$ and momentum $p$. The kinetic energy of emitted electrons is equal to their charge times the accelerating potential, $V$. This can be substituted into the Bragg relation to yield:

$$\sin(\theta) = n\frac{h}{d\sqrt{2meV}} \tag{2.9}$$

The Bragg relation is one dimensional, yielding a set of solutions as a function of $\sin(\theta)$. Equation 2.9 shows that these solutions are separated by an integer multiplier. This can be represented by a vector which is inversely proportional in magnitude to the lattice separation $d$, and also to the square root of the electron energy $eV$.

While depicted in Fig. 2.9 as a single element, the screen in a LEED system is in reality a set of 4 or 5 mesh grids, which can be held at independent potentials. This allows the grids to serve as a retarding field analyser, which selects the energy of incoming electrons to reject inelastically scattered electrons and allow only the elastically scattered electrons to pass through and interfere, resulting in the observed pattern.

By collecting the absolute intensities (or current, I) of each diffraction spot (also called a 'beam') as a function of electron energy (or accelerating potential, V), it is possible to produce a set of spectra for a sample. This process is called IV-LEED, and when combined with simulation and modelling, can be used to determine the positions of individual atoms in suitably crystalline samples. In this thesis, LEED has been used only in the fundamental, static energy mode, which only allows for the direct measurement of the surface cell symmetry. A thorough IV-LEED and simulation study is considered to be an interesting extension of the work shown herein.

## 2.3 Kelvin probe

Kelvin probe, or the Kelvin method, is a technique for measuring the work function of a sample. It can be performed in atmosphere or in vacuum 

# Chapter 3

# Literature Review

This chapter presents a review of published works which represent the relevant prior knowledge that motivated the investigations detailed in Chapters 4-7. This review is broken up into three sections, which represent three ways of looking at Group IV Terminated Diamond (GIVTD) surfaces. The first section reviews the papers which directly show the silicon termination produced by our group. I was a part of the team which undertook those studies, but the primary work was performed by Dr Alex Schenk. This section is included to show the firm foundation which was expanded upon in the studies contained in this thesis. The second section reviews a range of other diamond surface terminations, comprising selected studies from the past several decades, in order to show which other methods can be used to terminate diamond, and how that effects the observed nature of the surface. The final section aims to justify our understanding and model of the GIVTD systems by comparing SiTD to an analogous system, the (3x2) reconstruction of the (100) SiC surface.

## 3.1 Silicon terminated diamond

Since the body of this thesis describes several efforts to modify, adapt or exploit the silicon terminated diamond surface, I will give here a thorough description of that termination, and our understanding of it, based on the initial works which took place in the first year of my PhD research. These investigations were led by Dr Alex Schenk, mainly with the assistance of myself, Dr Anton Tadich, and Professor Chris Pakes. Dr Schenk also played a significant role in the direction of my work, and he is listed as an equal contributor to the papers in Chapters 4 and 5. This section is derived primarily from the papers by Schenk *et al.* in references [4, 18, 19], which describe work performed at the Australian Synchrotron and the Singapore Synchrotron Light Source.

The samples discussed in the studies described in this section were all produced using the same four step method of formation. First, *ex situ*, a boron-doped conductive diamond with (100) orientation was cleaned with a nitric:sulfuric:perchloric 1:1:1 triacid boil and subsequently hydrogen terminated by a H$_2$ microwave plasma treatment. Second, the sample was inserted into UHV and cleaned by a 1 hour anneal in vacuum at 450°C; at this stage the sample remains hydrogen terminated.

Third, a layer of silicon is deposited in situ upon the sample at room temperature, to a coverage of $1.05 \times 10^{15}$ atoms/cm$^2$. Finally, fourth, the sample + physisorbed layer is annealed to >950°C (920°C in the first study) in order to desorb hydrogen from the surface and allow bonding. At all stages the UHV chamber pressure remains $<5 \times 10^{-9}$ mbar. This method has been the basis of all the termination studies described throughout this thesis.

### 3.1.1 XPS

Core results:

- Silicon termination causes two different carbon chemical environments on the surface
- The intensity ratio of these species is approximately 2:1
- We propose that carbon atoms exist in two chemical environments on the surface, one with one silicon bond, and one with two silicon bonds
- We propose that silicon atoms each possess two bonds to diamond and two unsatisfied bonds
- To prove that we were able to chemically bond silicon to diamond, we used surface sensitive x-ray photoelectron spectroscopy at the Australian Synchrotron. Core level photoemission spectroscopy is an extremely surface sensitive and chemical-state sensitive probe, so physisorbed but unbonded silicon on the surface would not cause the formation of a distinct, energy shifted component in the carbon core level spectrum.

The silicon termination experiment used a hydrogen terminated diamond freshly prepared by plasma treatment, transferred via atmosphere and inserted into UHV. Before silicon termination, the surface could be represented by two components, one surface-associated and one bulk-associated. Our model for the hydrogen terminated diamond has since evolved [4] but the fit used here is consistent with the standard HTD fit used in literature, e.g. in Graupner *et al.* [20]

After the deposition of silicon onto this sample, the carbon core level retains the same structure, and the silicon core level appears to be a broad single peak. We took this to mean that no reaction had occurred, which matched our expectations that the silicon should be unreactive to the diamond while hydrogen was still bonded. This observation was matched in the germanium termination experiment detailed in Chapter 4, where the germanium also did not react with the hydrogenated surface, though it did spontaneously bond to the hydrogen-free surface which was also examined in that study.

When the sample was annealed to a temperature sufficient to liberate hydrogen, the silicon was induced to react, and the carbon core level developed three new

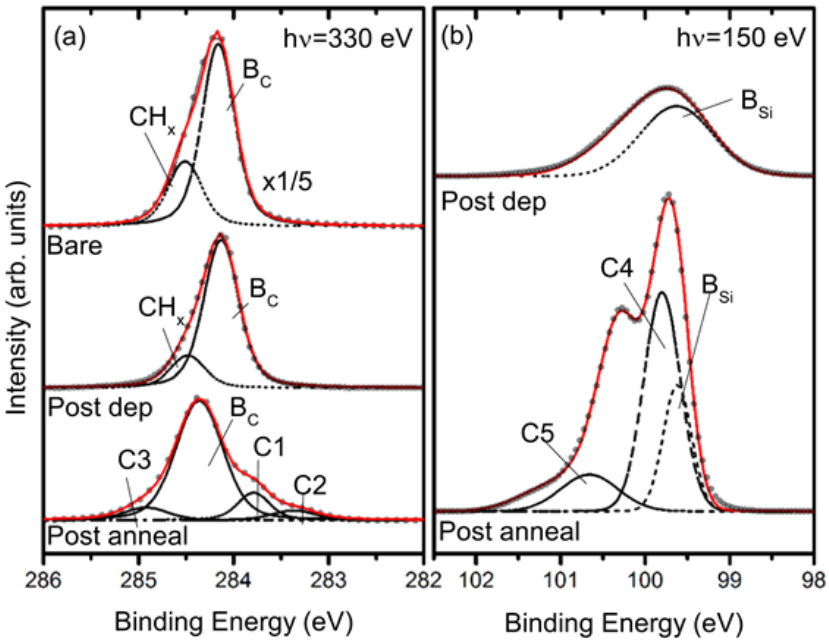


FIGURE 3.1: Carbon 1s and silicon 2p core level spectra of a (100) oriented diamond sample at various stages of silicon termination. Taken from Schenk *et al.* [4]

components, labelled in Figure 1 as C1, C2 and C3, where C1 was 2.2 times the magnitude of C2. The component C3 is associated with the relatively high proportion of oxygen which was present on this sample after annealing, and has not been present in most subsequent studies. We consider the components C1 and C2 to be the 'true' signature of silicon terminated diamond. These are assigned to surface carbon atoms attached to one (C1) or two (C2) silicon atoms at the surface. The justifications for this assignment are two. First, silicon has a lower electronegativity than diamond, so the formation of C-Si bonds should result in a peak shift to lower binding energy, and the formation of two C-Si bonds should drive the peak further to low binding energy. Second, there was a remarkable change in the surface symmetry, and the details of that change, and its effects on our interpretation, are given in the LEED discussion below.

The silicon 2p core level, after annealing, was fitted with three components. Just as the relative low electronegativity of silicon causes LBE shifts in the carbon region, the relative high electronegativity of carbon causes peak energy shifts to higher binding energy. Thus, the lowest BE component is assigned to excess silicon which is unbonded to the surface. The largest component in the spectrum, labelled C4 above, we attribute to silicon bonded to two surface carbon atoms. This is the component which represents the pristine or perfect silicon termination. This accounts for two of the four bonds for each silicon atom; we believe the remaining two bonds exist as dangling bonds, or possibly weakly coupled to adjacent silicon atoms. The reason for this assignment is given in the Structure section below.

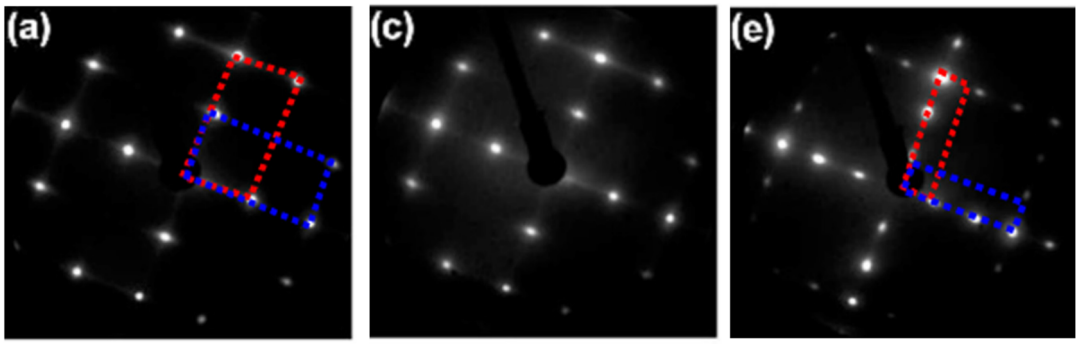


FIGURE 3.2: LEED patterns (70eV) throughout the silicon termination in Schenk *et al.* [4] Figure adapted from that paper. (a) Hydrogen terminated diamond, (c) after silicon deposition, (e) and after annealing.

The final component C5 is attributed, in this study, to oxidized silicon, which is a reasonable assignment given the presence of oxygen on the surface. Later work has shown that this peak is often present even when the surface density of oxygen is far below what would be necessary to assign it that way. Additionally, the exact magnitude of the peak changes from sample to sample. As such, we currently believe it should be attributed instead to silicon adsorbed on carbon step edges, as the 'atomically flat' diamond surface is known to possess only very small terraces. [21]

In this study, we also showed that silicon terminated diamond possesses a negative electron affinity, with $\chi = -0.7\ eV$.

### 3.1.2 LEED

Core results:

- Silicon termination results in a (3x1) surface symmetry
- Annealing is required to induce the reconstruction

The most compelling result in the first silicon terminated diamond study was the change in surface symmetry seen in low energy electron diffraction. While both hydrogen terminated diamond and hydrogen-free bare diamond (100) surfaces adopt a $(2 \times 1)$ reconstruction, and oxygen terminated diamond adopts a bulk-like $(1 \times 1)$ reconstruction, the result of the silicon termination was the formation of a clear, sharp $(3 \times 1)$ pattern. This is shown in Figure 2.

The square symmetry diamond (100) surface is characterized by a square pattern in LEED, with sharp diffraction spots at the $(\frac{1}{2}\ 0)$ and $(0\ \frac{1}{2})$ positions due to the $(2 \times 1)$ reconstruction of the hydrogen terminated surface. As the diamond cubic structure has a 90-degree rotation with each atomic step, the pattern shows overlayed $(1 \times 2)$ and $(2 \times 1)$ domains, indicated with red and blue rectangles in Figure 2 (a). Deposition of silicon onto the HTD surface resulted in an increase in background intensity without a change in symmetry, (c), an observation consistent with an adsorbed amorphous layer. Since there was also no change in the carbon 1s core level,

we concluded that the inert hydrogen terminated surface did not spontaneously react with the deposited silicon.

The sample was then annealed, which did result in a change in the surface symmetry, to our signature two domain $(3 \times 1)$ pattern, shown in (e). The features which distinguish that pattern are the two spots between the 0th order (center) and 1st order (edge) spots. Previously, on the HTD surface, there was a single half-order spot. After annealing, not only are the one-third-order spots formed, but the half-order spots are also completely removed. This says that the surface is entirely reconstructed into the $(3 \times 1)$ structure. In addition, there is no spot density in the center of the square regions which would suggest a $(3 \times 2)$ structure.

The $(3 \times 1)$ pattern observed here has not been seen experimentally on any other diamond surface, and serves as the most stark signature for all the Group IV terminations which are discussed throughout this thesis.

### 3.1.3 NEXAFS and ARPES

Core results:

- Four pre-edge peaks in NEXAFS and one non-dispersive feature in ARPES indicate that there are a range of surface states associated with the silicon termination
- The unoccupied states may interfere unfavourably with NV- centre

#### NEXAFS

Near edge x-ray absorption fine structure spectroscopy (NEXAFS) is a technique which measures the x-ray absorption by a material as a function of photon energy in the range of a few tens of electronvolts around core level absorption edges. Since NEXAFS requires tunable photon energy, it is a technique which can only be performed with a synchrotron source. By measuring intensity as the rate of electrons emitted into vacuum, NEXAFS has the same surface sensitivity as XPS, being a probe sensitive to primarily the top few atomic layers of the sample. The fine structure which gives the technique its name is a result of the amplified absorption which occurs when the photon energy is in resonance with a core level to excited state transition. In addition, NEXAFS uses linearly polarized light, and enhanced absorption therefore also occurs when the axis of the photon's electric field is aligned with the axis of a bond during excitation. By measuring spectra with a range of different angles of incidence to the sample, angular-dependent peak intensity can yield information about the alignment of bonds at the surface. This effect is only evident on highly homogenous and ordered samples. [22]

The carbon K-edge NEXAFS spectrum of diamond represents a transition from the 1s core level to unoccupied states in the conduction band or vacuum. Surface reconstructions and bonded adatoms which induce surface electronic states within the

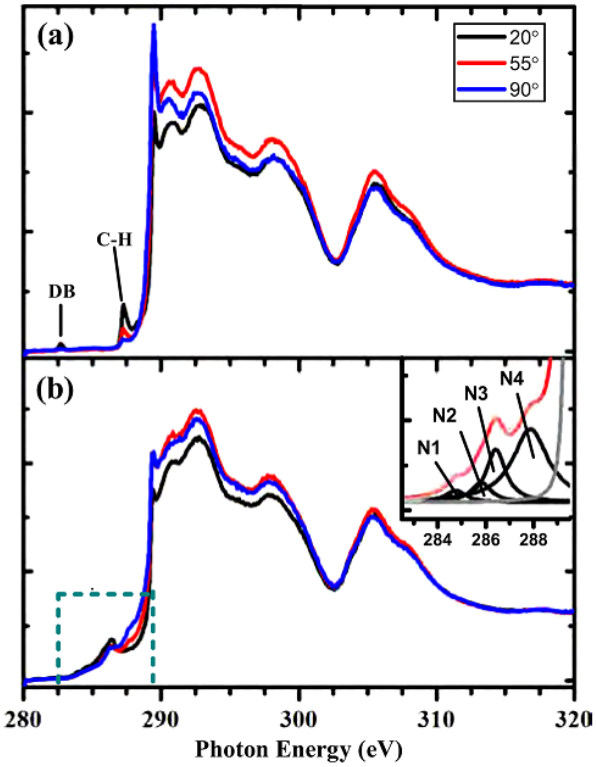


FIGURE 3.3: NEXAFS spectra for hydrogen (a) and silicon (b) terminated (100) diamond. Taken from Schenk *et al.* [18]

band gap, then, may be observed in NEXAFS as pre-edge peaks. Schenk *et al.* used a combination of NEXAFS and ARPES (detailed below) to probe the surface states induced by the silicon termination. [18] This work was performed at the Australian Synchrotron (NEXAFS) and the Singapore Synchrotron Light Source (ARPES).

The hydrogen terminated diamond spectra in Figure 3 demonstrate how angular dependent NEXAFS spectra may be used to gain information about the direction of bonds on the surface. The peak labelled C-H represents hydrogen bonded in the standard $(2 \times 1)$ dimer structure; this bond is known to be aligned close to perpendicular to the crystal surface. With a low angle of incidence, the vertically polarized light possesses an electric field vector which is also close to perpendicular to the surface, thus the C-H peak shows a higher intensity (black curve) compared to the spectrum recorded with the beam aligned at a high angle of incidence (blue curve). The HTD spectra also show a small component associated with dangling bonds at the surface.

Figure 3.3 (b) shows the NEXAFS spectra recorded at three angles for the sample after silicon termination. The inset shows the four peak decomposition which was used to fit the pre-edge region. Each of these peaks was attributed to a state within the band gap caused by the silicon termination. The peak labelled N4 in the inset can be seen to possess some angular dependence, showing the strongest signal with 90° incidence, suggesting that the state which it is associated with is aligned approximately parallel to the diamond surface. The weak angular dependence of the other

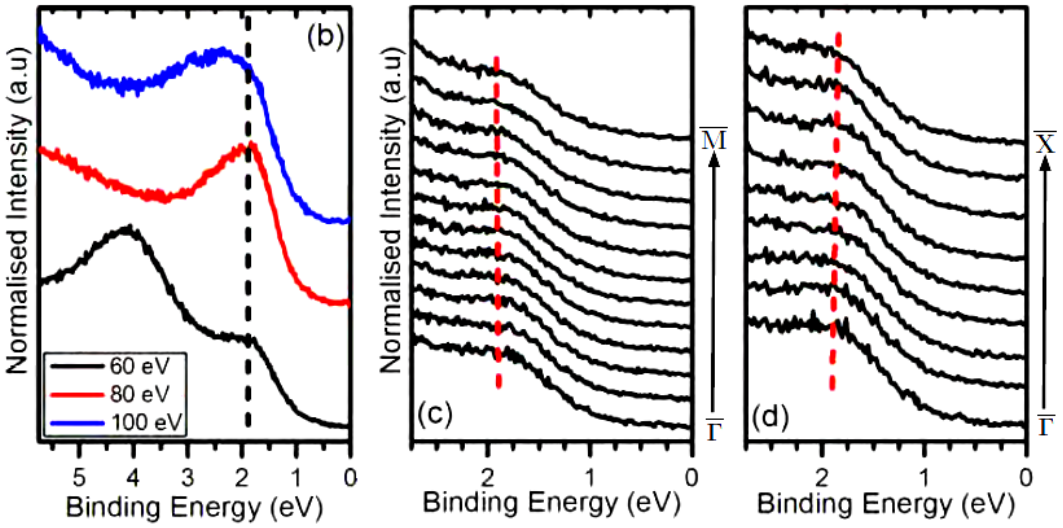


FIGURE 3.4: ARPES results showing the non-dispersive nature of the silicon terminated diamond surface state. Adapted from Figure 3 in Schenk *et al.*[18]

species is not sufficient to draw conclusions about the alignment of those states.

### ARPES

The work contained within this thesis uses primarily angle integrated x-ray photoelectron spectroscopy, which provides highly detailed information about the chemical states of species on the surface by observing binding energy shifts in core level spectra. Angle resolved photoelectron spectroscopy (ARPES) yields information about the momentum-dependent band structure of a material. In order to probe this, the photoelectron intensity must be measured as a function of both energy and angle of emission.

The momentum of electrons emitted from the sample during photoemission may be described by two components, a momentum parallel to the surface, $k_{\parallel}$, and one perpendicular to the surface, $k_{\perp}$. A result of conservation of momentum for electrons emitted from the material is that the $k_{\perp}$ component is proportional to their kinetic energy, or equivalently, to the binding energy of the state from which they originated and the photon energy which excited them. Since bulk-like states have a 3D Brillouin Zone, ARPES measurements of 3D states with different photon energies show energy dispersion—the measured binding energy changes with photon energy. Conversely, ARPES measurements of surface states, which are 2D, do not disperse with changing photon energy. A derivation of this result may be found in Chapter 8 of "Photoelectron Spectroscopy Principles and Applications" by Hüfner. [23]

Using this phenomenon, Schenk *et al.*[18] were able to identify an occupied surface state lying within the valence band in silicon terminated diamond. This state is marked by the black dashed line in Figure 4 (b), which shows that the peak does not

change in binding energy position with 60, 80 or 100eV photons. The surface state peak was also observed to have minimal dispersion with changing $k_{\|}$, as seen in Figure 4 (c,d) for two directions in k-space. The binding energy position and lack of dispersion was identified as similar to the dangling bond surface state seen in silicon carbide by Emtsev *et al.*, [24] suggesting that the silicon terminated diamond state may be similar in nature. This result is not conclusive, but the similarities between silicon terminated diamond and silicon carbide are discussed below at length.

The combination of ARPES and NEXAFS allowed Schenk *et al.* to identify both occupied and unoccupied surface states, yielding a good approximation for the band structure of the silicon terminated surface. There is an ambiguity in the derivation of the band alignment from the NEXAFS spectrum as the origin of the core hole is unknown. This leads to three possible versions of the determined band structure, assuming the core hole is associated with the bulk peak or the C1 or C2 peaks from XPS. These band alignments are shown in Figure 5, including the occupied state identified by ARPES (blue), and the unoccupied states found by NEXAFS (red).

Figure 5 also includes the energy levels for the technologically relevant states of the negatively charged nitrogen vacancy defect centre. A current problem with the application of near-surface NV- centres is the quenching which occurs due to the hole accumulation layer which forms on hydrogen terminated diamond in atmosphere. Unoccupied states in the band gap also provide possible traps for NV- state electrons, which is a problem for the application of SiTD to NV- devices. Further modification of the silicon termination may remove or alter these surface states; this was a motivating factor in the further work which led to this thesis.

### 3.1.4 Oxidation

The first study which attempted to modify the silicon termination used the element to which silicon is notably reactive: oxygen. Schenk *et al.* [19] dosed several silicon terminated diamond samples with oxygen in various forms, using (separately) water and $O_2$ gas dosing in vacuum, and exposure to atmosphere by removal from vacuum. All three of these treatments resulted in a significant degree of oxidation of the silicon without simultaneous oxidation of the underlying carbon. This means that the silicon was able to bond while retaining its bonds to the diamond, suggesting that it possesses unsatisfied bonds.

For the purpose of this review of the established knowledge of the silicon termination, I will highlight only the sample which was most effectively oxidized, the atmosphere exposed sample, as the alternate methods only differ in the degree of surface oxidation, they do not produce any chemical difference in the surface.

The silicon 2p core level XP spectrum is shown in Figure 3.6 before (top) and after (bottom) exposure to atmosphere and subsequent reintroduction to UHV. Before oxidation, the silicon core level is similar to the clean silicon termination shown above, albeit with a small excess (BSi component). After oxidation, the spectrum can be seen to have near completely converted to the +2 state, indicating that the

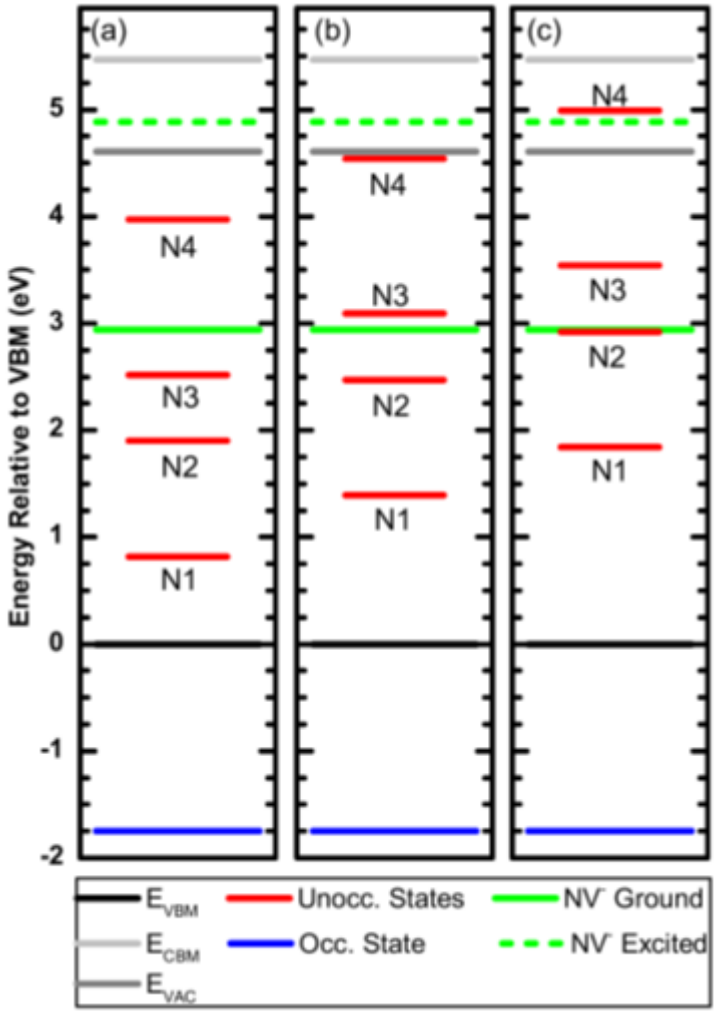


FIGURE 3.5: Silicon terminated diamond band structure models derived from ARPES and NEXAFS. (a) Assumes that the states seen in NEXAFS originate from the Bulk state in the C1s core level, (b) from the C1 state, (c) from the C2 state. Taken from Schenk *et al.* [18]

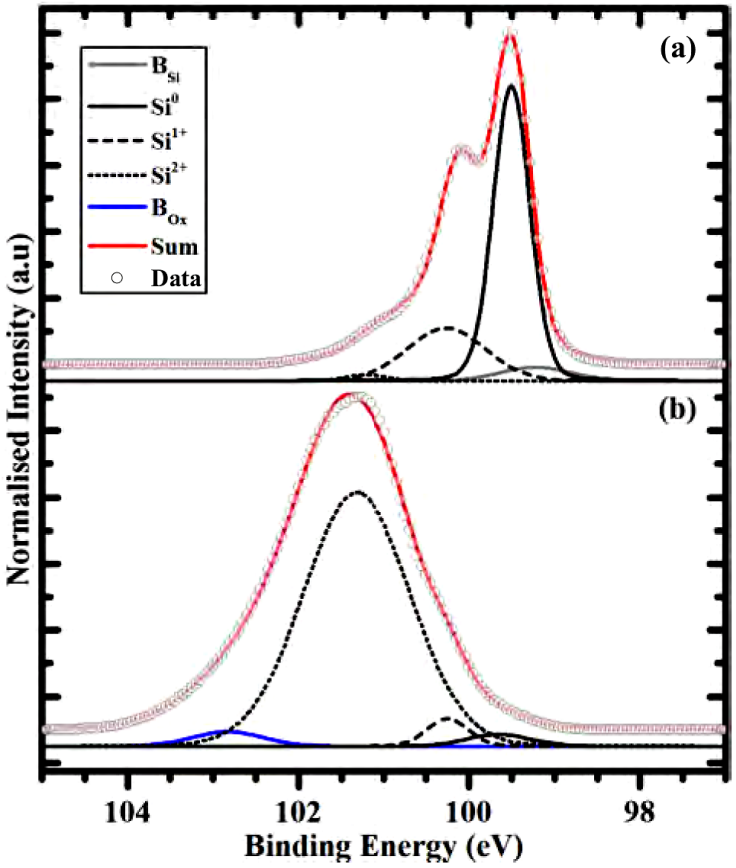


FIGURE 3.6: Silicon 2p core level spectrum for the clean and oxidized silicon termination explored in Schenk *et al.* [19] Adapted from Figure 6.

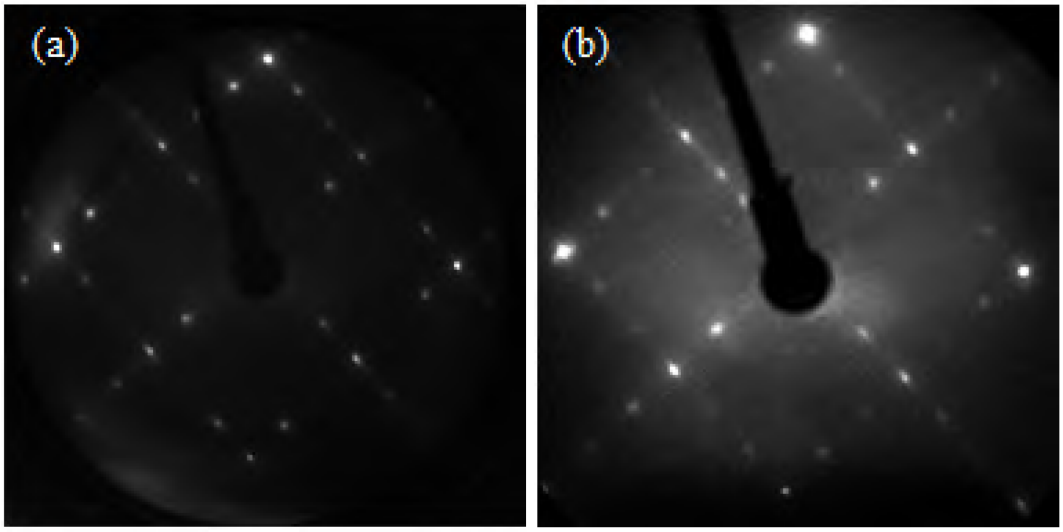


FIGURE 3.7: LEED patterns for silicon terminated diamond before (left) and after (right) oxidation by atmosphere exposure. Taken from Schenk *et al.* [19]

silicon has mostly bonded to two oxygen atoms. While the silicon core level has converted to an oxidized state, the carbon core level does not change, and the LEED pattern (shown in Figure 3.7) remains in the $(3 \times 1)$ pattern, albeit with an increased background signal. As the silicon is able to bond to oxygen without disturbing the symmetry which was induced by carbon-silicon bonding, we concluded that the two unsatisfied bonds on the SiTD surface were susceptible to passivation with oxygen, resulting in a heteroatomic two-layer termination comprised of a layer of silicon with a second layer of oxygen. As a final note on the oxidized silicon termination, it should be emphasized that the structure which has been formed by our group is different from alkyl-silane terminations which have been shown in some works, [25–27] which are characterized by carbon-oxygen-silicon bonds at the surface, compared to the direct carbon-silicon bonds in our termination.

### 3.1.5 Structure

With the information gained from these studies, which comprise four techniques, we have developed a structural model which we believe represent the (3x1) silicon terminated diamond (100) surface. A model of this structure is shown in Figure 3.8.

The density of bonded silicon on the surface was extracted from XPS; it was found that this corresponded to 2 silicon atoms per 3 surface atoms. [4] The $(3 \times 1)$ dimensions are a result of alternating dimers and monomers on the surface. For the two dimer-type carbon atoms, they are bonded to one silicon atom, and for the monomer atoms, they are bonded to two silicon atoms; this matches the 2:1 intensity ratio we saw in XPS.

The surface silicon atoms are incompletely satisfied; with two bonds to the diamond, each possesses two other bonds which are unaccounted for. The two most

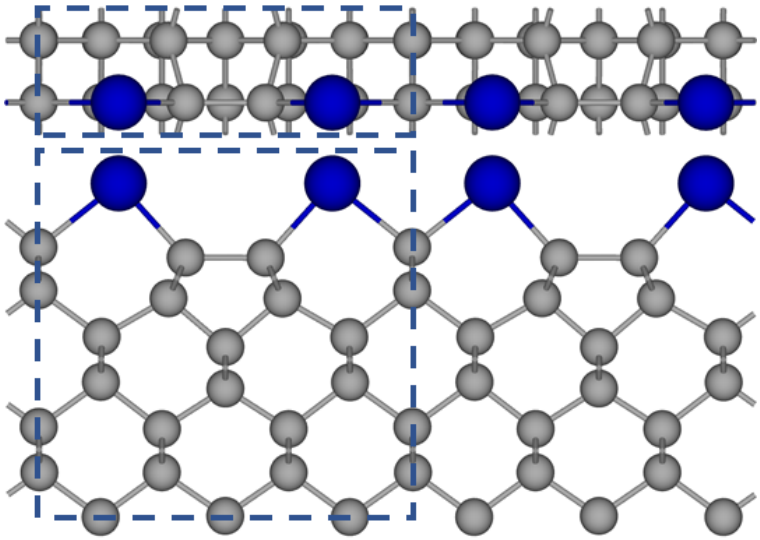

FIGURE 3.8: Our proposal for the structure of silicon terminated diamond (100). Top down view (top) and side view (bottom).

likely options are that (1) these atoms remain as dangling bonds, or (2) they bond along rows parallel to the short direction of the cell. This latter option is unlikely because it involves a significant angular deflection from the ideal tetrahedral bond arrangement, and a high degree of bond strain. The former option is also dubious because it implies a high density of dangling bonds on the surface, which is energetically unfavourable. However, the similarity between the occupied state seen in the SiTD ARPES and the dangling bond state seen by Emtsev *et al.* [24] weakly supports this assignment. The high reactivity of the silicon terminated surface to oxygen is also evidence for the dangling bond hypothesis, as such a surface should be very reactive.

This was the state of our understanding of the silicon terminated diamond system early in the timeline of the research which comprises this thesis. The goal of this work was to deepen our understanding of this termination, and to investigate how it can be modified, functionalized and used.

## 3.2 Other terminations

A goal of this thesis is to examine the possible termination structures which can be created using the silicon termination method developed by our research group in 2015. In order to highlight the significance of the GIV termination family, I will discuss here other diamond terminations which have been explored in literature. This discussion does not cover at length the hydrogen and oxygen terminations which have been thoroughly explored in literature; a brief summary of these is given below.

The noted low chemical reactivity of the diamond surface has been a limiting factor in the fabrication of diamond terminations. Additionally, the small size of the

carbon atoms and thus the diamond unit cell, present a steric barrier to full termination with large species such as many metal elements. These features manifest as poor coverage and homogeneity in the studies discussed in this review, and are an ongoing problem in diamond surface modification.

For the purposes of contrasting with the GIVTF, the features of each termination I will highlight are their method of formation, details of their proposed or demonstrated applications, details of their chemical variability, and when possible, details of their atomic structure. Within the larger context of this thesis, this review seeks to highlight methods which can allow for bonding at the diamond surface, common features of diamond terminations, such as the harsh methods required to access the chemically inert surface, and atomic structures which are known on the diamond surface as weak evidence for the atomic structure we espouse for the GIVTD surfaces. The chemical terminations which I will discuss are: nitride, amine, halogen, and light-metal oxides, as these represent the significant majority of published diamond surface chemistry studies.

### 3.2.1 Hydrogen termination

The hydrogen terminated (100) surface of diamond is the most thoroughly and extensively studied throughout the literature.[28, 29] This stems from its nature as a passive, stable, complete and homogenous termination, that can be prepared atomically flat by a simple treatment with a hydrogen plasma. While I will briefly highlight the major features of this termination here, for a thorough overview the reader is directed to Kawarada. [30]

The exploration of diamond on the atomic scale has only become popular relatively recently (circa 1990) due to the previous difficulty encountered in achieving ordered, epitaxial growth of atomically flat crystals. It is now known that ordered, oriented diamond layers with a hydrogen terminated surface may be formed by a number of methods, including atomic hydrogen dosing, hydrogen plasma treatment and ex situ oil polishing. Notably, epitaxial diamond grown by chemical vapour deposition possesses a 'natural' hydrogen termination as a result of growth, which proceeds with a small (1-5%) concentration of methane, or occasionally other alkanes, in a molecular hydrogen carrier gas. [30, 31]

The hydrogen terminated (100) surface possesses a $(2 \times 1)$ surface reconstruction, wherein each surface atom satisfies one dangling bond by dimerizing with a neighbour, resulting in the formation of rows, while the other bond is satisfied by a hydrogen atom. The structure of this surface is shown in Figure 3.9 (a). As each atomic layer step, on the (100) surface, represents a 90° rotation, the LEED pattern for HTD possesses a two-domain structure, as shown in Figure 3.2 (a), above. In vacuum, the HTD surface is known to be stable to about 900°C, at which temperature, the hydrogen will rapidly desorb, leaving the clean surface, unhydrogenated surface. [32]

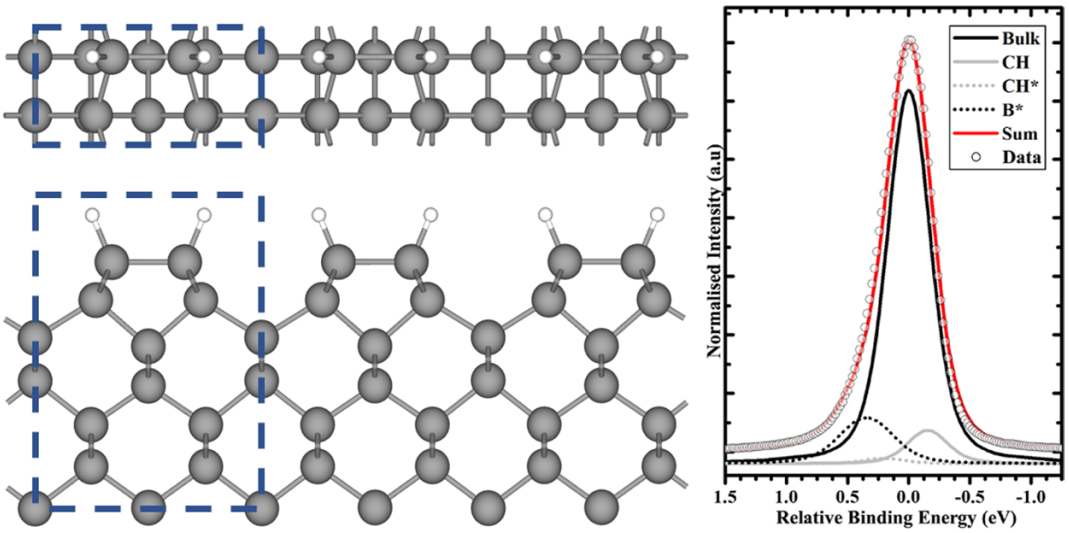


FIGURE 3.9: (a) The surface structure and top few layers of the (2x1) hydrogen terminated diamond surface, and (b) the corresponding C1s core level spectrum taken from Schenk *et al.*[33]

A thorough analysis of the structure of the C1s core level as observed by x-ray photoelectron spectroscopy has recently been published by Schenk *et al.*[33] describing the core level as comprised of a large component associated with bulk diamond (in Figure 3.9 (b) this is labelled 'B'), a second smaller component which is the result of final state effects causing a binding energy shift in carbon atoms near to the surface 'B*', a third component associated with H bonded carbon atoms at the surface, 'CH', and a fourth component due to vibrational effects on those surface C-H carbon atoms, 'CH*'. This fitting model, published in the *Journal of Physics: Condensed Matter* in 2016, was the motivation for the inclusion of a final state 'B*' peak in all the papers included in this thesis, as it should be present on all diamond surfaces, though the chemical shift is highly sensitive to the individual surface.

Technological interest in the hydrogen termination stems from the very unusual negative electron affinity which is found at the surface. Despite the large band gap of bulk diamond, hydrogen terminated surfaces in atmosphere have historically been observed to possess p-type conductivity at the surface as far back as 1989 by Landstrass and Ravi.[34, 35] The origin of this surface conductivity was a matter of some debate, being attributed variously to hydrogen induced surface acceptors,[36] to an acceptor subsurface region created by incorporation of hydrogen[37] or to a buried acceptor layer.[38] It is only as recently as 2000 that Maier *et al.*[2] fully elucidated the true mechanism behind this phenomenon, attributing it to the band alignment which occurs due to the negative electron affinity (NEA) at the H terminated surface.

Negative electron affinity means that the conduction band maximum lies above the vacuum level, a situation which is vanishingly uncommon among all semiconductors. The hydrogen-induced NEA at the diamond surface is caused by the formation of a very strong surface dipole potential; the strength of the potential stems from the highly polar C-H bond, and its short bond length, as well as the very high

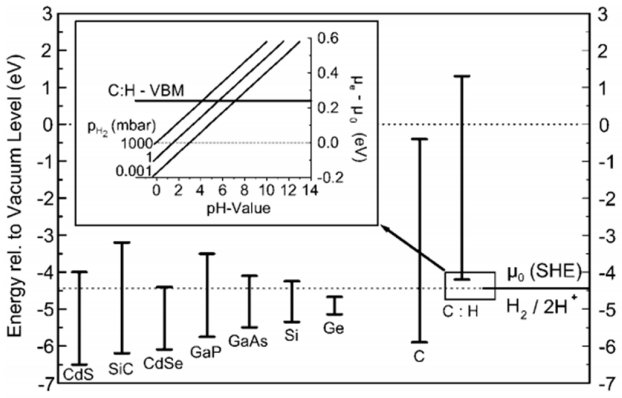


FIGURE 3.10: Diagram indicating the band gaps of a range of common semiconductors, relative to the vacuum level, and to the chemical potention for reduction of water. Taken from Maier *et al.*[2]

density of C-H bonds due to the small lattice parameter of diamond. The surface dipole acts as an accelerating potential, and the small width of the potential barrier allows for escaping electrons to easily tunnel through. While hydrogenated silicon and germanium (100) surfaces exhibit the same structure as diamond, the electronegativity of carbon is larger than hydrogen, while the opposite is true for Si and Ge. This electronegativity relationship, combined with the large band gap of diamond, are what allow the conduction band maximum to be driven above the vacuum level, resulting in a reported NEA as large as $\chi = -1.3\, eV$. [32]

Figure 10 shows the band alignment for hydrogen terminated diamond, as well as a range of common semiconductors, and this graphic shows why diamond is able to form an NEA while silicon carbide, for example, is not. The conclusion reached by Maier, *et al.* [39] was that the surface conductivity exhibited by hydrogen terminated diamond is a result of the fact that the electrochemical potential for water reduction lies below the HTD valence band maximum. That allows electrons to transfer out of the diamond and into the water layer which naturally adsorbs in atmosphere; this is the surface transfer doping model which is now accepted and well understood.

Since the development of the doping model, it has been shown that several molecular species which act as acceptors are also able to dope hydrogen terminated diamond when deposited on the surface. This includes molecules such as C60 fullerenes [28], various fluorofullerenes [28, 40], F4-TCNQ [41, 42], and various transition metal oxides including molybdenum trioxide [43, 44]. The use of MoO$_3$ for transfer doping the oxidized silicon terminated surface is the focus of the study comprising Chapter 5 of this thesis.

### 3.2.2 Oxygen termination

The oxygen terminated diamond (OTD) surface is a contrast to the hydrogen termination in almost every conceivable way. Instead of an atomically flat $(2 \times 1)$ reconstructed surface, oxidation methods invariably etch or damage the surface, leaving a $(1 \times 1)$ bulk-like surface symmetry. Instead of a single homogenous chemical species, it possesses a mixure of different oxygen states. And instead of the characteristic NEA of the HTD surface, the OTD surface possesses an electron affinity of $\chi = +1.7\ eV$, a full three electronvolts higher. [41]

#### Surface Chemistry

While the hydrogen termination bonds in a single, homogenous configuration, and results in atomically flat surfaces, the oxygen terminated surface is instead known to bond in a range of different moieties, including ether-style bridging between surface carbons, carbonyl-style C=O double bonds, peroxide-style C-O-O-C bridges, and hydroxyl C-OH bonds. This remains true whether the source of oxidation is plasma treatment [45, 46], acid treatment [47, 48], or atmosphere exposure of the vacuum dehydrogenated surface. [49]

This effect has been neatly shown by Torrengo *et al.* [46] in a study which explores the effect of oxidation on the subsequent amination of ultra-nanocrystalline diamond. In that study, oxygen terminated surfaces were prepared by three different methods: plasma oxidation (RF plasma, 50 W, $O_2$ gas), UV irradiation in pure $O_2$ gas, and acid etching ($H_2SO_4$, $H_2O_2$ in proportion 3:1 at 110 °C for 4 h). XPS spectra of the initial hydrogen terminated surface, and the oxidized surfaces resulting from each method are shown in Figure ?? where it can be seen that all methods possess a mixture of states in the O1s core level, and multiple oxygen related peaks at high binding energy of the diamond bulk, in the C1s core level.

Another example of this effect was shown by Notsu *et al.* [50], wherein the authors prepared two oxygen terminated samples, one by RF-plasma, and one by 'anodic polarization'. This latter electrochemical method used a platinum counter electrode and a silver reference electrode, and the diamond sample was immersed in a 0.1 M solution of $H_2SO_4$ held at +2.4 V. Neither of these two methods produced unique oxygen related states on the diamond surface.

Frequently, in order to maximize the oxygen termination, or to try and prefentially achieve a particular variant of the oxygen termination, OTD surfaces will be prepared with a series of oxidation methods. Martin *et al.* [51], for example, use a 1 hour treatment in fuming nitric acid, *followed by* 30 minutes exposure to UV activated ozone, but they do not report any improved results in terms of uniqueness.

As the oxygen terminated surface inevitable possesses an unpredictable mixture of atomic species, it is little surprise that there is no long range order seen in OTD LEED patterns. An interesting feature of the oxidized silicon and germanium terminations is that they retain the $(3 \times 1)$ symmetry of the underlying GIVTD surface.

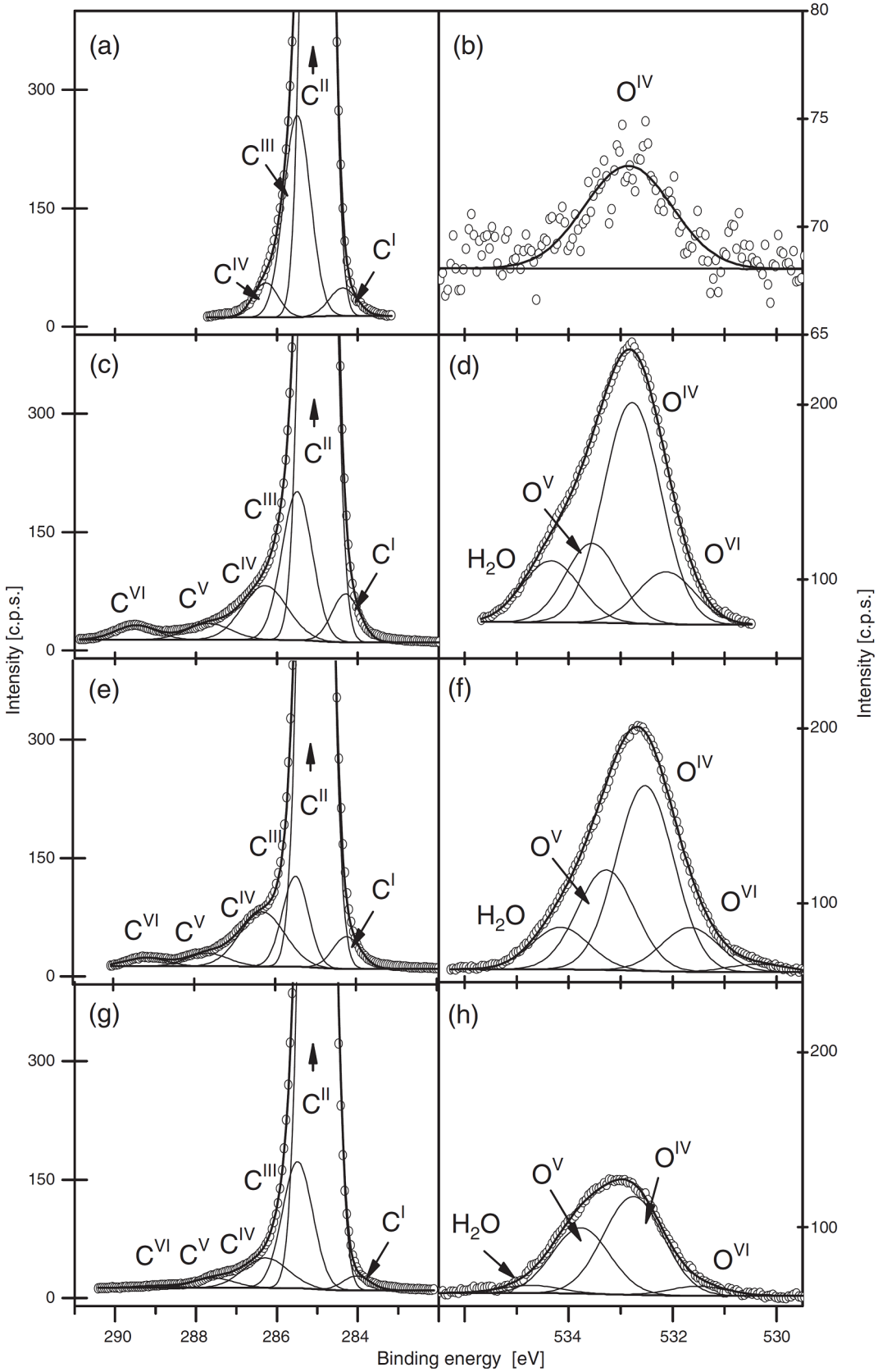


FIGURE 3.11: XPS spectra showing the mixture of states which result, regardless of oxidation method. The samples are UNCD, with C1s core level left, and O1s core level right. (a,b) H-terminated, (c,d) plasma oxidation, (e,f) piranha acid oxidation, (g,h) UV oxidation. Taken from Torrengo *et al.* [46]

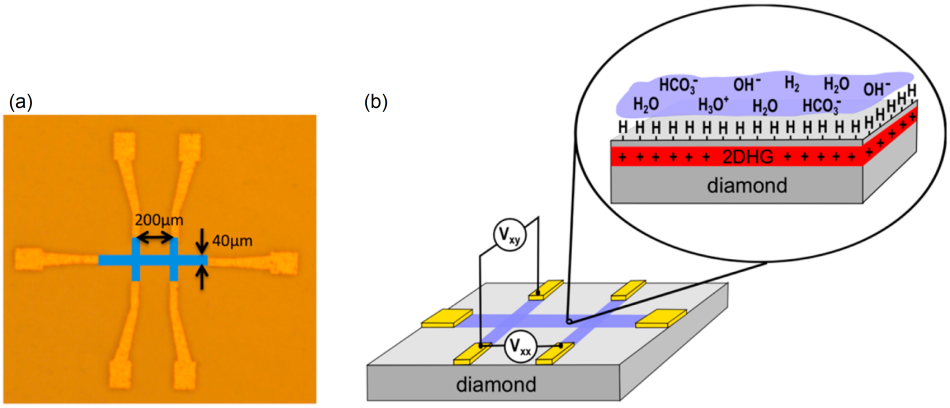


FIGURE 3.12: (a) Optical microscope image showing the Hall bar device fabricated on the diamond surface. The blue region indicates the area which is hydrogen terminated. (b) a schematic of the same device, with a zoomed image showing the induced conductivity in the presence of a water adlayer. Adapted from Figure 1 of Edmonds *et al.* [3]

This ordered oxygen may be technologically valuable, if it exhibits different properties to the disordered oxygen terminations of bare diamond. This is discussed within the study presented in Chapter 6.

### Electron Affinity

Unlike the negative electron affinity of hydrogen terminated diamond, the EA of oxygen terminated diamond has been observed to be +1.7 eV. This drives the surface well out of the range of surface transfer doping with water, and this means that confined conductive and insulating regions can be created by patterning terminations on the surface.[41]

An example of a practical realization of this effect was shown by Edmonds *et al.* in a study published in *Nano Letters*. [3] This work described the fabrication of a surface conductive electronic device on a (100) single crystal diamond substrate, as shown in Figure 3.12.

The device used by Edmonds *et al.* consists of a Hall bar fabricated by a standard photolithography process. The initially hydrogen terminated sample was masked by a photoresist, and the area outside of the blue region in Fig. 3.12 was exposed and stripped. The sample was then exposed to an $O_2$ RF plasma for 5 minutes. A further photolithography process was used to fabricate the electrode contacts, which were comprised of a titanium (10 nm), platinum (10 nm), gold (100 nm) trilayer. With this device, the authors were able to show that the hole accumulation layer in HTD supports a p-type two-dimensional conductivity.

This demonstration of the practical usefulness of termination-patterned devices was a core motivator in the exploration of new functionalized diamond surfaces in this thesis. The demonstration of fluorine passivation of the SiTD surface, shown in the study in Chapter 7 is particularly relevant for this application.

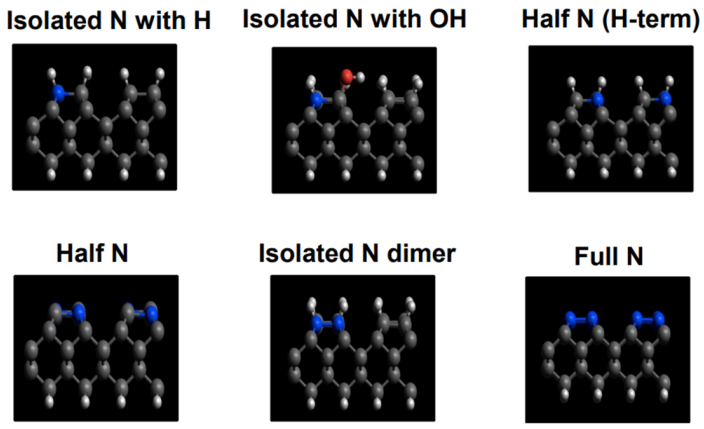


FIGURE 3.13: Some of the DFT calculated structures for a nitrogen terminated surface. Taken from Supplementary Figure 1 in Stacey *et al.*[52]

### 3.2.3 Nitride termination

There is a broad and well-established range of chemistry between carbon and nitrogen—this stems in no small part from the ubiquity of C-N moieties in biomolecules. Exploration of nitrogenic systems, then, is a logical pathway for functionalizing the diamond surface.

A feature of the oxygen terminated diamond surface is that all methods for its formation result in a mixture of different types of bonding at the surface. This remains true whether the source of oxygen is a plasma, a wet chemical treatment, or via the exposure of a dehydrogenated surface to atmosphere. With the variety of carbon-nitrogen bonding arrangements which exist in molecules, it is little surprise that published literature reflects a similar behaviour for nitrogenated diamond.

Nitrogen terminations in literature are generally formed by exposure of the HTD surface to a source of activated nitrogen species, either originating from $N_2$ or $NH_3$ gases, or from nitrogen containing organic molecules.

The possible bonding structure of a nitrogen terminated diamond surface was discussed at length in the 2015 paper by Stacey *et al.*,[52] wherein a range of reasonable bonding arrangements were analysed by density functional theory. Among the range of structure which were simulated, the most common bonding arrangements involved either substitutional replacement of one or both carbon atoms in a $(2 \times 1)$ surface dimer, or using nitrogen as a bridging atom, analogous to ether-bonded oxygen.

In addition to the computational work, the paper also shows XPS results for several nitrogen terminations formed by microwave plasma treatment. The most effective plasma treatment in this paper uses a plasma made of pure nitrogen gas, in contrast to other works, and the authors demonstrate that this leads to a higher coverage of N, as measured by XPS. The NEXAFS study contained within the paper shows that by varying the hydrogen content of the plasma feed gas, a surface

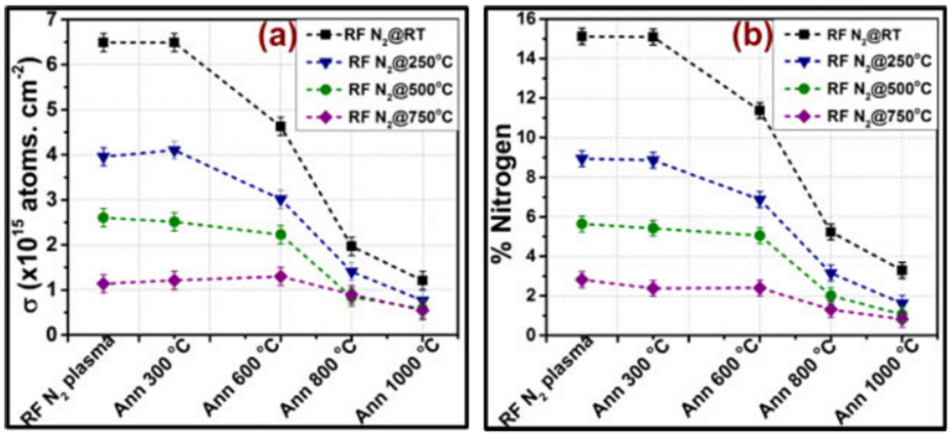


FIGURE 3.14: Plot demonstrating the low thermal stability of the nitrogen termination created. Taken from Figure 3 of Chandran *et al.*[53]

comprised of substitutional nitrogen (representing N-N bonds) and of mixed N-H (representing N-C bonds) terminations can be created. Stacey *et al.* also make note of the fact that their nitrogen terminated surface does not display induced conductivity in air, in contrast with hydrogen terminated diamond. This may be useful for NV center research, as it indicates the lack of formation of a 2D hole gas.

As with the GIV terminations, a goal for the development of nitrogen terminated diamond has been the creation of a PEA surface with a low density of surface spins, for use with NV centers. Chandran *et al.* detail a nitrogen termination realized by indirect RF $N_2$ plasma [53] which they go on to discuss in their 2015 letter [54] as a possible candidate for this purpose. Indirect, in this context, refers to the use of plasma to generate radical and ionized species, which then impact the surface, without the surface itself being within the plasma. In this case, the composition of the nitrogen termination was investigated by XPS, and shows that the plasma treatment results in a mixture of surface nitrogen species, including C-N-C and C=N much like the behaviour seen in oxidized diamond surfaces. The surfaces in this study also contain a large contribution from unterminated surface carbon, indicating the difficulty in creating a complete bonded nitrogen layer. A similar nitrogen termination was also produced by Denisenko *et al.*[55] using the same RF plasma method. Notably, that study showed that electrochemical oxidation of the nitridated surface led to the formation of both N-O and C-O bonds; arguably the latter may stem from unterminated surface regions as seen by Chandran.

Further work by Attrash *et al.*[56] reports that surface damage induced by the RF plasma treatment (as opposed to the microwave method used by Stacey *et al.*[52]), may be minimized by the use of a grounded grid between the plasma and diamond, to increase the ratio of radical to ionized nitrogen atoms impacting the surface. The metric which is used to assess surface damage in that study is the relative increase in the FWHM of the C1s peak. That study finds a $(1 \times 1)$ reconstructed nitrogen terminated surface, and, importantly, desorption of N from the surface at 210°C and 560°C.

Computational work by Chou *et al.*[57] suggests that nitrogen terminated (111) diamond surfaces present an extremely appealing platform for NV centers, and may be fabricated by the same plasma termination method as in the above studies. The study by Attrash *et al.*[56], as mentioned above, as well as by Kuntumalla *et al.*[58] both show that the thermal stability of surface nitrogen species is significantly less than that of bulk diamond. As a platform for device fabrication this property is suboptimal, since it limits the temperature of processing steps which can be used. In addition, the use of NV centres requires their thermal activation, which would also be limited by the desorption temperature of the nitrogen termination.

### 3.2.4 Amine termination

The method of nitridation by plasma seeks to overcome the low reactivity of the diamond surface by generating very highly reactive atomic species. While this method, as shown, does lead to the creation of carbon-nitrogen bonds, the method also risks severely etching the surface. Additionally, attempts to generate a "pure" nitrogen surface do not seek to use this nitridation as a platform for further functionalization, and are instead considered an end goal in themselves. An alternative pathway involving C-N bonding at the diamond surface is via the bonding of amines.

Notably, for the purpose of comparison with the studies which comprise the main text of this thesis, very few studies of aminated diamond use a single crystal sample, and as such do not make much note of atomic scale bonding arrangement or surface reconstructions. It is debatable whether these surfaces should be discussed in the context of 'terminations' rather than as 'functionalizations', but a review has been included here to highlight the variety of methods used to induce surface C-N bonds.

#### Radical beam

Separate from the goal, discussed above, of generating surfaces which are suitable for NV center devices by nitrogen and/or nitride terminations, a motivation for termination with amines is often to produce a platform for bonding biomolecules to the diamond surface, for further use as a biosensor. The ideal case of a surface homogeneously covered in primary (NH$_2$) amines is highly useful for biofunctionalization with other species.[59] This idea of a surface termination which may be further functionalized is a primary motivator in the silicon termination studies which comprise the main body of this thesis.

An example of amine termination was shown by Suaebah *et al.*[60] as a proof of

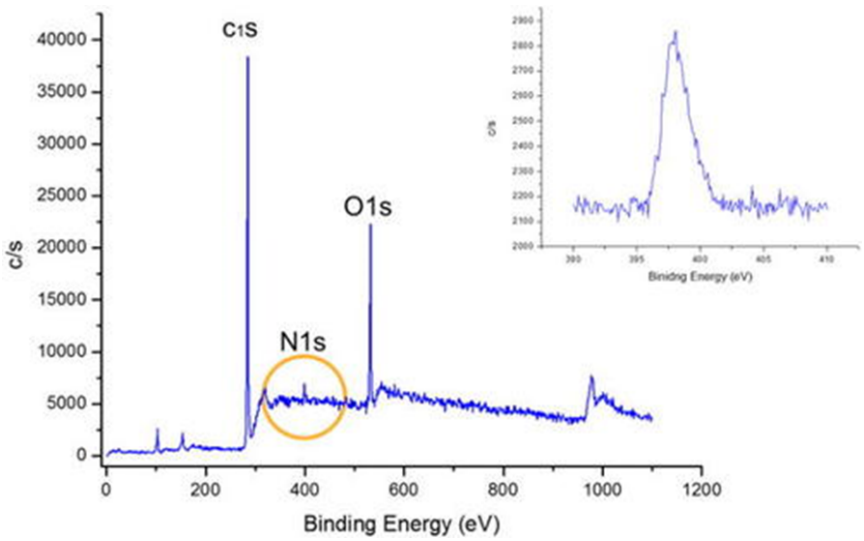


FIGURE 3.15: Survey spectrum demonstrating the relative nitrogen and oxygen coverages on an amine terminated diamond surface. Taken from Figure 3 of Suaebeh *et al.* [45]

concept for this application. The termination was performed by exposure of an oxidized diamond surface to a controlled beam of radical species generated from a mixture of $N_2$ and $H_2$ molecules. The sample used in this study was subsequently patterned by standard photolithography processes, and un-nitrogenated areas were fluorinated by $C_3F_8$ plasma treatment and the bonding of DNA and adenosine triphosphate molecules to the aminated area was tested.

This study again demonstrates the difficulty in generating a complete N coverage of the diamond surface; the XPS survey spectrum taken on a nitrogenated area shows an enormously higher contribution from oxygen over nitrogen (also, notably, an apparently significant degree of silicon contamination which is not discussed in the paper). The authors also note that the breadth of the nitrogen peak is indicative of multiple nitrogen species on the surface, much as seen in the nitridation studies above.

Regardless of the apparently low nitrogen coverage achieved in this work, the authors still were able to demonstrate selectively stronger binding for the DNA molecules on the nitrogenated regions compared to the adjacent fluorinated regions. As the preparation of this surface involved direct radical exposure, the work by Attrash *et al.*[56] would suggest that the degree of surface damage should be low, though this is not addressed in the paper.

### Plasma

Plasma treatments can also be used to generate a purportedly aminated surface.[61] Koch *et al.*[62] have reported that the exposure of a hydrogen terminated film of ultrananocrystalline diamond to an $NH_3$ plasma causes a change from a hydrophobic to a hydrophilic surface, and concurrent adsorption of amine to the surface. As

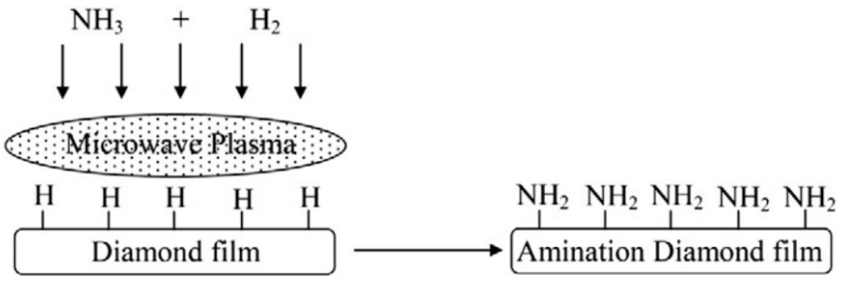


FIGURE 3.16: Conceptual schematic of microwave plasma amination. Taken from Wei *et al.*[59]

with previous discussed nitrogen plasma treatment studies, they also point out that the nitrogen "termination" results in a large increase in oxygen on the surface, as measured by XPS. This mixture of chemical species at the surface is a disqualifying feature for the use of aminated surfaces as a quantum computing platform but is not necessarily so for biosensing applications. The Koch *et al.*[62] study goes on to show that a biomolecule which is expected to bond to NH$_2$ groups does bond to the surface, as evidence for the nature of the surface nitrogen on their sample.

While the previous study involves the treatment of a hydrogen terminated UNCD diamond film with an RF plasma in a PECVD paper, in contrast the work by Wei *et al.*[59] shows an NH$_3$ plasma treatment in a microwave plasma CVD chamber, and the authors highlight the presence of both NH and NH$_2$ radical species in the ammonia plasma, which may be a contributing factor in the generation of multiple varieties of nitrogen species on the surface as noted in both this and other amination studies.

Compared to the UNCD film studied by Koch *et al.*, the sample investigated by Wei *et al.* was a polycrystalline film with average particle size of 5 µm. The plasma treatment in this study, according to the authors, did not alter the surface morphology and microstructure, a desirable feature for maintaining the integrity of a functional sample. An interesting note on this study is the observation that increasing the flow rate of ammonia in the plasma increased the ratio of primary amine to secondary and other surface nitrogen. It may be that a singular species amine surface can be fabricated, but that remains unproven.

### Other methods of amination

An alternative method of generating an aminated surface was reported by the Kawarada group in 2006. In contrast to the radical atom beam or plasma treatments in the previously discussed studies, the paper by Zhang *et al.*[63] describes a treatment method whereby a hydrogen terminated polycrystalline diamond film is exposed to UV light in the presence of ammonia gas. This amination, which they highlight as 'direct', as in from hydrogen terminated diamond, in contrast to amine bonding

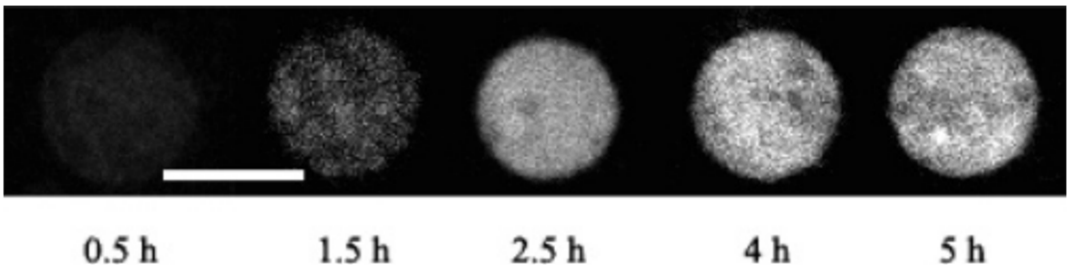


FIGURE 3.17: Increasing the duration of amination results in increased fluorescence after DNA binding, implying an increased degree of amine coverage. The fluorination appears to plateau by 2.5h of exposure. Taken from Zhang *et al.*[63]

by substitution of chlorine or alkyl group, results in a surface which is, once again, significantly contaminated with oxygen.

This paper is worthy of note because it both introduces a new method of surface termination, and also demonstrates the useful functionality of that surface. Zhang *et al.* generated their aminated surface and then deposit a layer of gold, which they patterned by a photolithographic masking procedure. They then treated the unmasked areas of the surface with a fluorine plasma. After stripping of the mask, spatially resolved XPS showed no fluorine in the formerly masked, aminated, areas, and conversely fluorine with no nitrogen or oxygen in the unmasked areas. Finally, a reaction allowed DNA to be bonded to the aminated regions via the cross-linker molecule glutaraldehyde, and fluorescence indicated that a significant treatment time of 2.5 hours was necessary to maximize the amine coverage.

The Kawarada group[63] suggests that the oxygen present on the surface after amination is a result of contamination in the $NH_3$ gas during illumination; UV amination was also demonstrated by Torrengo *et al.*[46] in a study which tried to ascertain in depth the role of oxygen in that UV amination method. They found that the rate of amine uptake for a hydrogen terminated sample with a pure $NH_3$ gas was relatively low, and that a much higher degree of amination could be achieved using oxygen terminated diamond, or a mixture of $NH_3$ and $O_2$ gases. This is further bad news for hopes of a chemically pure amine surface. An interesting method of amination was shown by Simon *et al.*[64] which consists of immersion of a hydrogen terminated surface in a 0.1M solution of ammonium persulfate in pure liquid ammonia, which leads to an apparent mixture of amine species, as well as surface oxygen.

Some studies which show an aminated surface do so via the attachment of a nitrogen-containing organic molecule, often aided by UV illumination. A flaw in this approach is that the large size of the organic molecules provides an inevitable kinetic barrier to complete 1:1 adsorption of nitrogen to the diamond surface carbon atoms.

Amine terminations have also been prepared in other studies indirectly, by modifying the surface first by chlorination or alkylation. The work by Strother *et al.*[65]

shows an alkylated surface being replaced by an amine-containing molecule, while those of May *et al.*[66], and Miller and Brown[67] both show a chlorinated surface (detailed below) being aminated by exposure to $NH_3$ under UV light. These studies do not present proof of a complete termination, though notably the latter study shows that the amination can be performed on both (100) and (111) surfaces.

Nitrogen and amine terminations may be prepared by a range of methods. Consistently in every treatment method, nitrogenation is associated with oxygenation, and some works propose that the presence of oxygen is not just inevitable but in fact necessary to produce or stabilize the nitrogen termination at all. Most methods involve generating highly reactive and/or radical species, to overcome the low reactivity of the diamond surface. The presence of oxygen, and the mixture of surface nitrogen species may present problems for nitrogen vacancy center quantum computing architectures, but $NH_2$ surfaces might be useful for biosensing.

### 3.2.5 Fluorine and chlorine terminations

I have shown how the generation of radical species can be used to induce a nitrogen-terminated surface, though doing so results inevitably in a mixture of bonding moieties, probably due to the tendency of nitrogen to form 3 bonds. It is also possible to produce, by plasma or other means, reactive or radical species of halogen elements like fluorine and chlorine. Since these elements tend to form only a single bond, they present an attractive target for the creation of a chemically homogenous terminated diamond surface, in the same manner as hydrogen terminated diamond.

The atomic structure of fluorine terminated diamond, in contrast to NTD, is fairly well understood. It has been observed by low energy electron diffraction that the (100) surface adopts a $(2 \times 1)$ reconstruction under the influence of fluorine, and shows primarily a single C-F component in x-ray photoelectron spectroscopy (in addition to the $sp^3$ diamond peak. This is taken to mean that the surface retains the same bonding arrangement as hydrogen terminated diamond, comprised of rows of dimerized atoms with a single available bond each, and that bond is satisfied by a fluorine atom. On the (111) surface, again similar to the hydrogen termination, a single dangling bond arrangement is assumed, with bulk-like $(1 \times 1)$ symmetry and each vacuum-adjacent carbon atom is satisfied by a single fluorine atom.[68]

The work of Cai *et al.*[69] has discussed the possible use of the fluorine terminated (100) and (111) diamond surfaces as a platform for a "large-scale quantum simulator", highlighting the bonded fluorine atoms as a nuclear spin array which can be arranged with either rectangular ( (100) ), or triangular ( (111) ) symmetry, which allows for tuning the interaction strength between fluorine spins. The $(2 \times 1)$ symmetry of previously reported fluorine terminations was a motivator for the study discussed in Chapter 6, which demonstrated the formation of a $(3 \times 1)$ symmetry array of surface-bonded fluorines, allowing a potential third, distinct system for the quantum simulator model.

**Plasma termination**

A primary motivator for the interest in FTD stems from the observed increased proportion of negatively charged NV centers in fluorinated diamond, which was first reported by Cui and Hu.[70] The desire to exploit near-surface NV centers for various devices is hampered, currently, by the detrimental effect of the hydrogen terminated surface. This stems from its near-surface hole accumulation layer, which forms spontaneously in atmosphere, as a result of transfer doping to an adsorbed water layer.[2] This is able to occur because of the energy level alignment caused by the negative electron affinity of the HTD surface. Fluorine, being a highly electronegative atom, leads to a strong positive electron affinity. This means that significantly less NV fluorescence quenching occurs for the fluorinated surface. The authors also showed that the higher proportion of negatively charged NVs persists for at least 10 days in air, which is notably positive for the prospect of using the FTD surface for practical NV devices.

In the study by Cui and Hu, they prepared a fluorine terminated surface by the treatment of an oxygen terminated surface with a $CF_4$ plasma, using an RF plasma reactor. Their fluorinated surface was confirmed by x-ray photoelectron spectroscopy, and showed a pair of surface fluorine species assigned as CF and $CF_2$, as well as the retention of a large graphitic, sp2, C-C peak. This suggests that their treatment either does not fully terminate the surface, or does result in the removal of damaged graphitic carbon from the surface. In notable contrast to the studies discussed above for nitrogen terminated diamond, the fluorine plasma DOES remove a significant majority of oxygen from the surface. Unlike nitrogen, fluorine has a higher electronegativity than oxygen, leading to a strong, partially ionic bond between C and F.

The work of Cui and Hu has garnered significant interest in recent literature, and has received over 50 citations in just five years. I note this to emphasize the high relevance of diamond surface chemistry studies within the scope of current scientific inquiry.

A variety of fluorine containing molecules have been used as a radical source in plasma fluorination studies, including $CF_4$, $CHF_3$ and $C_4F_8$.[71–80] Variations in the feed gas do not appear to meaningfully impact the nature of the resulting fluorine termination, though they may cause difference degrees of surface damage. Works by Kondo *et al.* [80] and Denisenko *et al.* [79] show RF plasma treatments using $CF_4$ resulting in satisfactory coverages of C-F, with the former showing that extended treatment results in surface damage, and the latter showing that a range of fluorocarbon species are formed. These studies used oxygen terminated diamond as a starting state.

Investigations into the nature of the mixed fluorocarbon species suggest that in addition to the actual termination, fluorine treatments tend to generate a layer of a polytetrafluoroethylene-like polymer. A recent work by Jelezko *et al.* [81] used an inductively coupled plasma of sulfur hexafluoride in an effort to minimize both the

surface damage and the formation of these polymer species. Notably, the $SF_6$ treatment was reported to be more effective in stabilizing negatively charged shallow NVs than in $CF_4$ plasma works.

### Other methods of fluorination

An alternate pathway for generating reactive atomic fluorine has been explored by Smentkowski *et al.* [82] and Rietwyk *et al.* [83, 84] which involves deposition of a fluorocarbon molecule upon the surface, followed by thermal or photoinduced decomposition of the molecules. The liberation of atomic fluorine on the surface provides a source of fluorine without the associated high energy of a plasma, and by lowering the surface concentration, a mixture of F and H functionalities can be achieved.

FTD has also been prepared by atomic beam bombardment; Freedman and Stinespring [85] demonstrated such a termination of the (100) surface, though the result did not show a $(2 \times 1)$ termination, and did have a significant $sp^2$ component. It has also been performed by exposure to highly reactive gases atomic fluorine, HF and $ClF_3$. [83, 86, 87] As with the nitrogen termination, all these methods demand the generation of reactive species. Unlike NTD, however, most methods of fluorination result in an oxygen-free surface, likely due to the larger bond strength of C-F compared to C-O, which is a result of fluorine's larger electronegativity.

Practical use of the fluorine termination has been shown as a high stability terminating species in surface conductive diamond devices, where a patterned fluorinated region acts as an insulator around the conductive hydrogen terminated regions.

An advantage of fluorine over chlorine, as a terminating species for diamond, is the fact that a complete, stable coverage is theoretically possible. This was discussed by Tiwari, *et al.* [88] in the context of a computational study, where they investigated the stability of F and Cl terminations for (100) and (111) diamond, finding that the increase in adsorption energy with coverage for chlorine is such that a complete coverage is energetically unfavourable, while a complete F coverage is predicted to be stable.

Nonetheless, chlorinated surfaces have been created in a number of studies, [66, 67, 89] and have been used as a method of further functionalization, by allowing substitution of the chlorine moiety with some other species. The fabrication of Cl-TD follows much the same methods as for FTD, with less of an emphasis on plasma treatments.

Widmann *et al.* [89] describe a chlorine treatment with a $Cl_2$ plasma, starting with an oxidized surface which is theoretically primarily OH terminated, though the photoelectron spectrum shows a large ether bridge component in addition to the C-O peak, as well as a very large $sp^2$ peak, suggesting that the surface is significantly graphitized or unterminated. The chlorine termination does not induce a notable distinct component in the C1s spectrum reported, though the large oxidized species may be masking its presence. After demonstrating that both oxygen and

chlorine begin desorb at the low temperature of about 250°C, the authors conclude that their chlorine termination is co-adsorbed with water. Given the poor adsorption, low thermal stability, and noticeable surface damage, I agree with the authors' conclusion that the chlorine termination by itself does not present a valuable platform for device fabrication.

Freedman [90] reported an investigation into atomic beam chlorination of diamond (100) and (111) using both atomic and molecular chlorine, which resulted in only very poor chlorine uptake, and near-total loss of adsorbed chlorine after light annealing to 423K. Freedman's assessment concurs with that of Widmann in stating that "atomic chlorine will exhibit a less significant role [than fluorine] in the surface chemistry of diamond deposition systems."

### 3.2.6 Metal oxide terminations

Diamond has also been investigated as a material of interest as a field electron emitter, ideally exploiting its ability to form a negative electron affinity surface which allows extremely high efficiency generation of photocurrent.

Himpsel *et al.* [91] conducted a study in 1979 on the negative electron affinity bare (111) diamond surface, using total photoemission quantum yield measurements. Notably, while the authors repeatedly describe the surface as 'natural', and 'clean', and claim not to observe any significant coverage of a terminating layer, they also observe a $(1 \times 1)$ LEED pattern, and no band-gap surface states, both features which are characteristic of H-terminated (111). They found that the NEA surface results in an extremely high quantum yield of 40-70%, and conclude that diamond surfaces present a very interesting prospective platform as a vacuum photocathode. As a reminder, negative electron affinity means that the conduction band lies above the vacuum level, and the resulting electron emission properties have thus been described as "barrier free".[92]

High probability of electron emission by excitation is desirable in a range of applications, such as image amplification, current signal multiplication, and for vacuum cathodes.[93] The observation that the negative electron affinity surfaces of diamond allow for barrier free electron emission was the motivation behind a range of recent studies, published since 2010, performed primarily by Cherns and O'Donnell *et al.*[1, 51, 93–96]

The concept of these experiments follows from the method for the formation of a negative electron affinity surface on gallium arsenide, which involves a complex surface treatment resulting in a cesium oxide surface layer. The physical interpretation of this structure is to consider the low electronegativity of cesium and the high electronegativity of oxygen as a strong dipole layer. The CsO layer provides both significant p-type doping, which induces downward band bending to the extent that the CBM is below the vacuum level (NEA), and an accelerating dipole. This CsO on GaAs structure is still in use as a high efficiency vacuum cathode in modern vacuum electronics.[93, 97]

Cesium oxide layers have been shown on diamond by cesiating the oxidized surface, by Loh *et al.* [98, 99], Pickett *et al.* [100], and Geis *et al.* [101] In these studies, the cesiated diamond was produced in the same general way: various diamond surfaces were prepared in vacuum, and cesium is deposited upon it from a vacuum deposition cell.

Loh *et al.* [98] investigated the (111) surface of bare and oxygenated diamond with ultraviolet photoelectron spectroscopy, and showed that cesium was able to bond to both surfaces, inducing a large, sharp peak characteristic of negative electron affinity. They report downward band bending on both surfaces, attributed to charge transfer, suggesting in particular that the cesium is able to populate defect states on the adsorbate-free surface. Notably for practical applications, the NEA of both of these surfaces was shown to be resistant to atmosphere exposure. After 3 hours in air, the NEA peak was only slightly attenuated, and a 0.5 eV shift in binding energy, consistent with oxidation of the cesium. Further work by that group[99] showed that the cesium oxide diamond surfaces were stable to 500°C annealing, the desorption temperature of oxygen on diamond.

Both the works of Loh *et al.* and of Geis *et al.* [101] consistently show that cesium deposited on hydrogen terminated diamond is neither chemically nor thermally stable, supporting the hypothesis that cesium does not bond to the hydrogenated surface. This comports with the understanding of hydrogen terminated diamond as chemically inert. It also does not show significantly enhanced electron emission properties.

Following this same concept of exploiting low electronegativity metals, O'Donnell *et al.* showed first by DFT[95], and then by experimental photoemission work[51] that the oxidized surface of (100) diamond could be dosed with lithium to form a strongly bonded lithium-oxide layer. The preparation of this surface is interesting; the authors prepared an oxidized diamond surface by acid treatment and UV activated ozone exposure, and deposited a 50nm layer of lithium. They removed most of this lithium by washing the surface in water. Because lithium is very highly soluble in water (forming LiOH) this process completely removes lithium when it is deposited on a *hydrogen* terminated surface, but leaves a thin layer on the oxidized surface, indicating that the strong oxygen-lithium bond is stable to removal by water.

An intriguing aspect of the lithium oxide termination is the formation of a negative electron affinity only after the surface has been annealed to 600°C. This is intriguing in the first instance because 600°C is above the reported temperature of oxygen desorption in other studies of the 'clean' oxygen terminated surface. The authors see a further spectacular enhancement of the NEA after annealing further to 800°C. Their results are shown in Figure 3.18. Photoelectron spectra of the lithiated OTD surface before and after 800°C annealing show a noticable loss of peaks in the high binding energy region of the C1s spectrum, which is suggestive of a loss of C-O. This would make sense, as that temperature is well above the desorption point of

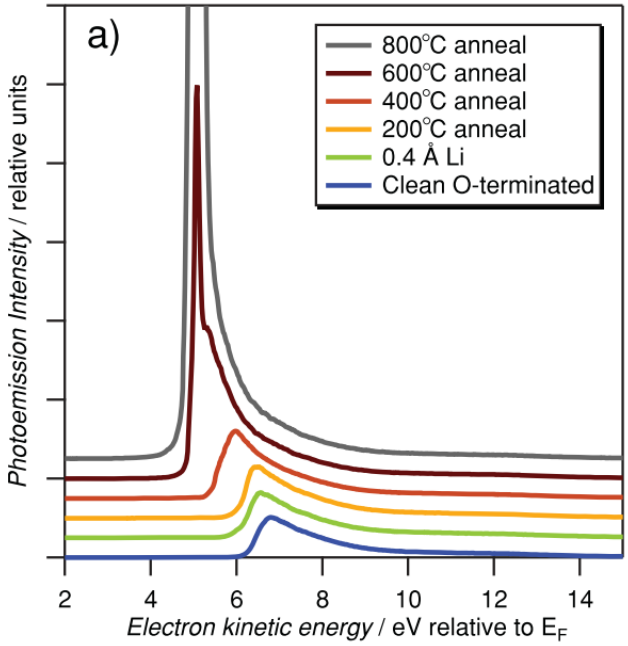


FIGURE 3.18: Shifts in photoelectron cutoff, followed by the formation of a large NEA peak, after a series of anneals of the lithiated oxygen terminated diamond surface. Taken from O'Donnell *et al.* [93]

oxygen. The O1s spectrum, however, does not show a large loss of intensity, but it does see a shift to higher binding energy. The authors conclude that the annealing causes a change in the structural arrangement of lithium and oxygen, leading to the large NEA enhancement.

Given that their LiO diamond surface is not just resilient to, but in fact activated by high temperature annealing, and possesses a negative electron affinity, it would seem to be a highly technologically useful surface for high electron emission applications.

Continuing the same concept, O'Donnell *et al.* have also shown the creation of magnesium-adsorbed oxygen terminated diamond [92] which possesses the largest negative electron affinity reported in literature, at -2.0 eV. Unlike the previous surface, the authors report that MgO terminated diamond does not need to be thermally activated, possessing an NEA immediately after deposition of magnesium. They propose that it is the formation of structures where the metal adatoms coordinate to two surface oxygen atoms which allows the negative electron affinity states, and that this can occur with no extra energy for Mg, but not lithium.

While both the magnesium oxide and lithium oxide terminations do have an NEA, neither of these surfaces were able to be transfer doped. This is attributed, in these studies, to poor band alignment with doping states, or to Fermi level pinning due to LiO or MgO surface states.

The relevance of this work for comparison with the studies described in Chapters 6 and 7 is that they all show the formation of a bilayer terminating structure. The studies discussed in this section all rely on the strong bonds between oxygen and low

electronegativity metals; our Group IV terminations present a completely chemically different variation of a similar bilayer termination concept.

Chapter 5 shows a transfer doping experiment on a bilayer termination (silicon oxide), in which transfer doping is successfully acheived, despite the much more positive electron affinity (around +0.07 eV, compared to -2.0 eV for MgO).

## 3.3 Silicon Carbide (3x2)

The results chapters of this thesis represent attempts to understand and modify Group IV terminated diamond surfaces, both (100) and (111). The unique feature of these terminations are their (3x1) surface symmetry, which has not been observed on any other diamond system. In order to gain an intuition for the likely behaviour of this systems, it is worth considering the most similar previously studied system to C(100)-(3x1):0.667Si, which I believe is the $(3 \times 2)$ reconstruction of cubic silicon carbide.

Much like silicon and diamond, silicon carbide is a semiconductor comprised of Group IV atoms bonded in $sp^3$ arrangement to four neighbours; SiC forms many different polytypes which are stoichiometrically identical but differ by the arrangement of its three equivalent layers, however only one of those (denoted 3C-SiC) has the cubic symmetry of the diamond and silicon. The ideal $(1 \times 1)$ (100) surface of cubic silicon carbide, as cleaved, may present a carbon-rich or silicon-rich face, with two dangling bonds per atom. In real crystals, to lower the surface energy by reducing the dangling bond density, the ideal surface forms a range of reconstructions. The simplest of these is a $(2 \times 1)$ bridge bonded dimer, but SiC is also known to form $c(2 \times 2)$,$c(4 \times 2)$, $(3 \times 2)$, $(5 \times 2)$, $(7 \times 2)$ and $(n \times 2)$ $(n \geq 8)$ reconstructions. [102–104] The $c(2 \times 2)$ surface has been proved to form on the carbon-rich face, while the rest present under various preparation circumstances on the silicon-rich face.

Of these models, the one which should stand out, for the purpose of comparison with our surface of interest, is the $(3 \times 2)$ reconstruction. This surface, which is a silicon rich tetrahedral semiconductor, comprised of silicon atoms bonded to carbon, and possessing a $(3 \times 2)$ surface symmetry is quite obviously worthy of comparison to the silicon terminated diamond.

Given the broad range of silicon carbide reconstructions which can be formed at the (100) surface, it should be queried as to whether the formation of the SiC $(3 \times 2)$ is similar to the formation of the SiTD $(3 \times 1)$. Under the influence of annealing at temperatures >900°C, silicon carbide loses silicon from the surface. Eventually, this will result in the remaining carbon-rich face graphitizing, so in order to combat this, during surface preparation a flux of atomic silicon deposited simultaneously with annealing. The $(3 \times 2)$ surface is the result which has the highest silicon coverage of the reconstructions described above, the most stable and can be reliably prepared by annealing samples at 900°C – 1100°C under a silicon flux as described by several studies. [102, 105–108] Despite this, the atomic structure of the $(3 \times 2)$ surface has

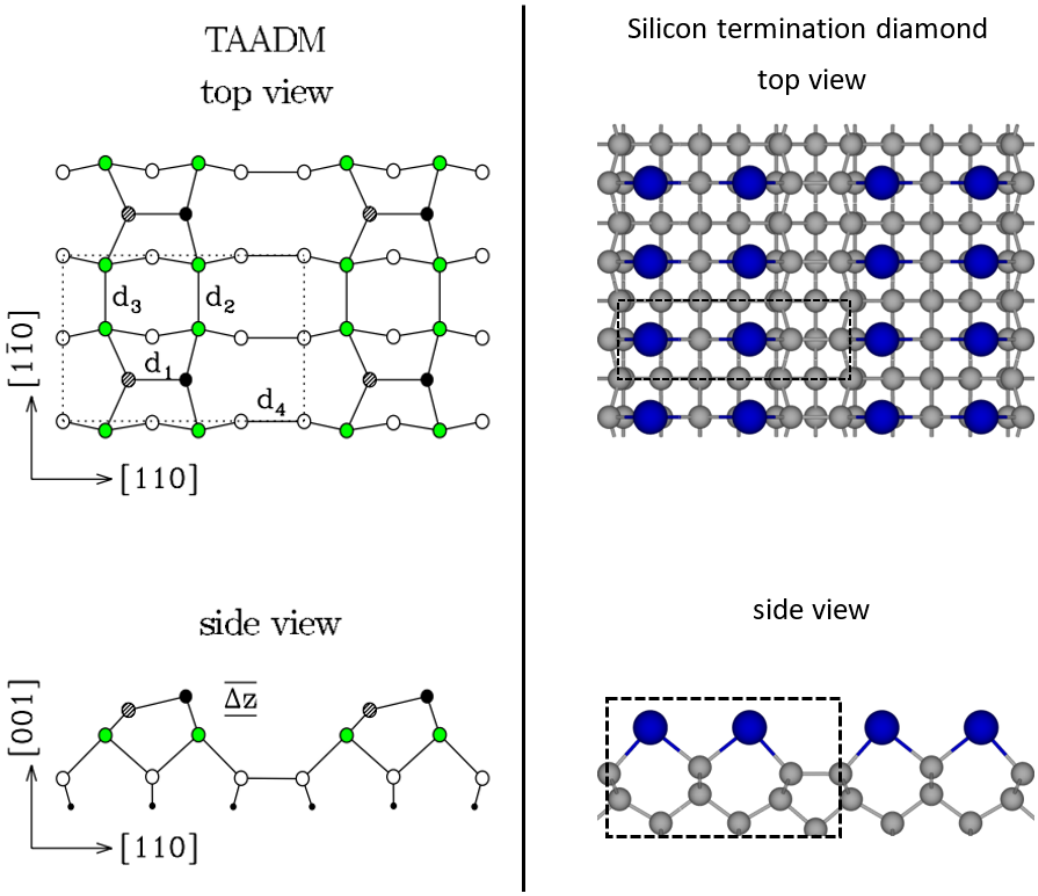


FIGURE 3.19: Left: The two adlayer alternating dimer model of the SiC(100)-$(3 \times 2)$ reconstruction, adapted from Figure 17 in Pollman and Krüger [102], compared with right: our model of the silicon terminated C(100)-$(3 \times 1)$ reconstruction.

been the subject of significant debate, and the now-accepted model has only been confirmed by experimental results recently.

While a variety of atomic arrangements have been proposed, the most agreed upon and current model is denoted the "two-adlayer alternating dimer model" or TAADM; a schematic of this structure is shown in Figure 3.19, with the silicon terminated diamond structure shown for comparison.

The TAADM describes a silicon faced surface of silicon carbide which has three layers. The primitive silicon face atoms (the open circles in Figure 3.19) are each bonded to two carbon atoms in the bulk lattice, this represents one full monolayer, and possess two unsatisfied bonds. On top of this layer, there is two thirds of a monolayer (the yellow circles) which each bridge two of the primitive face silicon atoms, and, themselves, have two dangling bonds. This causes the lower layer to adopt an alternating dimer-monomer (ADM) structure in the [1 1 0] direction, and is the source of the '3x' symmetry. The model further has 1/3ML of excess silicon on top of that layer (the shaded and black atoms) which bridge between two of the 3x cells of the lower layer, and adopt a Jahn-Teller distorted tilt to relieve their

own dangling bonds. The top view further shows that the middle bridging layer is comprised of dimers in the [1 -1 0] direction, which is the source of the x2 part of the symmetry, resulting in the overall $(3 \times 2)$ structure. The total coverage of silicon on this surface is 1 + 2/3 + 1/3 = 2ML. The method of the experimental confirmation of this three-layer structure is not relevant to this thesis, as it derives significantly from grazing incidence x-ray diffraction, and the reader is directed to D'Angelo *et al.* [109] for further details.

To compare this to our proposed model of the silicon terminated diamond surface, I have looked at the similarities and differences between the two structures. The largest similarity is the pair of bridging silicon atoms (SiC, yellow, and SiTD, blue) atop an ADM layer. The most obvious difference is that the lower layer for the SiC cell is silicon, while in diamond it is carbon. The second obvious difference is the lack of a third layer in our SiTD model. Both of these discrepancies are explained by the same feature: the much larger size of the SiC lattice.

The silicon carbide lattice parameter, 4.360Å, is more than 20% larger than the diamond parameter, 3.567 Å. That means that significant distortion is necessary to form C-C dimers on the SiC surface, and in the case where silicon is available, this does not occur. By the same token, the extra compression in the diamond lattice would result in much too high a bond strain for the adlayer silicon to form the ADM structure on diamond. The carbon, on the other hand, is perfectly within range to dimerize on the diamond (100) surface, as indeed it does on the hydrogen and fluorine terminated surfaces.

On the SiC surface, the top layer already alternates between bridge and dimer bond to relieve stress, [109] and possesses an interlayer spacing 50% larger than for bulk silicon carbide; an adsorbed extra layer on SiTD would necessarily be under further stress and be in a further awkward position, so it makes sense that our observations do not comport with the presence of such a layer. Without the presence of the top bridging layer on SiC, the cell reduces from $(3 \times 2)$ to $(3 \times 1)$ symmetry, exactly as we observe on silicon terminated diamond.

The maximum Si-Si dimer distance observed on the SiC$(3 \times 2)$ surface is 2.41Å while the diamond surface cell dimension is 2.52Å. This suggests that dimerization may be possible on SiTD, though we have yet to observe it in any experiment.

## 3.4 Conclusion

I have summarized in this chapter, several surface chemical structures which are relevant for understanding our attempts at modifying the Group IV terminations of the diamond (100) surface.

I have shown that our understanding of the silicon termination in the early part of my PhD came from work lead by Schenk, with which I assisted in developing. The key points which are relevant going forward are that: the silicon termination

is characterized by a $(3 \times 1)$ symmetry which is unique to the system, and by C-Si bonds seen in XPS; that it appears to have dangling bonds which can be further functionalized; and that is has a negative electron affinity, suggesting that it could be transfer doped.

I have summarized the major research avenues in diamond surface chemistry which have been pursued by other groups. This included a short summary of hydrogen and oxygen terminated diamond, which have been well explored in literature, and discussion of salient features of the other major types of terminations which have been explored in literature, namely the nitrogen based terminations, nitride and amine, the halogen based terminations, fluorine and chlorine, and the metal oxide terminations, CsO, LiO and MgO.

Finally, I have described the most closely analogous system to silicon terminated diamond that we have found in literature, the $(3 \times 2)$ reconstruction of silicon carbide. The existence of this surface was the basis of much of my intuition in understanding possible structure and bonding arrangements for the $(3 \times 1)$ diamond surfaces, and lead us to the consideration of SiC surface chemistry as inspiration for our own studies.

With these considerations in mind, I now turn to presenting my own results.

# Chapter 4

# Germanium terminated (100) diamond

## 4.1 Preface

Demonstration of successful silicon termination of the (100) diamond surface by Schenk *et al.* opened a broad range of investigations which could be pursued to adapt and expand upon that structure. A natural avenue to explore is the application of the method of silicon termination to germanium, given that they share a valence and bonding structure, and are similar in size and electronegativity. A germanium terminated surface would offer access to significant sulfur bonding chemistry which is not provided by either diamond or silicon, and would be an appealing platform for biosensing devices, combining the strength and biocompatibility of diamond with the strong and reversible disulfide bond. Bonding germanium to the (100) surface would also show that the deposition-annealing method which was used to produce silicon terminated diamond is applicable to other systems.

This chapter presents the combined results of X-ray Photoelectron Spectroscopy (XPS) and Low Energy Electron Diffraction (LEED) measurements investigating the formation of a germanium terminated diamond surface. While Ge-C bonding and a $(3 \times 1)$ reconstruction was observed at the surface, it was also found that the germanium terminated surface does not form a complete monolayer termination. Despite attempting a number of variants of the original process in an attempt to improve surface wetting and access to active carbon sites, the bonded germanium coverage saturates at approximately 0.63 ML, independent of the preparation method used. This shows that the termination method we have employed (depositing onto hydrogen terminated diamond, followed by annealing) will work to some degree with species other than silicon.

This work has been published in *Journal of Physics: Condensed Matter* 29.14 (2017): 145002 and the article is presented below. No changes have been made to the published work except those required to make the formatting consistent with the rest of this thesis.

## 4.2 Author contribution:

The experimental plan was conceived by Sear and Schenk. Sear, Schenk, Tadich, Spencer, Wright and Stacey performed the experimental work during a beamtime at the Australian Synchroton. The data was analysed by Sear and Schenk. The manuscript was prepared by Sear and Schenk, with feedback and input from Pakes. Sear and Schenk made equal contributions to this body of work.

## 4.3 Germanium terminated (100) diamond

Michael J. Sear[1], Alex K. Schenk[1], Anton Tadich[2,1], Benjamin J. Spencer[1], Christopher A. Wright[1], Alastair Stacey[3], and Chris Pakes[1]

[1)] *Department of Chemistry and Physics, La Trobe Institute for Molecular Sciences, La Trobe University, Victoria 3086, Australia*

[2)] *Australian Synchrotron, 800 Blackburn Road, Clayton, Victoria 3168, Australia*

[3)] *Centre for Quantum Computation and Communication Technology, School of Physics, The University of Melbourne, VIC 3010, Australia*

### 4.3.1 Abstract

An ordered germanium terminated (100) diamond surface has been formed and characterised using a combination of low energy electron diffraction and synchrotron-based core level photoemission spectroscopy. A number of preparation methods are explored, in each case inducing a two domain $(3 \times 1)$ surface reconstruction. The surface becomes saturated with bonded germanium such that each $(3 \times 1)$ unit cell hosts 1.26 Ge atoms on average, and possesses a negative electron affinity of -0.71 eV.

### 4.3.2 Introduction

Functionalised (100) diamond surfaces have long been investigated as a platform for a number of device applications, including high efficiency electron emission sources [45, 110, 111], biosensors [112, 113] and high power, high frequency electronic components such as field effect transistors [113, 114]. The suitability of the diamond surface for such a range of diverse applications stems from the ability to significantly alter the surface properties with a simple change in the terminating species. Due to the wealth of carbon chemistry, there are a number of chemical species which have the potential to be covalently bound to the diamond surface, using a variety of methods. Until recently, this has included only those atomic species which may be formed easily through plasma treatment, harsh chemical or photochemical processing and, of these, only hydrogen and oxygen have been significantly exploited as terminations for device applications. Hydrogen termination results in a two domain $(2 \times 1)$ reconstructed surface which exhibits a negative electron affinity [47], as well as a transfer doping-induced subsurface 2D hole gas [2, 40] which possesses a tunable spin-orbit coupling [3, 115]. The oxygen termination conversely has a positive electron affinity and produces a complete passivation of the surface. However, it has the undesirable property of leading to an uncontrolled combination of oxygen-containing functional groups at the surface and a less ordered structure [47], as most easily shown by low energy electron diffraction(LEED). Given the increasing interest in developing near-surface device architectures in diamond, it is desirable to widen the pool of available terminations, expanding into processing methods which ideally would preserve the high degree of order following a prior hydrogen plasma treatment as well as exhibiting novel chemical and electronic surface properties.

In previous work we have developed a robust silicon termination for the (100) oriented diamond surface [4] and characterised its electronic structure [116]. An interface between a common semiconductor such as silicon and the diamond surface opens up new possibilities for surface-based semiconductor heterojunction devices which rely on the excellent thermal properties of diamond, as well as its optical defects [81] and wide band gap. As an additional benefit, the preparation of a surface termination where the adlayer itself possesses dangling bonds [116] may make it possible to further tune the properties of the surface by attaching molecules to the bonded adlayer. This is particularly beneficial as the termination is prepared from the atomically flat C(100)-$(2 \times 1)$:H surface, and involves no steps which are expected to etch the surface, thereby producing a monolayer termination which is similarly flat but with an engineered chemistry and electronic structure. However, silicon is not the only Group IV semiconductor which has well established chemistry with carbon and it is natural to consider whether other such terminations, which offer alternative properties or functionalisation chemistry, can be prepared. For this work we have chosen germanium as the adlayer. This choice is based on the observation that silicon and germanium have the same valency, a similar covalent radius (1.11 Å for Si vs. 1.20 Å for Ge) [117] and similar Pauling electronegativities (1.9 for Si vs. 2.1 for Ge), suggesting that germanium may similarly bond with the (100) diamond surface. Additionally, the established chemistry between germanium and sulfur [118] may offer a platform for biofunctional diamond devices in future work.

Here we present the results of a number of variations on the preparation of a germanium terminated (100) diamond surface. The results show that it is possible to bond germanium to the (100) diamond surface and that the resulting structure is highly ordered and possesses a two domain $(3 \times 1)$ symmetry. Irrespective of preparation method, the results indicate that the germanium terminated surface is limited to a coverage of 0.63 monolayers (ML). On the basis of our observations, we attribute this to a steric limitation inhibiting the bonding of more germanium above this coverage.

### 4.3.3 Experimental Details

The diamond samples used throughout this study were obtained as electronic grade IIa single crystal (100) oriented diamond substrates from Element Six, upon which a (100) oriented boron doped overlayer was grown, at the Melbourne Center for Nanofabrication (MCN), to prevent charging in the course of measurements. After growth, the samples were hydrogen plasma treated and transferred to a UHV environment for all subsequent measurements.

The experimental work for this study was performed at the Soft X-Ray Spectroscopy (SXR) beamline of the Australian Synchrotron [119]. The UHV endstation is equipped with a SPECS Phoibos 150 Hemispherical Analyser, quartz crystal microbalance (QCM) for monitoring deposition rate, a reverse-optics Low Energy Electron Diffraction (LEED) system for observing the surface reconstruction and a Kelvin

probe (KP Technology) for determining sample work function. Once introduced to the endstation, samples were annealed to 450°C for 30 minutes to remove atmospheric contamination. Sample cleanliness was confirmed using x-ray photoelectron spectroscopy (XPS) prior to further experimental steps. Grazing Incidence (GI) Carbon K-Edge near edge x-ray absorption fine structure spectroscopy (NEXAFS) was used to confirm the presence of the hydrogen terminated surface and LEED was used to confirm a high quality two domain $(2 \times 1)$ reconstruction. Depositions of germanium was performed using a commercial Knudsen effusion cell (MBE Komponenten) containing germanium powder (99.99% purity, Sigma Aldrich) heated to a temperature of 1150°C. The deposition rate was estimated using the QCM and the total Ge coverage for each sample was more accurately determined using photoelectron attenuation measurements of the C1s core level signal from the substrate.

Soft x-ray photoelectron spectroscopy (XPS) measurements of the C1s and Ge3d core levels were performed using photon energies of 350 eV and 100 eV respectively, in order to maximise surface sensitivity. The binding energy (BE) of all spectra were referenced to the Fermi level either by setting the $Au4f_{7/2}$ core level BE to 84.00 eV (C1s spectra) or by monitoring the Fermi edge of a gold foil in electrical contact with the sample (Ge3d spectra). Core level spectra were fitted by symmetric Voigt components with Lorentzian widths of 0.15 eV for C1s [20] and 0.17 eV for Ge3d [120] after applying a Shirley background correction [15]. For the Ge3d core level, the usual restraints were imposed: a spin-orbit splitting of 0.59 eV and a branching ratio of 3:2 [120]. The photon energy resolution of the beamline is estimated to be 10 meV for measurements performed at 100 eV (Ge3d core level), and 34 meV for measurements performed at 350 eV (C1s core level) [119]. Combined with an analyser resolution of 140 meV for a pass energy of 5 eV, the combined instrumental resolution is 140 meV for data acquired at 100 eV, and 144 meV for measurements acquired at 350 eV.

For this study, all samples were initially prepared in an identical hydrogen terminated state. The standard process flow detailed below was used on each sample for the subsequent formation of the Ge terminated surface unless otherwise stated. That preparation involved the deposition, onto the room temperature substrate, of at least 1 ML of germanium. In this work we define 1 ML as 2 Ge atoms per $(3 \times 1)$ unit cell, as seen in our previous Si termination work [4]; this corresponds to an areal Ge density of $1.05 \times 10^{15}$ cm$^{-2}$. This was followed by annealing the sample to 950°C for 20 minutes in order to detach the hydrogen from the surface [121], allowing the Ge to react with the bare carbon atoms, and then leaving the sample to cool to room temperature before characterisation with core level XPS and LEED.

### 4.3.4 Results and Discussion

Figure 4.1(a)-(c) shows the XPS and LEED data acquired for Sample 1 at each stage of the preparation: (a) the clean hydrogen terminated surface, (b) after depositing

[1]Split spots in the half order positions are indicative of surface twinning, a finding which is not expected to influence other results of this study.

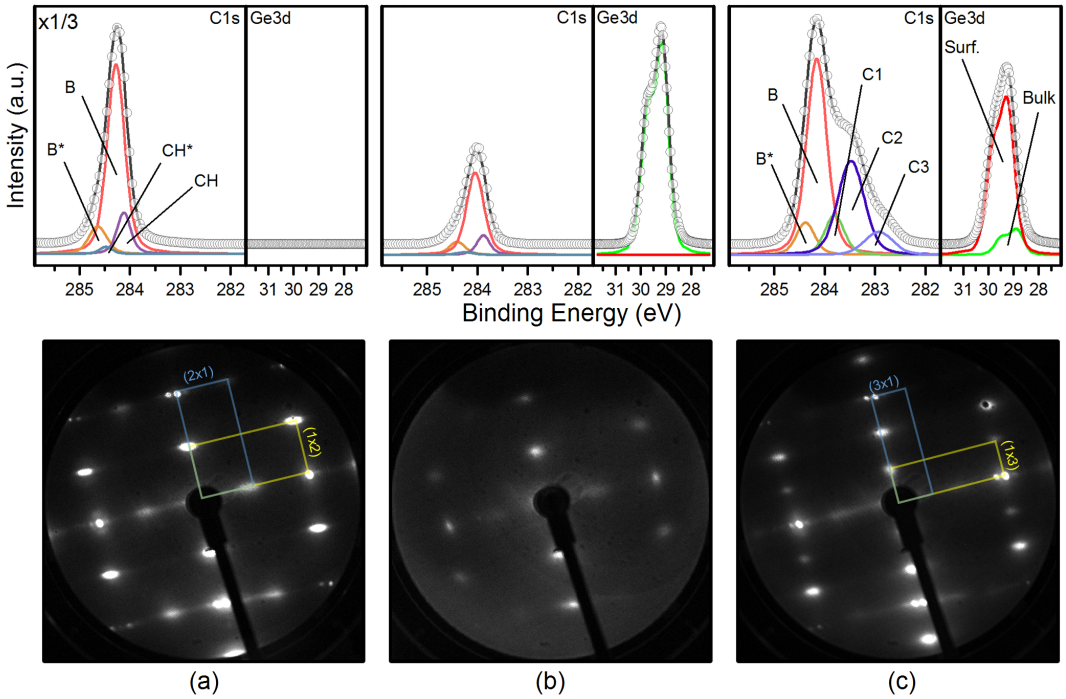


FIGURE 4.1: High resolution C1s (hv=350 eV, left panel) and Ge3d (hv=100 eV, right panel) photoemission spectra for Sample 1 at each processing step, with corresponding LEED patterns[1](70 eV), for (a) C:H, (b) C:H + Ge deposited, (c) C:Ge - 950°C anneal; components have been offset for clarity.

2.49 ML of Ge (an excess was deposited to account for germanium desorption in the subsequent annealing step, this will be discussed in detail below) and (c) after annealing to 950° C.

In Fig. 4.1(a) we see the two domain $(2 \times 1)$ LEED pattern of the hydrogen-terminated (100) diamond surface. The C1s core level for the as-prepared hydrogen terminated surface is as expected from the literature, and importantly no components attributed to surface oxidation are present. The core level has been fitted using the four component model recently proposed by Schenk *et al.* [17], in which bulk diamond is treated with two components, a large component (B) representing the majority of bulk $sp^3$ carbon, and a smaller component to higher BE (B*) which has an intensity equal to 15% of the B component, representing sub-surface carbon atoms experiencing a final-state effect shift [17]. This two-component bulk treatment has been maintained throughout all C1s fits presented here, with only the separation between the B and B* components allowed to vary due to the change in this final-state effect shift with surface termination [116].

Following the addition of the Ge adlayer, Fig. 4.1(b), the LEED pattern maintains the two-domain $(2 \times 1)$ structure seen for the pristine hydrogen-terminated surface, but displays an increase in the background intensity. Comparison of the C1s XPS core level before and after deposition shows that the same four components are still observable after deposition, with no change in the peak structure. As indicated in that figure, the peak intensity is also attenuated to approximately one sixth of the

pre-deposition intensity. As there is no change in the C1s structure or the LEED pattern (other than an increase in background intensity), and the satisfactory fit of the Ge3d core level with a single (doublet) peak, it is apparent that the adlayer is disordered in nature and is not chemically bound to the surface, only physisorbed. This result can be attributed to the passivating nature of the hydrogen termination [122, 123], which limits the chemical interaction between the surface and adlayer.

Annealing *in situ* to 950°C causes the LEED pattern to transition from a two domain $(2 \times 1)$ pattern to a two domain $(3 \times 1)$ pattern, as shown in Fig. 4.1(c). This shows that a significant change in surface reconstruction has been induced by the annealing process. We note that a similar transition was observed in our previous work on the developent of a silicon-terminated (100) diamond surface [4]. Concurrent with the change in symmetry there has been a reduction in the background of the LEED pattern, implying either that the excess germanium on the surface is predominantly ordered, or a significant portion of the excess has been removed by the annealing process. Based on the relative component intensities in our XPS survey scans, it appears that the latter is the case; the as-deposited 2.49 ML was reduced to 0.74 ML by the 950°C anneal.

Examination of the XPS spectra after annealing shows significant change in the C1s core level structure; the annealed surface exhibits three new components to lower binding energy of the bulk C1s, as would be expected to result from bonding germanium, a relatively electropositive element, to the surface. Relative to the bulk, *B*, these components are located at -0.35 eV (*C*1), -0.68 eV (*C*2) and -1.23 eV (*C*3). This spectrum is similar in appearance to the spectrum of the silicon terminated diamond (100) surface [4], although it includes an extra component which the following discussion will expand upon.

As the surface demonstrates a $(3 \times 1)$ symmetry LEED pattern, a physical model for that unit cell is considered here in the context of explaining the XPS data. The proposed unit cell structure contains alternating carbon monomer and dimer units, as shown in Fig. 4.2(a). From the atomic species in the complete unit cell (see Fig. 4.2), it is expected that the C1s core level will contain two surface-related components (attributed to the atoms A and B) in a 2:1 ratio (A:B). We attribute component *C*2 and *C*3 to atomic site A and B respectively on the basis of induction effect [124] arguments and the Pauling electronegativity difference between germanium (2.1) and carbon (2.5), and would therefore expect an approximate intensity ratio of 2:1 between these components if the surface were perfectly terminated with this type of cell [4]. However, as can be seen from Fig. 4.1(c) and the tabulated fitting parameters in the Supplementary Material, the *C*2 peak accounts for 28.3% of the C1s intensity and the *C*3 peak for 7.1%; or a peak intensity ratio of approximately 3.83:1.

This discrepancy between the intensity ratio expected from the model and the measured intensity ratios is attributed to incomplete $(3 \times 1)$ cells, such as the upper structure presented in Fig. 4.2(b). After the 950°C anneal, the Ge coverage was

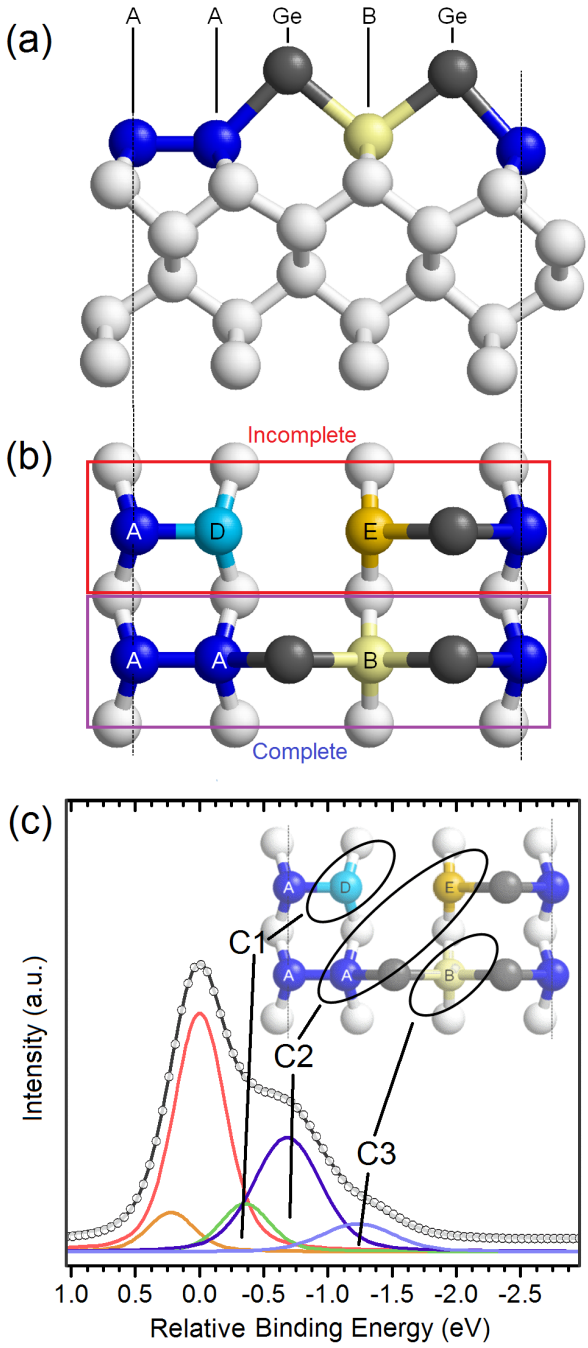


FIGURE 4.2: A schematic diagram of the top-down view, (a), and the side view, (b), of the possible structures of surface unit cells on C(100)-$(3 \times 1)$:Ge, and a visual assignment of the C1s components is shown in (c). The outlined structures in (b) represent the co-existing, but not necessarily adjacent, complete and incomplete $(3 \times 1)$ unit cells. A discussion of these structures is presented in the text.

reduced to 74% of a completely $(3 \times 1)$ terminated layer, which means that a significant portion of the surface is germanium deficient. As such, it is important to consider what influence the resulting unbonded carbon sites might have on the unit cell structure and the measured core level structure. We note that the proposed 'Incomplete' structure shown in Fig. 4.2(b), which would retain a $(3 \times 1)$ symmetry, is not necessarily the only configuration which might form in an incomplete unit cell: Ge adsorption on inter-dimer sites is also a possibility (see Supplementary Material for alternative structures). However, the LEED pattern measured after annealing (Fig. 4.1(c)) is a $(3 \times 1)$ pattern, without any features which would be attributed to co-existing domains of a different symmetry. This suggests that the majority of the incomplete unit cells present at the surface must also have a $(3 \times 1)$ symmetry, indicating a structure which does not differ significantly from that of the complete unit cell. The incomplete unit cell presented in Fig. 4.2(b) fulfils this requirement, and so our discussion is presented in the context of this unit cell, without excluding the possibility that alternative structures exist. Two distinct carbon species, the atoms D and E, arise as a result of the germanium atom missing from the 'Incomplete' structure in the upper panel of Fig. 4.2(b). Based again on the induction effect arguments which we used to attribute A and B to *C*2 and *C*3 respectively, we expect an upward binding energy shift of D and E relative to those positions.

We propose that the *C*1 component of the C1s spectrum is due to D-like atoms. As the upward shift is not restricted to be the same for the two components, this does not imply that component associated with E-like atoms should lie upward of the *C*3 by the same amount as the difference between *C*1 and *C*2. The C1s component associated with E carbon sites may be shifted to the same position as A sites, and incorporated indistinguishably in the *C*2 component, contributing to the width and intensity of that peak. Further, as each E site represents a missing B site, every incomplete cell both subtracts intensity from *C*3 and adds intensity to *C*2. This assignment of atomic species to their corresponding peaks, shown in Fig. 4.2(c), is consistent with an observed intensity ratio in excess of the 2:1 expected from a complete C(100)-$(3 \times 1)$:Ge reconstruction and with the observed sub-monolayer coverage. The existence of the E and D components should also generally increase the degree of surface disorder, likely contributing a broadening effect to the Gaussian widths of all peaks in the spectra.

Turning now to analysis of the Ge3d core level spectrum, only one peak is expected in this region, as both of the surface Ge atoms in the complete unit cell are in the same chemical environment. As the spectrum for that region, Fig. 4.1(c), also contains a small component on the low binding energy side, where a bulk contribution would be expected, we infer that there is some germanium remaining on the surface which has not bonded with the underlying carbon lattice. The relative intensity of these components implies that the actual coverage of germanium bonded to the surface is $0.63 \pm 0.06$ ML. This corresponds to, on average, 1.26 Ge atoms per $(3 \times 1)$ unit cell.

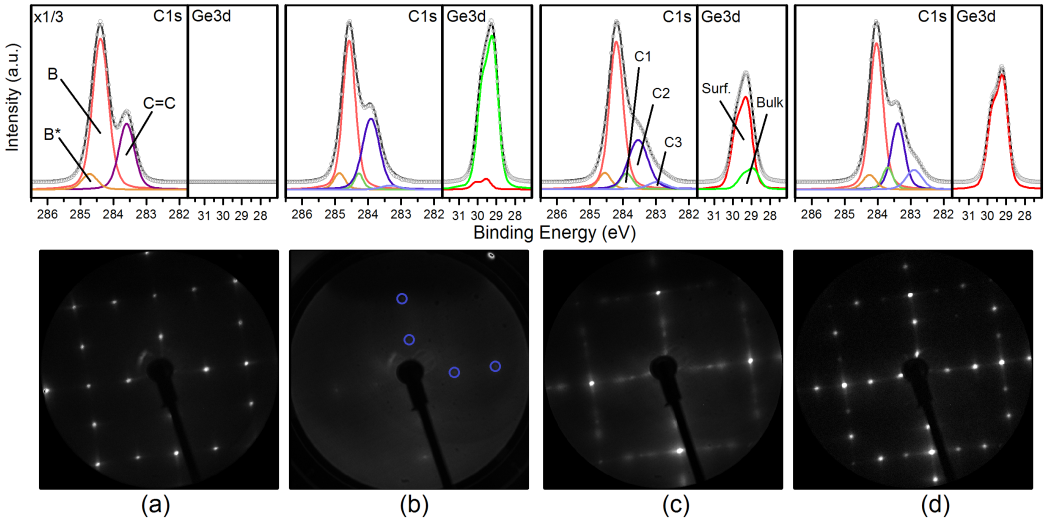


FIGURE 4.3: High resolution C1s (350 eV, left) and Ge3d (100 eV, right) photoemission spectra for Sample 2 at each processing step, with corresponding LEED patterns (70 eV), for (a) the bare (100) diamond surface; (b) after Ge deposition; (c) 500°C anneal, 75 minutes; (d) 950°C anneal, 20 minutes; components are again offset for clarity and a guide to the eye is given in (b)

By combining our photoemission results with Kelvin probe measurements, we are able to calculate the electron affinity $\chi$ of the surface as a result of bonding the germanium to the surface with the 950°C anneal. In order to do so, we rely on the equation $\chi = \Phi_D + (E_F - E_{VBM}) - E_G$ where $\Phi_D$ is the sample work function (WF), $E_F - E_{VBM}$ the separation between the diamond Fermi level and valence band maximum (VBM), and $E_G$ the diamond band gap (5.47 eV). The sample work function is determined from contact potential difference (CPD) measurements performed with Kelvin probe after calibration against a gold reference foil for which the work function was measured using the secondary electron cutoff method. To calculate $E_F - E_{VBM}$ we follow the approach of Maier *et al.* [47], using the binding energy (BE) of the C1s bulk core level component (B) measured using photoemission and the fixed energy separation ($283.9 \pm 0.1$ eV) between the VBM and the C1s core level. The relevant experimentally measured values are presented in Table 4.1. The electron affinity for the surface after the 950°C anneal is found to be -0.71 eV. A negative electron affinity was also seen on the silicon terminated $(3 \times 1)$ surface [116], and the result on this surface is consistent with the similar electronegativity of these elements.

We now consider alternative preparations to determine if higher germanium termination coverages could be prepared. We have shown that the 950°C anneal causes the sample to form a Ge-terminated $(3 \times 1)$ surface. Concurrent with the formation of this surface, a significant percentage of the deposited germanium desorbed from the surface. This may be a result of our anneal temperature (950°C) being close to the melting point of germanium (938.3°C). The balance between these competing processes of bonding-and-reconstruction versus desorption was investigated on a

TABLE 4.1: Summary of measurements used in determining the surface electron affinity for Sample 1 after 950°C anneal

| | |
|---|---|
| Probe WF (eV) | 4.57 |
| Diamond CPD (eV) | -0.05 |
| Diamond WF (eV) | 4.52 |
| Diamond Bulk C1s BE (eV) | 284.14 |
| Diamond $E_F - E_{VBM}$ (eV) | 0.24 |
| Diamond EA (eV) | -0.71 |

second, identically prepared, sample by depositing germanium onto a bare (100) surface, Sample 2. This bare, reconstructed surface, C(100)-$(2 \times 1)$:R, was prepared by annealing in vacuum the hydrogen terminated surface [121] to 950°C and the successful removal of hydrogen was confirmed by NEXAFS spectroscopy. Due to the absence of hydrogen passivation, we infer this surface will have a lower barrier to reactivity [125], and the surface is known to have a higher sticking coefficient than the H-terminated surface, two factors which might both favour the formation of a complete $(3 \times 1)$ surface over the thermal desorption of the Ge adlayer.

Figure 4.3(a) shows the LEED pattern recorded from Sample 2 for the reconstructed hydrogen free surface. Clear, sharp half-order spots are observed, indicating the $(2 \times 1)$ reconstruction caused by the surface carbon dimers. The C1s spectrum for this surface is also shown in that figure, containing the B and B* components, with a single reconstruction related peak at 0.79 eV to lower binding energy of the bulk peak, attributed to $C = C$ bonds [126].

Germanium deposition (2.27 ML) onto this surface results in extremely high background, with low intensity $(2 \times 1)$ spots as shown in Fig. 4.3(b). As with the previous sample, this implies that the deposited germanium is primarily an amorphous adlayer and does not show any indication of spontaneous $(3 \times 1)$ formation.

Contrasting with the previous case where hydrogen passivation prevented bonding, Ge deposition induced a change in the C1s from the bare surface, even without annealing. We are able to fit this spectrum using the component regime applied to Sample 1. The $C2$:$C3$ ratio is approximately 9.4:1 for this spectrum. The LEED pattern indicates that the surface still exhibits $(2 \times 1)$ symmetry, therefore the peak here labelled $C2$ likely includes a contribution from $C = C$ environment carbon atoms. While the small chemical shifts of all the possible components prevent the selection of a unique set of fitting parameters (and thus prevent a unique decomposition of the $C2$ component to account for the different environments), the sample is clearly far from the 2:1 ratio expected from a complete C(100)-$(3 \times 1)$:Ge reconstruction. The presence of $C = C$ intensity is reinforced by the Ge3d core level analysis, which indicates that only 5% (0.11 ML) of the adsorbed germanium is bonded to the surface. This value does not account for the effects of photoelectron attenuation, however this is unlikely to increase this value to more than 10% (0.22 ML).

It is worth emphasising that, based on the data in Fig. 4.3(b), while carbon-germanium bonds may form spontaneously on the (100) diamond surface, the $(3 \times$

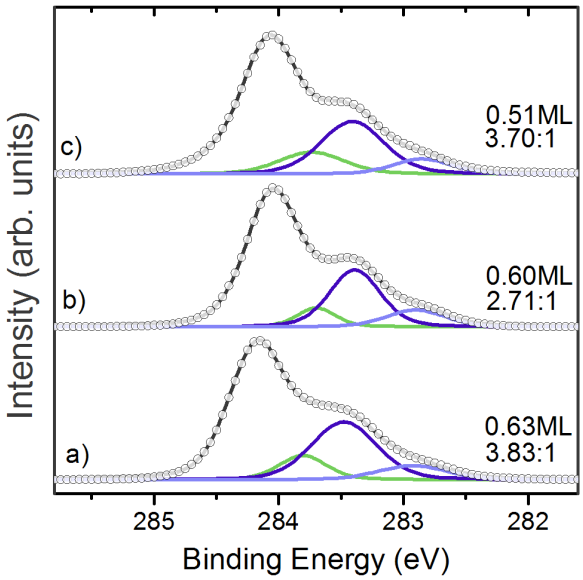


FIGURE 4.4: C1s spectra for 950°C annealed samples (bulk components omitted); (a) Sample 1, (b) Sample 2, (c) the low initial coverage sample; the corresponding germanium coverage and the C2:C3 ratio for each sample is included to the right of each spectrum.

$1)$ unit cell does not. The C3 component in the C1s spectrum is associated with B-type atomic sites which may only form by breaking the pre-existing dimers of the $(2 \times 1)$ unit cell, to form an additional carbon-germanium bond when compared to the A or E sites. This indicates that, at room temperature, bond scission is energetically unfavourable but it may be possible to increase the density of B sites through thermal activation.

Figures 4.3(c) and (d) show the LEED and XPS core level data after subsequently annealing Sample 2 to 500°C and 950°C respectively. The anneal at 500°C for 75 minutes resulted in the data seen in Figure 4.3(c). The LEED pattern has prominent $(2 \times 1)$ half-order spots, but in addition has developed $(3 \times 1)$ one-third-order spots, suggesting partial reconstruction at this temperature. From this we infer that the surface is comprised of co-existing $(2 \times 1)$ and $(3 \times 1)$ domains. The associated XPS data shows that the coverage after this anneal has reduced from the deposited 2.27 ML to 0.75ML. The Ge3d core level spectrum has also changed to be 81% comprised of the bonded-type germanium, implying a bonded Ge coverage of 0.61ML. This is a significant change in both the bonded and unbonded germanium coverages after this low temperature anneal, and the observed C1s structure reflects these changes.

The same model was used to fit the C1s core level as on Sample 1. While the peak positions remained the same (and the $C1$ peak was still present), the $C2$:$C3$ ratio has reduced to 5.4:1. This is closer to the 2:1 ratio of a complete layer than was seen after spontaneous bond formation from deposition (a confirmation of the connection between the developing $(3 \times 1)$ unit cell structure and the presence of the $C3$ peak in the core level structure) but it is still significantly deviant from that

ideal ratio. The presence of the $C1$ peak and the sub-monolayer coverage indicate that there remains a significant proportion of incomplete cells on the surface, but most of the remaining germanium is bonded to surface carbon.

The broadness of the $(3 \times 1)$ spots in the LEED pattern suggests that either the regions reconstructed to that state are small (domain size on the order of the 10 nm coherence length of LEED imaging), or that the $(3 \times 1)$ unit cells have some variance in size. Intermediate-state or $(2 \times 1)$ cells adjacent to $(3 \times 1)$ reconstructed cells will change the geometry of those reconstructed cells from their complete-monolayer equilibrium positions; this would explain a variation in the unit cell dimension.

After annealing to 950°C for 20 minutes, the resulting LEED pattern (Fig 4.3(d)) showed a complete extinction of the $(2 \times 1)$ half-order spots, much sharper $(3 \times 1)$ spots, and a signal-to-background ratio on the order of that seen before deposition. This demonstrates, by measure of LEED at least, the most coherent, homogenous, fully reconstructed surface seen for this termination. The complete removal of $(2 \times 1)$ spots from the LEED pattern suggests that most of the C=C surface dimers have been converted to full or incomplete $(3 \times 1)$ surface unit cells.

From analysis of the XPS spectra, the impact of further annealing on the coverage of germanium was found to be minimal: from 0.75 ML (0.61 ML bonded) after the 500°C anneal it was reduced only to 0.60 ML, all of the bonded type. This further implies that only 60-70% of a monolayer readily bonds to the surface.

The C1s spectrum (Fig. 4.3(d)) was fit by the same regime as all previous steps. The smaller Gaussian width of the $C2$ peak relative to the 500°C anneal (see tabulated fitting parameters in Supplementary data for exact values) is consistent with the reduction of $C = C$ species intensity. The $C3$ intensity was found to increase after the anneal, consistent with a higher relative density of B-type sites as the surface reconstructs to $(3 \times 1)$ cells, a finding supported by change in the measured $C2$:$C3$ intensity ratio to 2.71:1.

Having demonstrated that two simple methods do not produce a complete monolayer coverage, further samples were prepared in an attempt to improve the final coverage while retaining the same reconstruction. A sample with a larger initial coverage resulted in 0.63 ML with C2:C3 ratio 4.51:1; a second deposition (to 12.6 ML total coverage) and anneal cycle on the same sample resulted in 0.55 ML (C2:C3 = 4.86:1); and depositing onto a surface at elevated temperature, to improve wetting, resulted in 0.58ML (2.63:1). These three variations all failed to increase the final coverage beyond about 60% of a monolayer, which implies a limit to the achievable coverage of the germanium terminated surface.

To confirm that the limiting factor for Ge coverage is not the germanium desorption rate, a H-terminated sample was prepared with an initial coverage of 0.56 ML and annealed for 20 minutes at 950°C, resulting in a final coverage of 0.51 ML (3.70:1, Fig. 4.4(c)). This suggests that the limiting factor in final coverage is not rooted in desorption kinetics. A possible explanation is that the atomic size of germanium or interactions between germanium atoms create a steric barrier [127] to the formation

of a complete monolayer, or that the complete unit cells contribute to surface strain which is relieved by the formation of incomplete cells. These effects would create a scenario in which Ge cannot bond to the surface in a sufficient density to form a termination comprised uniquely of complete $(3 \times 1)$ unit cells (see Fig. 4.2(b)). Density Functional Theory (DFT) modelling or Scanning Tunneling Microscopy (STM) measurements would be required to confirm these effects.

Finally, comments are made here about the possible bonding arrangement of the germanium adatoms bonded to the surface. As per the C(100):Si-$(3 \times 1)$ structure model [4, 116], the adatoms are bonded to two surface carbons, and have two unsatisfied dangling bonds. Alternatively, in the case of Ge, they may be satisfied by bonding to germanium atoms in adjacent cells; this distance is about 2.5 Å, close to the bulk Ge-Ge bond length of 2.449 Å [128], although the bond angles would not be ideal. If a desire to satisfy bonding is dominant, an induced angular strain could be a driver for an asymmetric buckled dimer surface. Buckled dimer structures have been observed on $(2 \times 1)$ bulk silicon and germanium surfaces, leading to $p(2 \times 2)$ and $c(4 \times 2)$ reconstructions [129]. The observed LEED pattern does not reflect the formation of such structures over extended domains. Previous terminations for diamond using adatoms capable of forming multiple bonds, such as nitrogen [52], have shown it is possible for such adatoms to displace carbon and thus form carbon-adatom dimers bound to the surface. We discount such a possibility in the case of germanium termination as the conditions which we use for inducing the reaction between germanium and the carbon lattice are not expected to produce surface etching. In contrast, nitrogen termination is accomplished by exposure to nitrogen plasma, which etches the surface, and it is this etching which is the driving force behind forming carbon vacancies and thus allowing carbon-adatom dimer formation in these systems. We intend to investigate the precise structure of this surface by STM, which could usefully illustrate the formation of different bond configurations locally.

### 4.3.5 Conclusion

This paper presents data demonstrating the ability to prepare a germanium-terminated (100) diamond surface using a number of preparation methods which all appear to produce minor variations of the same surface structure. The surface demonstrates a negative electron affinity of $-0.71$ eV, and can form a sharp $(3 \times 1)$ LEED pattern. Photoelectron spectroscopy shows that the surface does not form a complete monolayer termination, maximizing coverage at 0.63 ML. We have proposed a model for the surface which includes both completely and incompletely germanium terminated cells.

### 4.3.6 Acknowledgements

This research was undertaken on the Soft X-ray Spectroscopy beamline at the Australian Synchrotron, Victoria, Australia. This work was performed in part at the Melbourne Centre for Nanofabrication (MCN) in the Victorian Node of the Australian National Fabrication Facility (ANFF). MJS and AKS contributed equally to this work.

# Chapter 5

# P-type surface transfer doping of oxidized silicon terminated (100) diamond

## 5.1 Preface

One of the most unique and remarkable features of the hydrogen terminated surface is its negative electron affinity, stemming from the surface dipole formed by the relative electronegativities of carbon and hydrogen. The band alignment associated with the H-terminated diamond is the property which allows diamond to undergo surface transfer doping, and thus form a near-surface hole accumulation layer. While other diamond surfaces such as the LiO termination produced by O'Donnell et al. (*Adv. Funct. Mater.* **2013**, *23*, 5608–5614) have shown a negative electron affinity, even one much stronger than that of HTD, no other diamond surface has, to date, shown the ability to be transfer doped. Having previously shown a low negative electron affinity on oxidized silicon terminated diamond surface, it is worth determining whether transfer doping can be induced with the high electron affinity transition metal oxide $MoO_3$ to show that the Group IV termination family can yield technologically valuable functionality.

This chapter presents the combined results of x-ray photoelectron spectroscopy and contact potential difference measurements of sample work function, in order to determine the effect of gradually increasing doses of an electron accepting molecule. With these results, we show that a reduction in Fermi level to valence band maximum occurs as the areal concentration of $MoO_3$ increases: a signature of surface band bending and the formation of a hole accumulation layer.

This work has been published in *Applied Physics Letters* **110**, 011605 (2017) and the article is presented below. No changes have been made to the published work except those required to make the formatting consistent with the rest of this thesis.

## 5.2 Author Contribution:

The experimental plan was conceived by Sear, Schenk, Pakes and Tadich. Sear, Schenk, Stacey, Tadich and Pakes performed the experimental work during a beam-time at the Australian Synchrotron. The data was analysed by Sear and Schenk. Sear and Schenk made equal contributions in the preparation of this manuscript.

## 5.3 P-type surface transfer doping of oxidized silicon terminated (100) diamond

Michael J. Sear[1], Alex K. Schenk[1], Anton Tadich[2,1], Alastair Stacey[3,4], and Chris Pakes[1]

[1)] *Department of Chemistry and Physics, La Trobe Institute for Molecular Sciences, La Trobe University, Victoria 3086, Australia*

[2)] *Australian Synchrotron, 800 Blackburn Road, Clayton, Victoria 3168, Australia*

[3)] *School of Physics, The University of Melbourne, VIC 3010, Australia*

[4)] *Melbourne Centre for Nanofabrication, 151 Wellington Road, Clayton, VIC 3186, Australia*

### 5.3.1 Abstract

High-resolution core-level photoemission was used to examine the interaction between the oxidised silicon-terminated diamond (100) surface and the molecular acceptor $MoO_3$. An observed downward shift in the Fermi level position, accompanied by the appearance of two distinct charge states of $MoO_3$, indicates charge transfer from the surface into the $MoO_3$ adlayer in the form of surface transfer doping with an concurrent accumulation of holes in the diamond.

Diamond is considered an attractive platform for next generation electronics.[130] This is due to the high breakdown field, high thermal conductivity and wide band gap of diamond, as well as the two dimensional hole gas (2DHG) with strong spin splitting which may be formed at the hydrogen terminated diamond (100) surface[3, 115] through surface transfer doping using atmosphere exposure[2] or electron acceptor molecules such as $C_{60}F_{48}$,[40] $F_4$-TCNQ[41], $MoO_3$[44, 131] and other metal oxides.[43, 132] That the surface is hydrogen terminated is important for a number of reasons. The charge transfer is driven by the energy level alignment between the diamond surface and the acceptor layer, and so relies on the low ionisation potential (4.2 eV) of the H-terminated diamond surface and the high electron affinity (EA) of the acceptor molecule. This places the molecule LUMO beneath the occupied states of the diamond, resulting in spontaneous charge transfer from the diamond into the acceptor layer. The hydrogen terminated (100) diamond surface is chemically homogeneous with atomically smooth terraces. This, along with the chemically passivated nature of the hydrogen terminated surface reduces carrier scattering and improves the spin lifetime, important aspects to consider for exploitation of the 2DHG.

We have recently demonstrated terminations for the (100) diamond surface based upon Group IV elements–specifically silicon [4, 18] and germanium–as the terminating species. These surfaces are chemically homogeneous, possess atomically smooth terraces and have been shown to possess dangling bonds[18] which offer the potential to further tune the surface properties by using the Group IV termination as a bridging layer to bond other chemical species to the diamond surface. We have shown that the oxidised silicon terminated (100) surface possesses a high degree

of order as well as a low EA and so a low ionisation potential.[133] The electronic and adhesion properties such a silica-based termination offers for device fabrication make doping this surface an interesting field of study.

In this article we show the possibility of doping the oxidised silicon terminated (100) diamond surface using molybdenum trioxide ($MoO_3$). We observe both charged and uncharged $MoO_3$ molecules at the surface and the diamond Fermi level moving closer to the valence band maximum, results which indicate molecule-induced p-type surface transfer doping[40, 134, 135] in this system.

Experiments were performed using a single crystal (100) IIa diamond substrate (Element Six). An electrically conductive, 500 nm thick boron doped overlayer was grown onto this substrate using chemical vapor deposition to allow photoemission experiments to be carried out without charging. The thickness of this adlayer is much greater than the length scale which we may probe with photoemission and the length scale of the band bending in diamond due to surface transfer doping. The sample was H-terminated in a microwave hydrogen plasma for 10 minutes at 150 Torr, with the sample maintained at a temperature of 800°C, following growth.[33] All subsequent preparations and measurements were carried out under UHV conditions at the Soft X-ray Spectroscopy beamline of the Australian Synchrotron. The endstation is equipped with a SPECS Phoibos 150 Hemispherical Analyser, quartz crystal monitor for deposition rate calibration, a reverse-optics Low Energy Electron Diffraction (LEED) system for determining surface reconstruction and a Kelvin probe (KT Technology) for monitoring sample work function. The sample was mounted within a Ta envelope on a sample holder with an underlying e-beam heater and K-type thermocouple in direct contact with the sample envelope. An optical pyrometer was used to confirm the sample temperature during annealing.

After introduction to the UHV endstation, the hydrogen-terminated sample was annealed at 450°C for 45 minutes to remove atmospheric contaminants and then allowed to cool. The oxidised silicon-terminated (100) surface was prepared following the process developed in previous work.[133] First, a pristine silicon terminated surface is prepared by depositing 1 ML of silicon onto the clean H-terminated surface, followed by annealing to 950°C for 20 minutes. After cooling, the sample was oxidised by removing it from the UHV endstation and exposing it to ambient conditions for 10 minutes, after which it was re-introduced to the endstation and again annealed to 450°C for 45 minutes in order to remove atmospheric contamination. This treatment yields a high quality surface with a predominant peroxy oxygen termination and a regular $(3 \times 1)$ reconstruction.[133] The preparation was confirmed using x-ray photoelectron spectroscopy and LEED at each stage of the process. $MoO_3$ (Strem Chemicals, 99.999% purity) was deposited *in situ*, without breaking vacuum after the 450°C anneal, using a Knudsen effusion cell (MBE Komponenten) set to a temperature of 525°C. The sample was measured at pressures below $5 \times 10^{-10}$ mbar, and all *in situ* sample preparation was carried out at pressures less than $5 \times 10^{-9}$ mbar.

Core level spectra were analysed with OriginPro 8.6, using the Shirley background[15] and a Voigt lineshape for each component. Lorentzian widths of 0.15 eV,[20] 0.055 eV[136] and 0.20 eV[134] were used for the C1s, Si2p and Mo3d core levels respectively. For the doublet core levels the usual constraints were applied; a spin-orbit splitting of $0.59 \pm 0.02$ eV ($3.17 \pm 0.02$ eV) and a branching ratio of 2:1 (3:2) for the Si2p (Mo3d) core level.[134, 136] The binding energy (BE) scale of all XPS spectra are referenced to the Fermi level by measuring the $Au4f_{7/2}$ core-level of a gold foil in electrical contact with the sample and setting this to a BE of 84.00 eV.

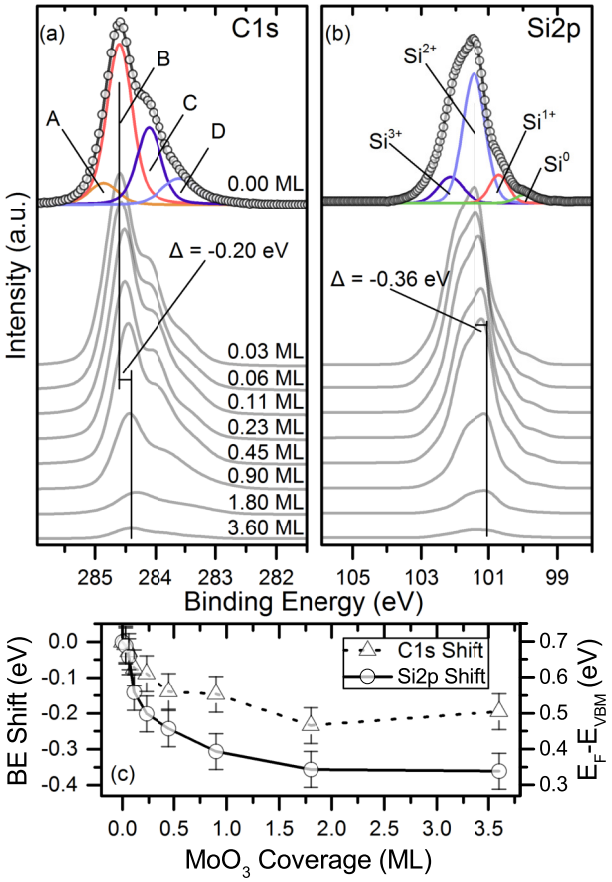


FIGURE 5.1: Details of the C1s ($\hbar\omega = 350$ eV) and Si2p ($\hbar\omega = 150$ eV) core levels acquired at each $MoO_3$ coverage. (a) and (b) show the fitting models applied to the C1s and Si2p core level respectively (only the [illegible] component is displayed for clarity), (c) shows the shift of the core levels as a function of $MoO_3$ coverage and the position of the Fermi level relative to the diamond valence band maximum, based on the C1s position.[47]

Figure 5.1 shows the C1s (a) and Si2p (b) core levels acquired at each $MoO_3$ coverage in this study. Following the model established in previous works[133], the C1s region is fit with four components, two associated with bulk carbon (A, B) and two surface related components (C, D) which appear in a 2.2:1 intensity ratio. The origin of these components is discussed in detail elsewhere[133], but in short, the surface components represent the two carbon environments present in the surface unit cell. For the Si2p spectra, the $Si^{2+}$ environment is the majority species at this surface, and

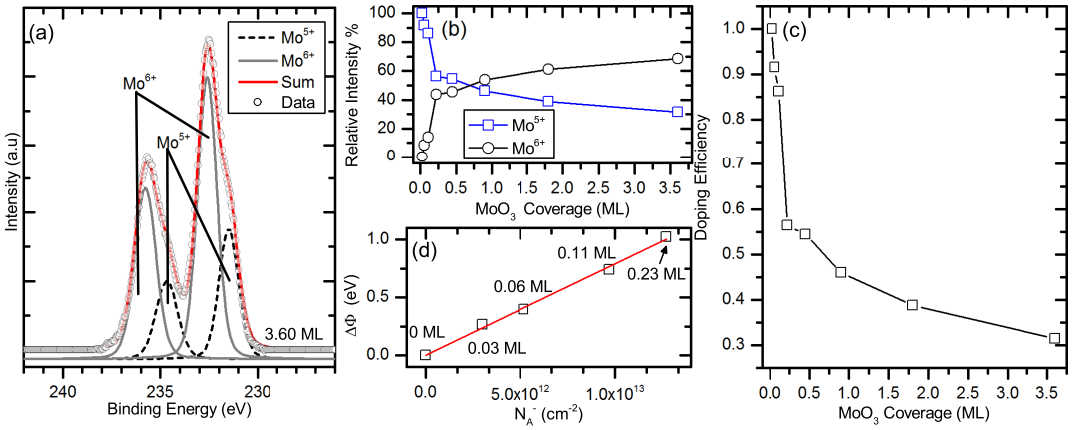


FIGURE 5.2: Details of the Mo3d core level ($\hbar\omega = 350$ eV) and derived parameters as a function of $MoO_3$ coverage. (a) shows the fitting model applied to each spectra in this series, (b) shows the intensity of the $Mo^{5+}$ (blue squares) and $Mo^{6+}$ (black circles), relative to the total Mo3d core level intensity, at each coverage, (c) the $MoO_3$ doping efficiency as a function of coverage, and (d) the change in surface dipole potential with increased charged molecule areal density.

the lower oxidation states are the result of a minority of the surface silicon which has not been completely oxidised in the treatment.[133] The $Si^{3+}$ environment is attributed to a small amount of excess silicon which has oxidised.[133] The C1s and Si2p core level structures are unchanged as a result of $MoO_3$ deposition, indicating that the adlayer does not alter the surface chemistry, as expected due to the passivating nature of the oxide layer. However, a shift in both the C1s and Si2p core levels to lower binding energy with increased $MoO_3$ coverage is observed. The shifts, presented in Fig. 5.1 (c), are calculated based on the position of the largest component in each spectrum (C1s: B, Si2p: $Si^{2+}$). A shift to lower binding energy is expected in a system where p-type transfer doping is occurring,[40] although we note that the Si2p core level shifts further than the C1s. We will return to this point later.

Given that the direction of the core level shifts is consistent with p-type transfer doping, we turn our attention to the Mo3d core level. Figure 5.2(a) shows the fitting model which has been applied to each spectra acquired in this series. Two doublets are required to fit the data, separated by $1.16 \pm 0.05$ eV. Greiner *et al.*[137] found the same seperation between the $Mo^{6+}$ and $Mo^{5+}$ states for $MoO_3$ (neutral and negatively charged $MoO_3$ molecules respectively) when depositing $MoO_3$ films on Mo substrates. The observation of both charged and neutral molecules, concurrently with no chemical modification of the surface, are a signature of surface transfer doping. Figure 5.2(b) contains the intensity (relative to the total Mo3d intensity) of these two doublets as a function of coverage. Initially the $Mo^{5+}$ doublet is the larger of the two, but as the coverage increases the $Mo^{6+}$ doublet begins to dominate the spectra. This behaviour is consistent with that of molecular acceptors on H-terminated diamond.[40, 44, 135] We are able to plot the doping efficiency

(Fig. 5.2(c)) $\eta = N_A^- / (N_A^- + N_A^0)$ as a function of coverage, where $N_A^-$ is the intensity of the $Mo^{5+}$ (negatively charged $MoO_3$) component and $N_A^0$ is the intensity of the $Mo^{6+}$ (neutral $MoO_3$). The doping efficiency has an initial value of 1 and then proceeds to decrease rapidly as additional $MoO_3$ is deposited. From the change in work function $\Delta$WF (measured via Kelvin probe) and the change in the Fermi level position relative to the diamond valence band maximum $\Delta(E_F - E_{VBM})$ determined from our photoemission measurements,[47] we are able to calculate the change in dipole potential $\Delta\Phi = \Delta WF - (E_F - E_{VBM})$ at the surface as a result of charge transfer. This calculation is only valid for low coverages, as the work function measured via Kelvin probe will begin to reflect the work function of the adlayer as the coverage approaches 1 ML. By assuming that one monolayer of $MoO_3$ is $1 \times 10^{14}$ $cm^{-2}$ molecules[134], the relative intensity of the $Mo^{5+}$ component can be used to calculate the areal density of charged molecules; a plot of the change in dipole potential as a function of the charged molecule areal density is shown in Fig. 5.2(d) in the low coverage regime. As the areal density of $Mo^{5+}$ $MoO_3$ molecules increases (ie as charge transfers from the surface), $\Delta\Phi$ increases. This changes the energy alignment at the interface, leading to the decreased doping efficiency at higher $MoO_3$ coverages. There is a linear correlation between $\Delta\Phi$ and the areal density of charged molecules, further evidence that we are observing charge transfer doping.[40, 134]

Finally, we turn to consider the energy level alignment at the diamond-$MoO_3$ interface, which dictates the charge transfer dynamics. Figure 5.3 shows a schematic diagram of the diamond-$MoO_3$ interface, based on the measurements we have presented here and values found in the literature; we have aligned each component using the vacuum level as the common origin. As was done by Xue *et al.*,[138] Figure 5.3 presents a band model which estimates the silicon oxide layer as a thin barrier with the band structure of bulk $SiO_2$, interstitially positioned between the diamond and the $MoO_3$ layer. We may calculate an "acceptor energy" for $MoO_3$ based on the condensed phase EA for neutral $MoO_3$ (6.7 eV).[137, 139] The acceptor energy $\Delta_0$, defined as $E_{VBM} - E_{LUMO}$, is $-1.16$ eV. It is useful to compare this scenario with $C_{60}F_{48}$ on hydrogen terminated diamond, for which the acceptor energy is lower in magnitude (-0.6 eV),[40] and so less charge transfer would be expected. In the present work $E_F - E_{VBM}$ has decreased by 0.2 eV at 3.6 ML coverage, a smaller change than that observed for $C_{60}F_{48}$ on hydrogen terminated diamond where at 1 ML coverage $E_F - E_{VBM}$ has decreased by 0.64 eV.[40] The smaller $\Delta(E_F - E_{VBM})$ observed here implies that the achievable hole sheet density in this diamond in the present case is lower than that for $C_{60}F_{48}$ on H-terminated diamond, contrary to what one may expect based on the calculated acceptor energy. It is interesting to note that the dipole potential has increased by 1 eV at 0.45 ML in this work (Fig. 5.2), a substantially larger increase than is the case for $C_{60}F_{48}$ on diamond where the dipole potential plateaus at approximately 0.45 eV. This may be a contributing factor to the inferred lower hole sheet density, causing the doping efficiency to decrease faster than is the case for $C_{60}F_{48}$ on hydrogen terminated diamond.

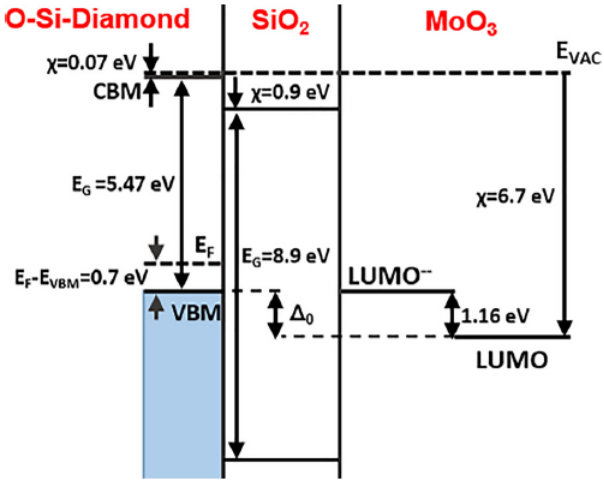


FIGURE 5.3: A schematic energy level diagram of the interface between the oxidised silicon terminated diamond and the $MoO_3$ LUMO.

However, it is important to consider that the interface in this work is more complex than in previous transfer doping investigations on diamond. The oxidised termination is in essence a bound silicon oxide monolayer which may complicate the process of charge transfer. The work of O'Donnell *et al.* saw no change in $E_F - E_{VBM}$, and thus no doping, when exposing the negative electron affinity MgO-terminated diamond surface to atmospheric conditions.[45] This was attributed to a high density of occupied surface states preventing the formation of an accumulation layer within the diamond. Such charge trapping would not play a dominant role in the present work, where the Fermi level has shifted closer to the valence band by 0.2 eV. We note that the Si2p core level also shifted to lower binding energy by 0.35 eV. This may indicate electron depletion has occurred within the oxidised silicon layer as well as in the diamond. Similar behaviour is seen in a molecular heterojunction on H-terminated diamond,[135] using zinc tetraphenylporphyrin (ZnTPP) as an intralayer between hydrogen terminated diamond and $C_{60}F_{48}$, where hole accumulation was observed both in the diamond and the ZnTPP layer. Our energy level diagram does not take into account surface states which form as a result of the termination, rather treating the ultrathin silicon oxide layer as a seperate layer in the system. Ultrathin silicon oxide layers have been explored on other systems in the past, notably on bulk silicon by Xue *et al.*[138], and it has been observed that the oxide layer provides a potential barrier which may be penetrated by silicon 'bulk' orbitals. Whether this is true for the surface states of diamond, and how the presence of this barrier effects the creation of a hole accumulation layer, is a question not easily addressed based on the current understanding of transfer doping.

The effects of depositing $MoO_3$ onto a silica-based terminated (100) diamond surface were explored using high resolution core level photoelectron spectroscopy and

Kelvin probe. A shift to lower binding energy for both the C1s and Si2p core levels was observed, along with the presence of negatively charged and neutral $MoO_3$ molecules, from which we infer that a hole accumulation layer has formed in response to dosing with the acceptor adlayer, with a proportion of the holes residing in the diamond layer and the rest in the silicon layer. Further electrical characterisation is required to verify the presence of surface conductivity, however the observation of subsurface band bending is promising. The hydrogen and oxidised silicon terminated surfaces both offer the desired atomically smooth and chemically passivated platform for surface-based electronic devices. However, the oxidised silicon-terminated surface presents potential for such systems. The dangling bonds which the pristine silicon-terminated diamond surface possesses open up the possibility of more targeted band engineering at the surface, while the silicon-based terminations will offer different adhesion properties when compared to the H-terminated surface which may favour device fabrication.

**Acknowledgements**

This research was undertaken on the Soft X-ray Spectroscopy beamline at the Australian Synchrotron, Victoria, Australia. This work was performed in part at the Melbourne Centre for Nanofabrication (MCN) in the Victorian Node of the Australian National Fabrication Facility (ANFF). MJS and AKS contributed equally to this work.

# Chapter 6

# Thermal stability and oxidation of Group IV terminated diamond surfaces

## 6.1 Preface

Chapter 3 of this thesis details a range of diamond surface termination procedures using elements other than hydrogen and oxygen. While many of these works intend to produce surfaces which are suitable for device development, few studies address in depth the practical concerns which limit their use in real life. The Group IV termination family involve preparation at temperatures sufficient to remove hydrogen, and the silicon termination produces a natural oxygen passivation layer when exposed to atmosphere. If these surfaces are to ever be used, it is important to understand how resilient they are to thermal and oxidative conditions.

This chapter presents the results of combined x-ray photoelectron spectroscopy, low energy electron diffraction, and contact potential difference measurements in order to show that the silicon and germanium terminations are stable to a significantly higher temperature of annealing than hydrogen or oxygen terminations, to show that the germanium terminated surface may be oxidized, and to investigate the stability of the oxidized SiTD and GeTD surfaces. Critically, we also demonstrate that both terminations provide a stabilizing effect on the surface, allowing the surface to be annealed above the point at which the bare surface graphitizes in vacuum. This strongly suggests that the GIVTF may be technologically useful for applications which involve thermal dopant activation in diamond, such as NV- center devices.

This work has been published in *Physica Status Solidi A* **2018**, *215*, 1800283 and the article is presented below. No changes have been made to the published work except those required to make the formatting consistent with the rest of this thesis.

## 6.2 Author Contribution:

The experimental plan was conceived by Sear. Sear, Schenk, Stacey, Tadich and Pakes performed the experimental work during several beamtimes at the Australian

Synchrotron. The data was analysed by Sear. The manuscript was prepared by Sear, after consultations with Schenk and Pakes.

## 6.3 Thermal stability and oxidation of Group IV terminated diamond surfaces

Michael J. Sear[1], Alex K. Schenk[2],1, Anton Tadich[3,1], Alastair Stacey[4,5], and Chris Pakes[1]

[1)] *Department of Chemistry and Physics, La Trobe Institute for Molecular Sciences, La Trobe University, Victoria 3086, Australia*

[2)] *Center for Quantum Spintronics, Department of Physics, Norwegian University of Science and Technology, NO-7491 Trondheim, Norway*

[3)] *Australian Synchrotron, 800 Blackburn Road, Clayton, Victoria 3168, Australia*

[4)] *School of Physics, The University of Melbourne, VIC 3010, Australia*

[5)] *Melbourne Centre for Nanofabrication, 151 Wellington Road, Clayton, VIC 3186, Australia*

### 6.3.1 Abstract

High resolution x-ray photoelectron spectroscopy was used to explore the thermal stability of as-prepared and oxidised silicon and germanium-terminated (100) diamond surfaces which form two domain $(3 \times 1)$ surface reconstructions. The as-prepared germanium and silicon-terminated surfaces are stable up to 1200°C, making them the most thermally stable surface termination for diamond (100). The oxidised forms of these surfaces can be created via exposure to $O_2$, $H_2O$ or atmospheric conditions and retain the $(3 \times 1)$ surface symmetry. The thermal stability of the oxidised surfaces exhibit differing behaviour. A 700°C anneal is sufficient to liberate oxygen from the germanium-oxide terminated (100) diamond surface, leaving the pristine germanium-terminated surface, while the silicon-oxide terminated surface is thermally stable up to 1200°C, at which point both silicon and oxygen are removed.

### 6.3.2 Introduction

Functionalised diamond surfaces have emerged as a promising device platform in many diverse application areas, such as high sensitivity nanomagnetometry [140, 141], biosensing [142–144], cold cathode electron emitters [145–147] and spintronics [3, 69, 115, 148]. The interest in diamond surfaces stems from the ability to engineer significantly contrasting properties with a simple change in the terminating species, as well as the advantages that bulk diamond properties offer for such applications. Extending the range of available terminations offers new possibilities for developing diamond surfaces as a technologically relevant platform. Typical elemental terminations include hydrogen [33], oxygen [149], nitrogen [52, 150] and fluorine [83, 84]; more complex terminations based around metal-oxides have been developed [45, 110], as well as biologically relevant organic functionalisations [151]. While the chemically inert nature of diamond is considered a benefit for a large number of

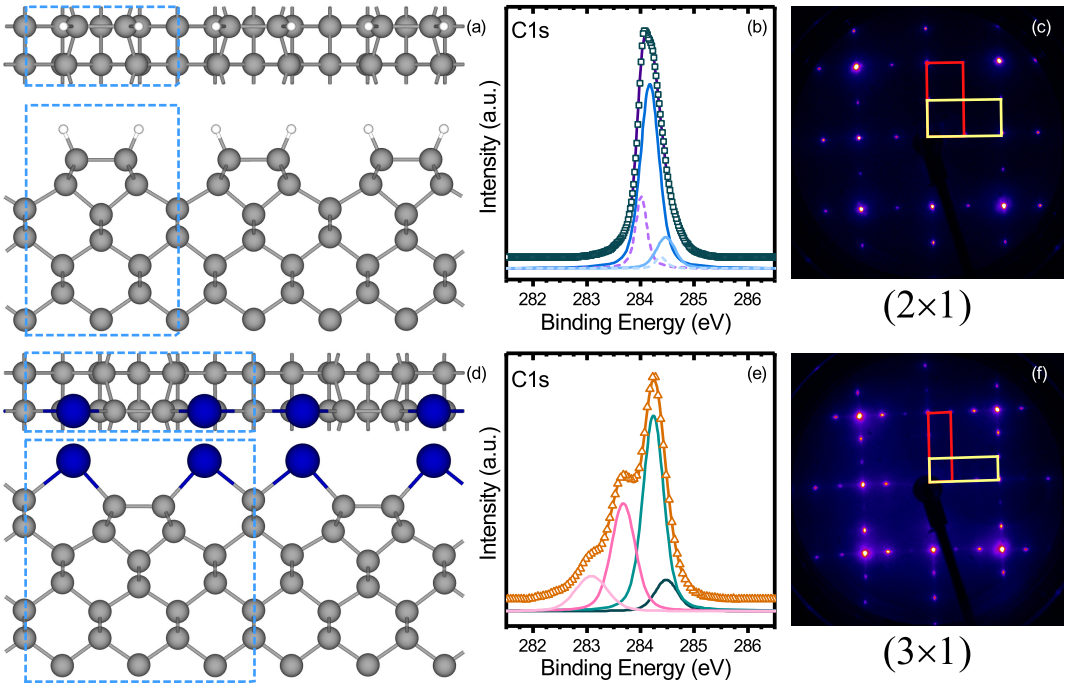


FIGURE 6.1: Schematic model with unit cell outlined, C1s x-ray photoelectron spectra ($\hbar\omega = 350$ eV) and LEED pattern for the $(2 \times 1)$ hydrogen terminated (a-c) and $(3 \times 1)$ silicon-terminated (d-f) diamond surfaces

applications, Raymakers *et al.* have shown that forming a covalent surface functionalisation with diamond is complicated by the stability and chemical passivity of the diamond surface [152]. Typical processing steps for terminating diamond surfaces require that the surface be exposed to harsh chemicals, or to radicals created through thermal cracking of molecules or in a plasma. Such treatments have a tendency to etch the surface and yield chemical inhomogeneity. While this does not necessarily impact the utility of diamond surfaces in all applications, the desire for surface-based electronics and subsurface defect center devices creates a need for greater control over the morphology and chemical structure of the diamond surface [148].

### Group IV terminations of (100) diamond

We have recently shown that the (100) diamond surface can be terminated with group IV elements, forming silicon-terminated (SiTD) [4] and germanium-terminated (GeTD) (100) diamond [153]. In both cases, the preparation procedure for these surfaces begins with the highly ordered C(100)- (2x1):H surface [33] and then proceeds in a manner which, in principle, should preserve the atomically flat terraces as associated with this surface, while modifying the surface electronic properties. Both the SiTD and GeTD surfaces possess a small negative electron affinity. Low energy electron diffraction (LEED) shows that both terminations cause the surface to transition from the two-domain $(2 \times 1)$ structure associated with the hydrogen-terminated

surface, to a two-domain $(3 \times 1)$ structure which we believe has the same origin in both cases. Figure 6.1 shows the alternating monomer-dimer model proposed for the $(3 \times 1)$ reconstruction, derived from the results of synchrotron-based X-ray Photoelectron Spectroscopy (XPS) and LEED characterisation of these surfaces. One feature of the proposed model is that each adatom forms two bonds with the underlying carbon surface and has two dangling bonds associated with it. This structure is supported by studies demonstrating the oxidation of silicon-terminated diamond [19], where chemical modification of the surface-bound silicon is evident, but the $(3 \times 1)$ reconstruction and the carbon chemical states are otherwise preserved.

While the proposed ideal reconstruction for the SiTD and GeTD surfaces is identical, in practice there are key differences. Importantly, while a completely silicon-terminated (100) diamond surface can be readily prepared [4], germanium-terminated surfaces have been prepared with a germanium coverage only up to 0.63 ML [153]. This limitation appears to be derived from steric hinderance due to the larger atomic size of germanium compared to silicon, rather than any kinetic barrier limiting the extent of the bonding reaction. This may limit the use of germanium terminated diamond in applications where surface homogeniety is critical. However, the group IV terminations of diamond have more to offer than simply the properties of their pristine as-prepared surfaces. For example, we have recently shown that when oxidised, SiTD can be p-type surface transfer doped with an adlayer of $MoO_3$ [154], in a similar fashion to hydrogen-terminated diamond [40, 132]. While forming a material interface with diamond may be difficult due to the conditions typically required for chemical functionalisation, silicon and germanium have a rich variety of functionalisation schemes [155, 156] and well-established fabrication protocols which may now be applicable to diamond through this Si or Ge bridging layer, fostering even greater tunability in the properties of the diamond surface. This may include the possibility to functionalise the surface with optically active or magnetic species.

The present work focuses on understanding aspects of Group IV terminated diamond which are relevant to integrating the Si and Ge terminated surfaces into real device systems. As a complimentary study to our previous work exploring the oxidation of SiTD [19], we explore the behaviour of GeTD when exposed to sources of oxygen, specifically $H_2O$ and $O_2$ dosed under ultra high vacuum (UHV) conditions, as well as full atmospheric exposure. As in the case of the oxidation of SiTD, the germanium oxidises in all three cases while the carbon-germanium bonding and $(3 \times 1)$ surface reconstruction are retained. The thermal stability of pristine SiTD and GeTD, as well as the oxidised form of these surfaces, is examined. The ability to anneal diamond samples without disturbing the surface has relevance to developing device architectures based on Group IV terminated surfaces, both because this may influence the processing steps which are compatible with these terminations and as the activation rate of bulk dopants is correlated with temperature. A crucial factor, then, is determining the temperature to which our group IV terminations are stable. We show that the pristine surfaces are stable up to 1200°C when annealed under UHV

conditions, considerably higher than for the hydrogen-terminated (100) diamond surface [20, 33, 121], where the hydrogen is removed with a 950°C anneal, leaving a highly reactive bare surface which furthermore begins to graphitise at 1200°C[47]. The oxidised surfaces present differing behaviour. Oxygen desorbs from oxidised GeTD with a 700°C anneal, reverting to the pristine germanium-terminated surface. In contrast, oxidised SiTD is stable to 1200°C, at which point the oxygen desorbs, liberating silicon from the surface with it. As shall be explored, this contrasting behaviour is attributed to the relative strengths of the Ge−C, Ge−O, Si−C and Si−O bonds.

### 6.3.3 Experimental Details

For the measurements presented in this work, each sample is a CVD-grown type-IIa single crystal (100) oriented substrate (Element Six) onto which a (100) oriented boron doped overlayer (B concentration in the range $1 \times 10^{16}$ - $1 \times 10^{18}$ B/cm$^{-3}$) was grown at the Melbourne Centre for Nanofabrication (MCN), to prevent charging in the course of measurements. Scanning Tunneling Microscopy studies have been performed to show that the grown overlayers possess atomically flat terraces with a terrace width of typically 30 nm [33].

#### Preparation of pristine Group IV terminated surfaces

Our preparation methods for the silicon [4] and germanium [153] terminated surfaces are reported in extensive detail elsewhere, and we summarise the key points here for the benefit of the reader.

The starting point of our preparation is a (100) oriented substrate which has been hydrogen-terminated by exposing the substrate to a microwave hydrogen plasma, such that it forms the well-known two-domain $(2 \times 1)$ reconstruction [33]. Following hydrogen termination, the selected substrate is loaded into a UHV environment where it is annealed at 450°C for at least 30 minutes to remove atmospheric contamination, and it is in this UHV environment that all subsequent preparation is performed. From this point, three processes must occur to successfully terminate the (100) diamond surface:

- Deposition of sufficient adlayer material (silicon or germanium) to satisfy the reconstructed unit cell
- Removal of hydrogen (achieved by annealing the sample to 950°C [20, 121])
- High temperature annealing to form the $(3 \times 1)$ reconstruction

To achieve these goals, silicon or germanium is evaporated under UHV conditions, with a pressure no higher than $5 \times 10^{-10}$ mbar during deposition. The silicon is evaporated by passing a DC current through a rectangular piece of silicon wafer (approximately 25 mm x 4 mm) until the temperature is sufficient to cause evaporation. Germanium is deposited using a commercial effusion cell (HTZ cell, MBE

Komponenten) equipped with a graphite crucible. In each case, the source is positioned approximately 30 cm from the sample.

Our model of the $(3 \times 1)$ surface contains two adatoms per surface supercell. That amounts to an atomic density of $1.048 \times 10^{15}$ cm$^{-2}$. Using a calculation of photoelectron attenuation we correlate this adatom density with a measurable ratio of XPS peak intensities, and use this metric to determine our coverages.

On the silicon terminated surface, excess deposited material cannot be removed, thus we aim for exactly 1 ML, whereas we have found that excess germanium will desorb during the annealing step, so we deposit in excess of 1 ML in order to maximize terminated coverage.

The samples were then annealed using an electron-beam heater incorporated in the sample plate for the removal of hydrogen and the surface reconstruction. The sample holder and deposition stage were thoroughly outgassed before the sample holder was removed from vacuum and the sample mounted. This was to mitigate as far as possible the evolution of oxygen during sample preparation, to maximize the quality of the pristine samples.

As we describe elsewhere [153], there is some flexibility in the order and implementation of these steps. The most commonly used process has been to deposit the desired material onto the hydrogen-terminated diamond surface, then to anneal the substrate to 950°C for 30 minutes. This anneal simultaneously both desorbs the hydrogen from the surface and enables the reaction and relaxation necessary to form the $(3 \times 1)$ reconstruction [4, 153]. As an alternative, we have also found that a high quality termination can also be achieved by annealing the sample to remove the surface hydrogen, then depositing material and finally annealing again for the surface to relax into the $(3 \times 1)$ reconstruction. Furthermore, while annealing at temperatures lower than 950°C will result in bonding between the adatom and the diamond (100) surface, we find that annealing at 950°C is required to produce a completely reconstructed surface [153].

**Surface characterisation and oxidation**

Measurements were performed at the Soft X-ray Spectroscopy (SXR) beamline of the Australian Synchrotron. The beamline end-station is equipped with a SPECS Phoibos 150 hemispherical analyser, leak valves for controlled gas dosing and a reverse-optics LEED system for monitoring the surface reconstruction. The samples were mounted inside a Ta envelope on a sample holder with an underlying electron beam heater, enabling annealing to temperatures of 1200°C reproducibly. A K-type thermocouple in direct contact with the sample envelope and an optical pyrometer were simultaneously used to monitor the sample temperature during annealing steps. All measurements were performed at pressures below $5 \times 10^{-10}$ mbar.

The samples were exposed to molecular $H_2O$ and $O_2$ using a precision leak valve for controlled dosing. During exposure, the dose (in Langmuirs, L) was estimated by monitoring the partial pressure of the species using a residual gas analyser (Stanford

Research Systems RGA 300). The recorded partial pressure curve was integrated following each exposure to precisely determine the administered dose.

High resolution XPS measurements of the C1s, Si2p and Ge3d core levels were performed using the photon energies listed in Table 6.1. In each case the photoelectron kinetic energy falls within the range 50-70 eV, maximising the surface sensitivity of these measurements. In addition, XPS survey scans were acquired to evaluate surface cleanliness using a photon energy of 850 eV. The binding energy (BE) scale of all XPS spectra were referenced to the Fermi level either by setting the $Au4f_{7/2}$ core-level BE to 84.00 eV (for C1s spectra) or by monitoring the Fermi edge of a gold foil in electrical contact with the sample (for Si2p and Ge3d spectra). Core level spectra were fitted using Voigt components with the Lorentzian widths listed in Table 6.1, after first applying a Shirley background correction. [15]

For the doublet Si2p core level, the spin-orbit split components of the $Si2p_{1/2}$ and $Si2p_{3/2}$ components have been constrained to have a binding energy separation of 0.6 eV and the required branching ratio of 0.5. For the doublet Ge3d core level, the $Ge3d_{3/2}$ and $Ge3d_{5/2}$ have a binding energy separation of 0.59 eV and branching ratio of 0.67. The relative and absolute binding energy uncertainties of our measurements are estimated as 0.05 eV and 0.1 eV for the Si2p and Ge3d core levels, respectively. For clarity, fitted core-level spectra illustrated in this paper show the $Si2p_{1/2}$ and $Ge3d_{3/2}$ components in transparency. [120, 153]

### 6.3.4 Results and Discussion

#### Thermal stability of pristine Si and Ge-terminated (100) diamond

Silicon and germanium terminated surfaces were prepared using the process described above and characterised after cooling to room temperature and after a subsequent annealing step at higher temperature (1200°C) to test whether these surfaces are stable to temperatures higher than the 950°C reconstruction temperature.

Figure 6.2 shows the C1s and Si2p core levels of SiTD, before and after a 1200°C anneal for 15 minutes. The surface related components of both the Si2p and C1s core levels have narrowed, leading to a sharpening of the spectral features. This may be qualitatively interpreted as an improvement in the quality of the reconstruction as a result of the high temperature treatment. Furthermore, a small amount of surface oxygen which was present following the initial preparation of the terminated

| Core level | $\hbar\omega$ (eV) | $w_L$ (eV) |
|---|---|---|
| C1s | 350 | 0.15 [20] |
| Si2p | 150 | 0.055 [136] |
| Ge3d | 100 | 0.17 [120] |

TABLE 6.1: The photon energies ($\hbar\omega$) used for measuring high-resolution, surface sensitive core level spectra in the current work and the Lorentzian widths ($w_L$) used during peak fitting analysis of the respective core levels.

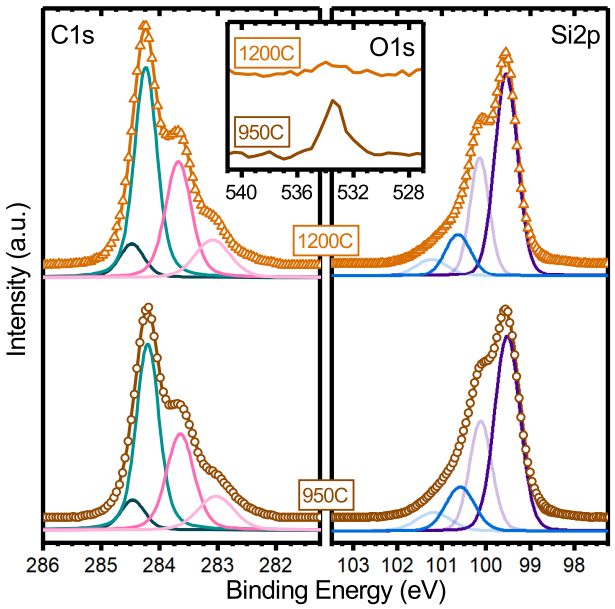


FIGURE 6.2: Fitted C1s and Si2p core level spectra obtained for a silicon-terminated diamond surface, (i) as-prepared and (ii) after a subsequent 1200°C anneal. Components are vertically offset from the spectra, and only the $Si2p_{3/2}$ components are displayed, for clarity. Inset shows the corresponding O1s core level from a survey scan

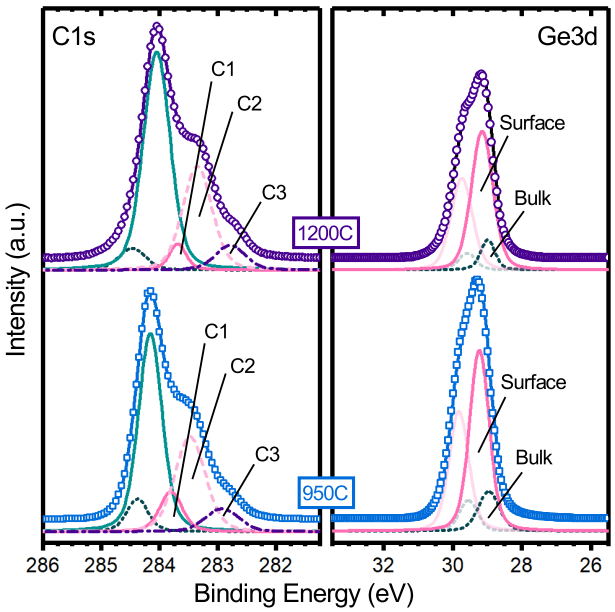


FIGURE 6.3: Fitted C1s and Ge3d core level spectra for a germanium-terminated diamond surface, as-prepared (bottom) and after a subsequent 1200°C anneal (top). Components are vertically offset from the spectra, and only the $Ge3d_{5/2}$ components are displayed, for clarity.

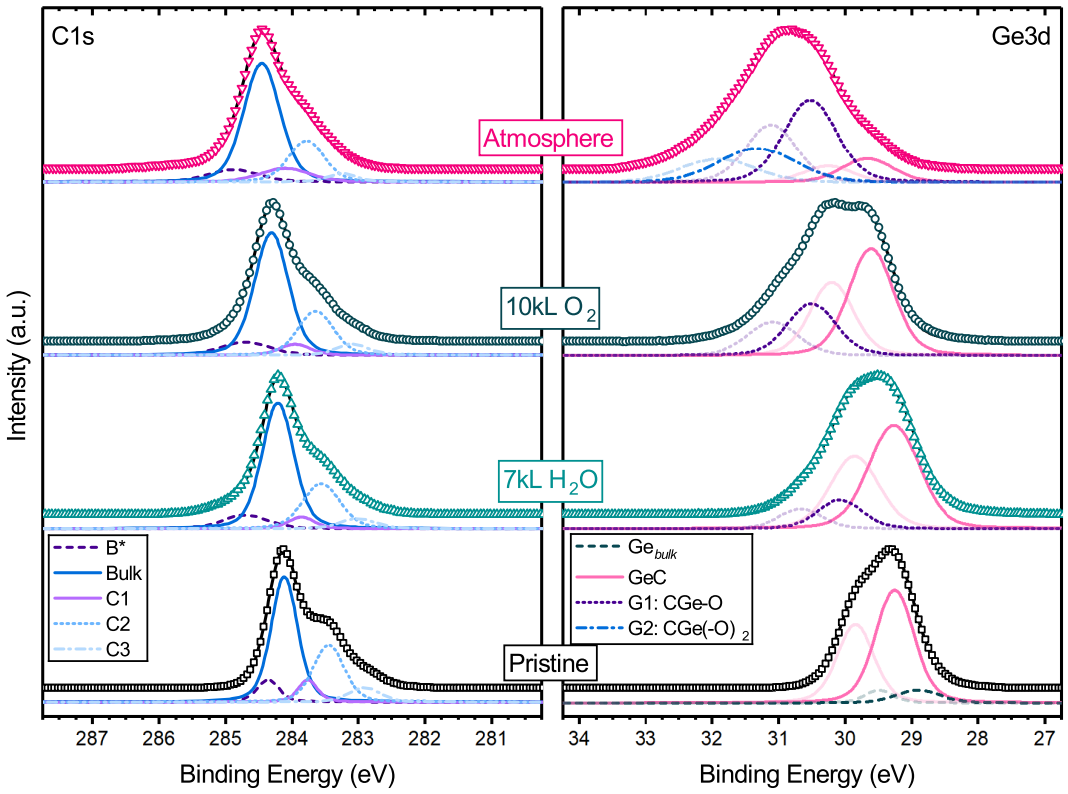


FIGURE 6.4: Germanium-terminated (100) diamond before (Pristine) and after exposure to $H_2O$ or $O_2$ *in situ*, and exposure to atmospheric conditions. Components are vertically offset from the spectra, and only the $Ge3d_{5/2}$ components are displayed, for clarity.

surface, as evident in the O1s core level (inset) was removed during the 1200°C anneal, further showing an improvement in the surface quality. For the case of the germanium-terminated surface, shown in Figure 6.3, the changes to the core level structure are more complex yet support a similar conclusion. As noted above, we have found that the maximum achievable germanium coverage on the germanium-terminated surface is approximately 0.63 ML [153]. As a result, some of the surface-related components are in part attributed to those unit cells which are "incomplete"; these are indicated in Fig. 6.3. Following an anneal of 1200°C, we observe a relative decrease in the component C1, which is attributed to sites in incomplete unit cells, accompanied by a relative increase in the C2 and C3 components which have been attributed to surface carbon atoms bonded to, respectively, one and two germanium atoms [153]. Concurrently, there is a relative decrease in the bulk-like component of the Ge3d spectrum (Fig. 6.3, right). In short, there are subtle changes which qualitatively reflect some improvement in the surface, but more importantly we do not observe any new indications that a high temperature treatment has removed any of the surface-bound germanium or caused the formation of any new components. Thus, our measurements indicate that annealing to 1200°C has little impact

on the as-prepared pristine silicon- and germanium-terminated (100) diamond surfaces, other than to perhaps improve the quality of the surface reconstruction in both cases.

**Oxidation of Ge-terminated (100) diamond**

We have previously explored the oxidation of the silicon terminated (100) diamond surface [19], and turn now to the behaviour of the germanium-terminated surface upon exposure to sources of oxygen. Figure 6.4 shows the Ge3d and C1s core levels of an as-prepared germanium-terminated (100) diamond surface for reference, along with the same core levels for surfaces subsequently exposed to $O_2$ (RGA integrated total exposure: 10852 L), $H_2O$ (RGA integrated total exposure 7128 L), and atmosphere (10 minutes, i.e. approx. $10^{11}$ L exposure to $O_2$ and $10^{10}$ L exposure to $H_2O$). The Ge3d spectrum for the as-prepared surface is dominated by a peak assigned to the pristine germanium-carbon termination (labelled GeC in the figure), with a smaller feature at lower binding energy attributed to excess germanium remaining on the surface after the initial preparation, as described in detail elsewhere [153]. We observe two changes in the Ge3d spectra that are attributed to oxidation. Firstly, the $O_2$ and $H_2O$ dosed samples show a single additional component (labelled G1 in the figure) to high binding energy of the component GeC.

Our fit for this new component is based on systematic fitting of spectra from these three samples, resulting in a core level shift of $0.85 \pm 0.05$ eV relative to the GeC component; the component positions are shown in Table 6.2. We attribute this component G1 to germanium which is bonded to a single oxygen atom, in addition to the underlying carbon lattice. Turning to the the atmosphere exposed sample, we find that the Ge3d spectrum is composed of three components. Two of these are attributed to the same GeC and GeO species as in the case of the $O_2$ and $H_2O$ exposed surfaces, with the GeO component (G1) shifted in binding energy by 0.86 eV relative to GeC. The third component (Ge2) appears at a core level shift of 1.65 eV relative to GeC and is assigned to $GeO_2$. For the atmosphere exposed sample, the measured Ge3d component shifts of 0.86 eV and 1.65 eV relative to GeC in both cases represent a shift of roughly half that seen in work on bulk germanium [157]. However, Kuhr and Ranke [158] describe a variation in chemical shift of $Ge^{1+}$ across a range 0.56 to 1.17 eV, and $Ge^{2+}$ across a range 1.72 to 2.03 eV, dependent on crystal orientation. Given these reported ranges, and the reduced induction effect due to the bonding of the Ge atom to the underlying (higher electronegativity) carbon lattice in this system, we are confident in the assignment of these peaks as described above.

In contrast to the oxidation of SiTD surfaces, the adsorption rate of oxygen containing species on the GeTD surface was observed to be very low. The GeO component, in the maximally exposed $H_2O$ ($O_2$) sample represents only 20% (34%) of the core level. In contrast, exposure to just 1170 L of $H_2O$ was previously shown to result in almost 50% oxidation of the SiTD surface [19]. Even in the case of the

atmosphere-exposed GeTD surface, the sum of both oxide species present in Figure 6.4 still represents only 85% of the total core level intensity. Our previous study of the oxidation of SiTD showed that the exposure to atmosphere resulted in not just near-total oxidation, but near-total conversion to the $Si^{2+}$ oxidised state. In contrast, here the $Ge^{2+}$ core level intensity is found to represent just 31% of the Ge3d core level spectrum for the atmosphere exposed surface. These results are in agreement both with the oxidation behaviour described for bulk Ge [157], where a significant formation of $GeO_2$ was only observed after exposure to atmosphere, and with measurements of the adsorption of water on bulk Ge [159] which showed that the sticking coefficient of water on germanium is quite low at room temperature, an effect which is apparently not mitigated in our system despite the known reactivity of dangling bonds. In bulk germanium, the low rate of $GeO_2$ formation by oxidant exposure in vacuum is attributed to the similar stability of GeO and $GeO_2$, whereas $SiO_2$ is significantly more stable than SiO [160]. This difference is a reasonable explanation for the contrasting behaviour we observed between these two Group IV terminations of diamond.

We now turn to a brief discussion of the C1s core level corresponding to each of the three oxidized GeTD samples. These are shown in Figure 6.4, along with the corresponding core level for the as-prepared surface. As noted above, the germanium termination achieves a maximum coverage below 1 ML, and thus it is reasonable to consider whether the surface carbon which has not bonded with germanium remains vulnerable to oxidation. Oxidation of the bare (100) diamond surface generates C1s components to high binding energy of the bulk diamond peak [45, 47]. For the C1s spectra shown in Figure 6.4, while there is some change in the distribution of spectral weight to the high binding energy side of the bulk diamond component, we do not attribute this to the oxidation of surface carbon based on the following argument. We have employed the same five component model in fitting the C1s core levels of both the clean GeTD C1s and those of the oxidised samples. The component to higher binding energy of the bulk component in this five component model (labelled B* in Figure 6.4, as in our previous work [33, 153]), makes up 15% of the bulk core level and is associated with near-surface atoms which experience a final-state shift [33]. Since the magnitude of this final-state shift and the width of this component are dependent on a number of complex factors, including the surface dielectric constant, it is expected that this peak will change with surface oxidation in a manner

| | Ge | GeC | GeO | $GeO_2$ |
|---|---|---|---|---|
| Clean | 28.90 | 29.26 | | |
| $H_2O$ | | 29.27 | 30.08 | |
| $O_2$ | | 29.61 | 30.50 | |
| Atmosphere | | 29.67 | 30.52 | 31.32 |

TABLE 6.2: Binding energy positions (in eV) and assignments of the $Ge3d_{5/2}$ components in the spectra shown in Figure 6.4

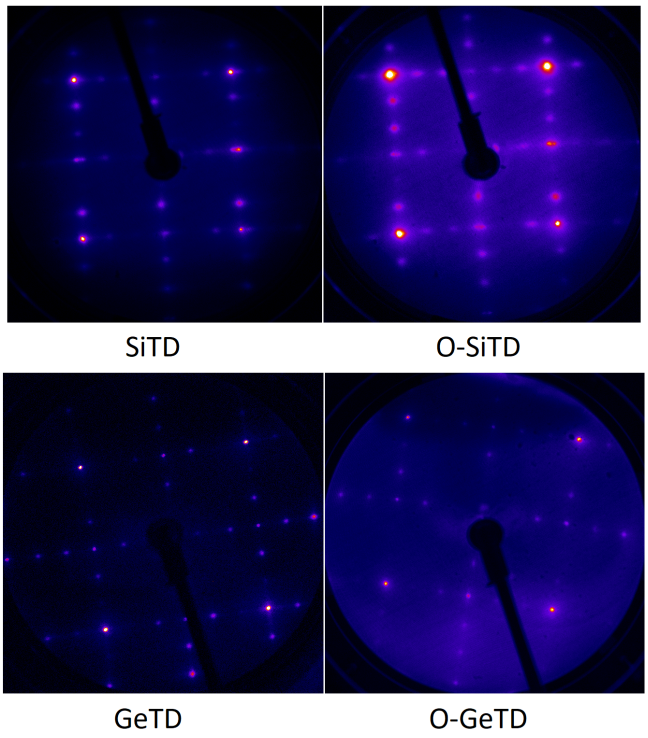


FIGURE 6.5: LEED patterns for pristine and oxidised Group IV terminated diamond surfaces. The rotation of the oxidised GeTD pattern relative to the pristine GeTD pattern is the result of remounting the sample after atmosphere exposure.

which cannot currently be predicted. As a result, we cannot rule out that this component may mask features related to slight oxidation of the surface. However, Maier *et al.* [47] describe a chemical shift of 2.5 eV to higher binding energy of the bulk peak for the C-O component, well beyond the range of the B* component employed in the present work; thus we state with some confidence that the surface is not oxidized to a meaningful extent. That oxidation of the surface carbon which is not bound to germanium is not observed may be interpreted as further support for our hypothesis that 63% represents a maximum surface layer packing, and sufficiently shields the surface carbon atoms from further bonding.

As a final point in the characterisation of the oxidised GeTD surface, we consider whether oxidation affects the two domain $(3 \times 1)$ reconstruction which is unique to the Group IV terminations. In previous work we showed that exposing the SiTD surface to oxidation sources causes the formation of (C−)SiO and (C−)$SiO_2$ related components in XPS, while retaining the characteristic $(3 \times 1)$ surface structure seen in LEED. Here we report this to be similarly true for the oxidation of germanium-terminated (100) diamond. Figure 6.5 shows the LEED patterns for Si, SiO, Ge and GeO terminations. In both the Si and Ge cases, oxidation causes an increase in the diffuse background signal, while the $(3 \times 1)$ symmetry is retained.

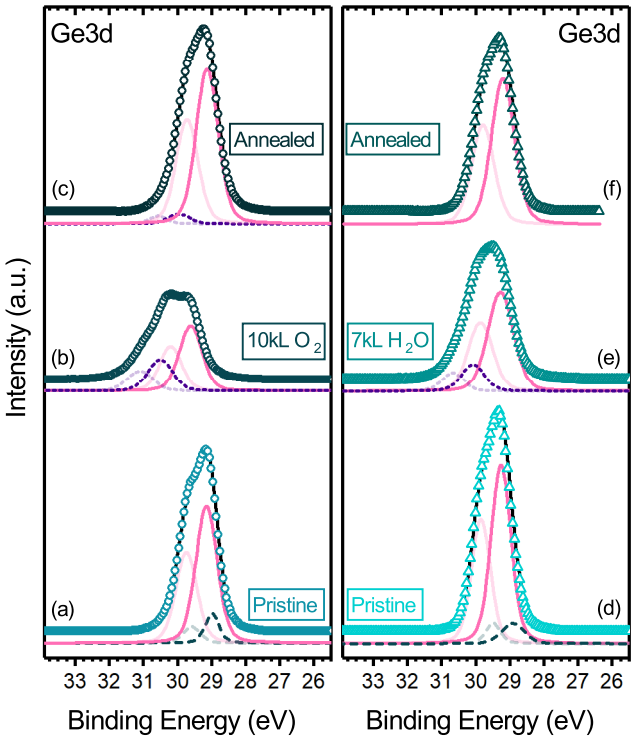


FIGURE 6.6: Ge3d spectra illustrating the thermal stability of the oxidized GeTD surface. (a,d) Pristine; exposed to (b) 10kL $O_2$, (e) 7kL $H_2O$; subsequently annealed for 15 minutes to (c) 700°C, (f) 300°C

**Thermal stability of oxidised Si and Ge-terminated (100) diamond**

In order to determine the thermal stability of the oxidised surfaces, the samples were annealed to increasingly higher temperatures until a change in the survey spectra, measured at room temperature after each anneal step, was observed. Here follows the results of annealing on three representative samples.

The first two samples were Ge terminated; the corresponding Ge3d core level spectra of the GeTD surfaces are shown in Figures 6(a) and 6(d). The two surfaces have the same Ge coverage (0.73 ML). For the case of Figure 6(a) a slightly higher bulk Ge component relative to the surface component is evident (0.15, compared to 0.13 in the case of Figure 6(b)) and the Gaussian widths of the surface components are also slightly higher in Figure 6(a) (0.64 eV compared to 0.59 eV), which is ascribed to a more inhomogeneous sample. This explains the slightly different spectra for the two as-prepared samples, however these factors do not affect the present study.

For the first sample investigated, the GeTD surface was exposed to 10kL of $O_2$, giving a GeO component of 34% of the total Ge3d core level intensity. This sample was annealed for 15 minutes at 700°C; the effect on the Ge3d core level is shown in Fig. 6.6 (a) to (c), where a clear similarity between the pre-oxidised and post-anneal core levels is observed. The post-anneal fit includes a GeO component comprising 3.5% of the core level, or about 10% of the amount of pre-anneal oxidation. For the

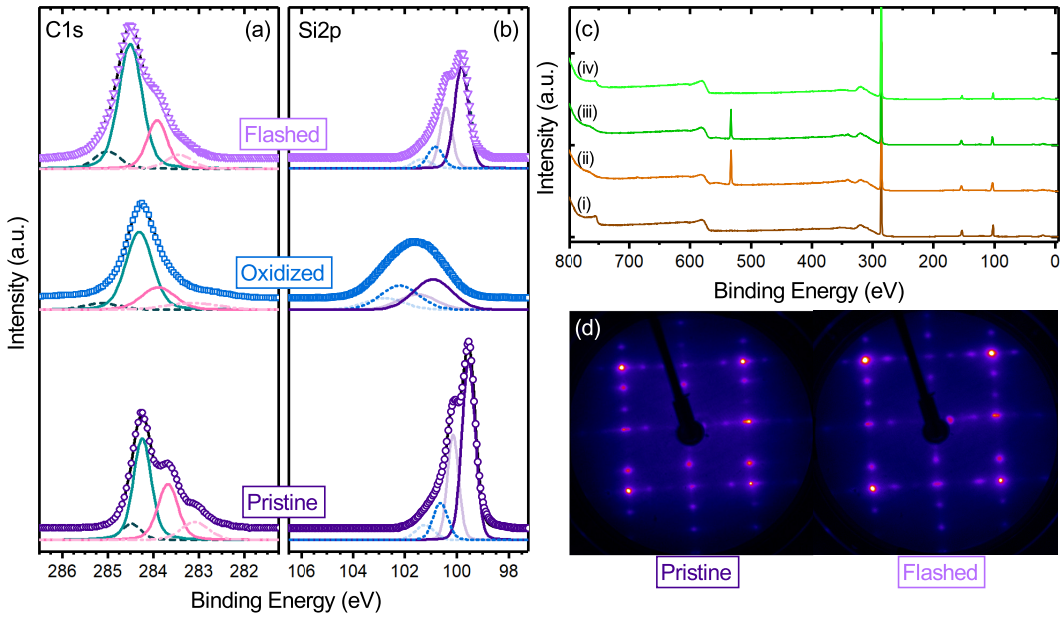


FIGURE 6.7: C1s (a) and Si2p (b) core level spectra demonstrating the thermal stability of the oxidized SiTD surface. Survey scans (c) show the clean (i), oxidized (ii), after being flashed twice at 1200°C (iii), and finally after two further flashes at 1400°C (iv); (d) LEED patterns corresponding to the pristine and post-treatments surface.

second sample, the GeTD surface was exposed to 7kL of $H_2O$, giving a GeO component only 20% of the Ge3d core level intensity. We noted, in the previous section, the relatively poor adsorption of water onto the germanium terminated surface. Furthermore, it was observed in [159] that adsorbed $H_2O$ dissociates into atomic oxygen at 450K. This sample was annealed to 300°C, for which the effect on the Ge3d core level is shown in Fig 6.6 (d) to (f). That low temperature annealing was apparently sufficient to cause the complete desorption of oxygen from the surface and conversion of (C-)GeO back to GeC. In this case, we did not need any GeO component to fit the core level. The relatively easy reversal of the oxidation of the germanium termination via low temperature annealing is contrasted now with the higher temperatures required to reverse the oxidation of the SiTD surface.

The C1s and Si2p spectra for the as-prepared, oxidised and annealed SiTD surface are shown in Figure 6.7. The as-prepared Si2p core level was fit with two components, at 99.55 eV and 100.63 eV, which account for 81.4% and 19.6% of the core level intensity respectively. As the ratio of oxygen to carbon as indicated by survey scan (also shown) is less than 1%, we attribute the higher binding energy component to step edge bonded silicon, which has a higher carbon co-ordination than the ideal termination. This sample was heavily oxidized in UHV by $O_2$ exposure, such that no unoxidized component was required for fitting; the core level consisted of 56% $Si^{1+}$ (100.92 eV) and 44% $Si^{2+}$ (102.22 eV). The corresponding growth of the O1s peak in the survey scan (approx. 530 eV) is illustrated in Figure 6.7 (c). After oxidation, the O1s to C1s peak ratio had increased to 28%. The C1s core level is broadened

and structure is lost, however it may still be fit using the four peak model of the as-prepared surface, with broadening attributed to scattering from the oxygen overlayer.

Due to the higher annealing temperatures required for the case of SiTD, the sample was flash annealed four times; that is, it was rapidly ramped to the temperature set point, held for 10 seconds, and then ramped down to room temperature over a period of 1 minute. The sample was flashed to 1200°C twice, causing a reduction in oxygen ratio to 17% in the survey scan. It was then flashed twice to 1400°C, reducing the oxygen to carbon ratio to below 1%. The Si2p core level resulting from this annealing is shown in Fig. 6.7 (b). Evident in this spectrum is a return to the chemical composition of the pristine SiTD surface, in this case the SiC component accounting for 81.5% and $Si^{1+}$ for 18.5%, similar to the pre-oxidation composition. However, it is also important to consider whether silicon is removed by this process. If we quantify the silicon coverage before and after thermal treatment, using the attenuation method we have used in previous work [4], we find that the coverage has gone from 1.44 ML pre-anneal to 0.73 ML after the flashing, a loss of about half the Si. As this is accompanied by a complete loss of the surface oxygen, we attribute this to desorption of silicon as a silicon-oxide moiety, although at this stage have no specific knowledge of the mechanism involved [161, 162]. While silicon remains on the surface, we cannot claim to have shown that the pristine termination would be resistant to 1400°C flashing. However, we do observe that surface silicon-carbon bonds are capable of resisting this treatment, and that the $(3 \times 1)$ termination is similarly resilient, as may be seen in Figure 6.7 (d).

### 6.3.5 Conclusion

This article has presented data showing the oxidation of the germanium-terminated (100) diamond surface and the thermal stability of pristine Group IV terminated (100) diamond surfaces, as well as the oxidised variants of those surfaces. The pristine GeTD surface is shown to be vulnerable to oxidation from $H_2O$ and $O_2$ *in vacuo*, and will oxidise on exposure to atmospheric conditions. However, the GeTD surface may be less vulnerable to oxidation when compared to SiTD [19], as atmosphere exposure for 10 minutes still leaves 15% of the surface germanium unoxidised, in comparison to SiTD where the surface has been shown to be near-completely oxidised after the same exposure. While the pristine GeTD surface has been found to reach a maximum coverage of 0.63 ML and thus some surface carbon should be exposed, we note that exposure to oxygen does not oxidise these surface carbon sites, a finding attributed to steric hindrance preventing oxygen from bonding to these sites.

When investigating the thermal stability of these surfaces, the pristine SiTD and GeTD surfaces are found to be stable up to at least 1200°C. Given that the hydrogen desorbs from the hydrogen terminated (100) diamond surface at 950°C [20, 33, 121] and the bare (100) surface graphitises at 1200°C [47], this shows that these Group IV terminated surface improve the stability of the diamond (100) surface. Such

high temperature annealing may be advantageous for optimisting the properties of nitrogen-vacancy centers [163] and boron doped layers [164, 165] in bulk diamond, or useful in enabling higher temperature treatment of near-surface dopant layers. The oxidised SiTD and GeTD surfaces show differing behaviour. It has been observed that an oxidised GeTD surface can be reverted to an as-prepared GeTD surface with an anneal of 700°C, with some species removed at 300°C. In contrast, the oxidised SiTD surface is stable up to 1200°C, at which point some oxygen species are removed; a heat treatment of 1400°C removes the oxygen completely but also results in removal of some surface silicon.

### 6.3.6 Acknowledgements

This research was undertaken using the Soft X-ray Spectroscopy beamline at the Australian Synchrotron, Victoria, Australia. This work was performed in part at the Melbourne Centre for Nanofabrication (MCN) in the Victorian Node of the Australian National Fabrication Facility (ANFF). This work was partly supported by the Research Council of Norway through its Centres of Excellence funding scheme, project number 262633, "QuSpin". This work was supported by the Australian Research Council under the Discovery Project (DP150101673).

# Chapter 7

# Fluorination of silicon-terminated (100) diamond via decomposition of $C_{60}F_{48}$

## 7.1 Preface

Chapter 6 showed that both the silicon termination and the germanium termination can be modified, to differing extents, with oxygen, and this oxidative passivation occurs naturally by exposure to atmosphere. An advantage of diamond is that by selecting from the range of terminations described in Chapter 3, the surface properties may be tuned as desired, from positive to negative electron affinity, and from very unreactive (hydrogen) to more reactive to hydrocarbons (amine). Ideally, the silicon terminated surface should show a similar level of tunability, as our structural model of the surface attributes to each silicon atom two dangling bonds which may be functionalized.

This chapter presents the results of combined x-ray photoelectron spectroscopy and low energy electron diffraction studies which demonstrate such a tunability, by terminating the silicon terminated (100) surface with fluorine. The fluorination was performed by decomposing fluorofullerene molecules which had been deposited on the surface, using two methods: electron-stimulated dissociation and thermal decomposition. We showed that the silicon terminated diamond can be modified with fluorine, and that the fluorine appears to be resistant to replacement by oxygen. As fluorine possesses a very high electronegativity, the effect of bonding fluorine to the surface should be to induce a high positive electron affinity; this has been seen in the direct fluorination of diamond (Rietwyk et al. *Appl. Phys. Lett.* **102**, 091604 (2013)). Since the clean and oxygen terminated SiTD surfaces have been observed to possess a negative electron affinity, and Chapter 5 showed that the oxidized surface can be transfer doped, this study suggests that termination-patterned surface conductive devices akin to existing diamond device architectures may be able to be fabricated on silicon terminated diamond.

This work has been submitted to the Journal of Physics: Condensed Matter, as of January 2019, and the submitted manuscript is shown below. No changes have been

made to the manuscript except those required to make the formatting consistent with the rest of this thesis.

## 7.2 Author Contribution:

The experimental plan was conceived by Sear, Schenk, Pakes and Tadich. Sear, Schenk, Stacey, Tadich and Pakes performed the experimental work during a beamtime at the Australian Synchrotron. The data was analysed by Sear and Schenk. Sear and Schenk made equal contributions in the preparation of this manuscript.

## 7.3 Fluorination of silicon-terminated (100) diamond via decomposition of $C_{60}F_{48}$

Michael J. Sear[1], Alex K. Schenk[2], Nikolai Dontschuk[3], Anton Tadich[4,1], Alastair Stacey[3,5], and Chris Pakes[1]

[1)] *Department of Chemistry and Physics, La Trobe Institute for Molecular Sciences, La Trobe University, Victoria 3086, Australia*

[2)] *Center for Quantum Spintronics, Department of Physics, Norwegian University of Science and Technology, NO-7491 Trondheim, Norway*

[3)] *School of Physics, The University of Melbourne, VIC 3010, Australia*

[4)] *Australian Synchrotron, 800 Blackburn Road, Clayton, Victoria 3168, Australia*

[5)] *Melbourne Centre for Nanofabrication, 151 Wellington Road, Clayton, VIC 3186, Australia*

### 7.3.1 Abstract

The functionalization of silicon terminated diamond [C(100)-$(3 \times 1)$:0.667Si] with fluorine is demonstrated. Atomic fluorine, generated by the decomposition of surface adsorbed fluorofullerenes, provides the source for silicon-fluorine bonding without modification of the underlying diamond surface, and without destruction of the silicon-diamond bonds which characterize the surface or of the $(3 \times 1)$ surface symmetry. This functionalization is also shown to be resistant to oxidation by atmospheric exposure.

### 7.3.2 Introduction

Functionalised diamond surfaces have emerged as an alternative platform to silicon for device development in a number of diverse application areas, such as high sensitivity nanomagnetometry,[140, 141] biosensing,[142–144] cold cathode electron emitters[145–147] and spintronics.[3, 69, 115, 148] The suitability of diamond surfaces for such diverse applications comes as a result of the ability to significantly alter the electronic and interfacial properties of the diamond surface through a simple change in the terminating species, allowing the surface properties to be engineered and optimised for a particular application.

We have recently demonstrated that an ordered $(3 \times 1)$ silicon-terminated reconstruction may be formed on (100) oriented diamond by depositing silicon onto a hydrogen-terminated (100) diamond surface and then annealing to high temperature.[4] The prevailing model for this reconstruction has a unit cell with two silicon atoms bonded to three carbon atoms; each silicon atom in the reconstruction possesses two dangling bonds, and as a result the surface is not atmosphere stable.[19, 166] However, these dangling bonds offer the possibility of further functionalising the surface through a silicon "bridge". While the chemically inert nature of diamond is a benefit for a large number of applications, Raymakers *et al.* have shown that

forming a covalent surface functionalisation with diamond is complicated by the stability and chemical passivity of the diamond surface.[152] This means it is often necessary to use strong acids or plasma exposure to successfully functionalise diamond surfaces, resulting in a significant degree of undesirable surface etching. Our investigations into oxidation of the silicon-terminated surface show that the resulting Si-O termination retains the highly-ordered $(3 \times 1)$ reconstructed nature of the silicon-terminated diamond surface,[19] in contrast to traditional oxidised diamond surfaces, and is stable up to temperatures of 1200°C.[166] Additionally, the surface possesses a negative electron affinity, and has been demonstrated to support p-type charge-transfer doping when exposed to $MoO_3$.[154] Given our previous success in modifying the pristine silicon-terminated diamond surface, and the rich variety of properties demonstrated by functionalised diamond surfaces, it is natural to explore whether the silicon-terminated diamond surface can be modified with other species with which silicon is known to bond.

Fluorine terminated diamond surfaces have been proposed as a diamond based quantum simulator.[69] One desirable feature in such a simulator is the ability to tune the interaction strength, which may be achieved by altering the symmetry and spacing of the fluorine atoms, and implemented through the use of different diamond surfaces such as the fluorine-terminated (100) and (111) surfaces. As the Group IV terminated surfaces of (100) diamond are the only diamond surfaces possessing a long range $(3 \times 1)$ reconstruction,[4, 153] successful fluorination of a Group IV terminated surface offers unique access to symmetries and spacings distinct from those currently offered by the (100) and (111) surfaces. Fluorine-terminated diamond surfaces have been produced through a number of methods, including exposing the surface to fluorine-containing plasmas,[70, 73, 77, 89] $XeF_2$[167] or atomic fluorine[85]. However, given the well-documented etching properties of reactive fluorine species, and that our silicon interface is one atomic monolayer, here we turn to fluorination of the silicon-terminated (100) diamond surface using the thermal and electron-stimulated dissociation of $C_{60}F_{48}$.

The thermal decomposition of fluorofullerenes including $C_{60}F_{48}$ has been demonstrated to generate active fluorine atoms which can bond to local surfaces including silicon carbide[168] under graphene, without etching, while fluorination through electron-stimulated dissociation was demonstrated on hydrogen-terminated diamond (100), as a result of the high secondary electron yield of this surface when subjected to synchrotron beam exposure.[84]

In this study, both electron-stimulated dissociation and thermal decomposition of $C_{60}F_{48}$ are employed to generate reactive fluorine at the silicon terminated diamond surface. These methods each result in a similar amount of surface fluorination, while higher fluorine density may be achieved by combining both processes. Further optimisation of the process is needed before a complete fluorine coverage may be achieved. We also demonstrate that the resulting fluorine termination of

silicon terminated diamond is stable against atmosphere exposure and low temperature annealing.

### 7.3.3 Experimental Methods

This work has been performed on a CVD-grown type-IIa single crystal (100) oriented substrate (Element Six) onto which a (100) oriented boron doped overlayer (B concentration in the range $1 \times 10^{16}$ - $1 \times 10^{18}$ B/cm$^{-3}$) was grown at the Melbourne Centre for Nanofabrication (MCN), to prevent charging in the course of measurements. The sample was H-terminated *ex situ* in a microwave hydrogen plasma for 10min at 150 Torr, with the sample maintained at a temperature of 800°C, following growth. This growth and termination process has been shown to produce (100) surfaces with atomically flat terraces, with a terrace width of typically 30 nm. [33]

All subsequent preparations and measurements were conducted at the Soft X-ray Spectroscopy beamline at the Australian Synchrotron. The beamline endstation is equipped with a SPECS Phoibos 150 hemispherical analyser for performing high resolution core-level photoelectron spectroscopy (XPS) and a reverse-optics Low Energy Electron Diffraction (LEED) system for monitoring the surface reconstruction. The sample was mounted inside a Ta envelope on a sample holder with an underlying electron beam heater, enabling annealing to temperatures of 1200°C. A K-type thermocouple in direct contact with the sample envelope and an optical pyrometer were simultaneously used to monitor the sample temperature during annealing steps. All measurements were performed at pressures below $5 \times 10^{-10}$ mbar. Following introduction to the UHV endstation, we prepared the silicon-terminated (100) diamond surface from the hydrogen-terminated diamond surface using the procedure which has been demonstrated in other works.[4, 18, 19] The initially hydrogen-terminated substrate is annealed at 450°C for 1 hour to remove atmospheric adsorbates. We then deposit silicon from a vacuum deposition cell, aiming for a surface atomic density of $1.048 \times 10^{15}$ cm$^{-2}$, or 2 silicon atoms per $(3 \times 1)$ cell. This amorphous layer is then annealed to 1000°C, in order to remove hydrogen from the surface and allow bonding between the silicon and underlying diamond substrate, as well as providing the conditions necessary for relaxation into the $(3 \times 1)$ reconstruction which is typical of the silicon-terminated (100) diamond surface.[4]

Following confirmation of the successful preparation of the silicon-termination with LEED and XPS,[4] a 3 Å layer of $C_{60}F_{48}$, as estimated from photoelectron attenuation, was deposited upon the silicon termination for this investigation. Due to the previously observed decomposition of $C_{60}F_{48}$ as a result of secondary electrons produced during photoemission measurements,[84] measurements were performed on fresh spots of the sample after all important steps, and the results compared to equivalent spectra on previously exposed regions. For this reason, a distinction between spectra acquired on fresh and heavily exposed regions of the sample will be made throughout this paper.

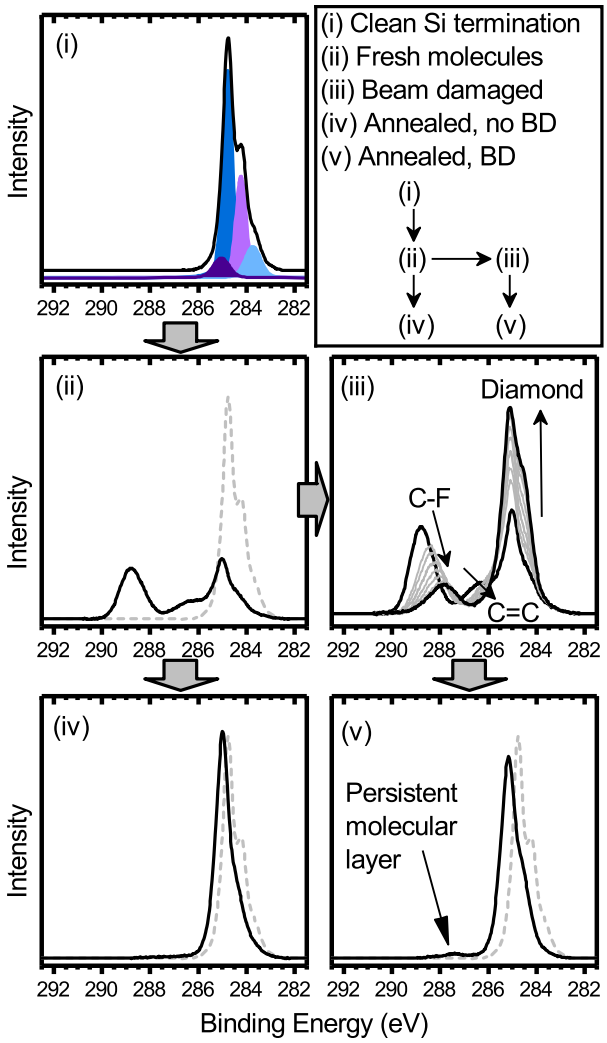


FIGURE 7.1: Evolution of the C1s core level throughout treatments, as detailed in text.

### 7.3.4 Results and Discussion

#### Carbon core level evolution

Given that previous studies have shown decomposition of $C_{60}F_{48}$ with extended synchrotron beam exposure[84] and annealing,[168] and that fluorine radicals might be expected to react with the diamond surface, we first examine the changes to the C1s core level under these conditions. Figure 7.1 shows the C1s core level of silicon-terminated surface before (i) and after (ii) deposition of $C_{60}F_{48}$. The C1s core level of the pristine silicon-terminated surface (i) matches previous work, with two components to lower binding energy (LBE) of the main bulk line caused by the two carbon environments which are part of the reconstruction,[4] and a single minor component to high binding energy (HBE) of the main bulk diamond peak, attributed to subsurface carbon.[19, 33]

After $C_{60}F_{48}$ deposition (Fig. 7.1 (ii)), the diamond core level components remain visible, with a shift (0.36 eV) towards HBE attributed to the electron-withdrawing effect of the fluorofullerenes, and an increase in Gaussian width due to scattering in the overlayer. In addition, the fullerenes themselves contribute to the high binding energy structure of the core level, creating a large, broad peak at about 289 eV, and a HBE shoulder on the bulk peak at about 285 eV, as observed in previous studies of this molecule.[40, 84]

The C1s evolution as a result of $C_{60}F_{48}$ on diamond being exposed to 350 eV synchrotron radiation for extended periods of time is shown in Figure 7.1 (iii). This series represents a total dose of $3.58 \times 10^{15}$ photons (80 minutes exposure at a photon flux of $7.46 \times 10^{11}$ photons/sec/200mA). Due to the close proximity of the C1s components from $C_{60}F_{48}$ and the beam damage components which would evolve during exposure[40] to the diamond components, it is not possible to determine at this stage of the experiment whether there is a component developing due to fluorination of the underlying diamond surface. However, the peak at 289 eV provides a clear marker for the presence of the fluorofullerenes; following deposition and measurement, the sample was then annealed to 550°C for five minutes to remove the molecules.[84] As mentioned, the molecules undergo beam-damage induced decomposition which may alter their properties, so a carbon core level spectrum was measured after annealing both on an area of the sample which had not been previously scanned (Figure 7.1 (iv)), and an area which had been beam-damaged (v). Both areas showed near-complete (>99%) removal of fluorofullerene-related components with the anneal, although the beam damaged area had a small feature at 288 eV. We attribute this to molecular fragments produced by the heavy irradiation subsequently rebonding into a more stable form.

After annealing, neither spectrum exhibited peaks to higher binding energy attributable to direct fluorination of the diamond surface,[84, 167] and the components to lower binding energy of the bulk attributed to the silicon termination are still present, indicating that annealing with a fluorine source does not strip silicon off

the surface. Rietwyk *et al.*[84] observed fluorinated diamond C-F peaks after annealing to 700°C, so we state with confidence that the molecular treatment in this case modifies only the silicon layer and not the underlying carbon. Having shown that $C_{60}F_{48}$ is able to adhere to the surface, and subsequently be removed by annealing, we move on to examining the effect of this process on the Si2p core level.

**Silicon core level evolution**

While $C_{60}F_{48}$ exposure does not result in fluorine bonding with the surface carbon, the converse is seen for the surface silicon. The Si2p core level for the as-prepared silicon termination, Figure 7.2 (i) (presented with the $Si2p_{1/2}$ component subtracted for clarity), matches that seen in previous studies.[4, 18, 19] It is comprised primarily (71%) of a component assigned to silicon atoms bonded to two carbon atoms, and possessing two dangling or weakly cross-coupled ('accessible') bonds; we refer to this component, below, as the '+0' species. An additional component (28% of the core level intensity) exists to higher binding energy, representing a higher oxidation state ('+1'). As the survey spectrum for this sample does not exhibit sufficient oxygen to attribute this state to $C_2SiO$, this component is attributed to step-edge silicon bonded to 3 carbon atoms, consistent with the work of Schenk *et al.*[18] Finally, there is a negligible (1%) component attributed to excess silicon—this component is removed immediately by molecular deposition and will not be discussed further in this work.

Deposition of $C_{60}F_{48}$ onto the pristine surface leads to the immediate formation of two higher binding energy components (See Fig. 7.2 (ii)). For reasons which will be discussed later, we denote these components as +2F and +3F, attributing them to silicon sites which have been fluorinated due to spontaneous abstractiuon of fluorine from $C_{60}F_{48}$. As observed in the previous section, extended synchrotron illumination decomposes $C_{60}F_{48}$, and we expect that this generates free fluorine atoms[84] and thus will increase the relative intensity of the components attributed to the fluorine-bonded silicon atoms. This expectation is bourne out in Fig. 7.2 (iii), which shows the silicon core level structure after the beam damage treatment. While no new chemical species form, the +2F and +3F components increase in intensity, concomitant with the decrease in the +0 state, the unfluorinated surface silicon. This occurs in step with the decrease in intensity of the molecule-related peaks seen in the C1s spectrum, Fig. 7.1 (iii), indicating that this process liberates fluorine which then bonds to the unsatisfied silicon dangling bonds. For the sake of quantitative comparison, the stacked column chart in Figure 7.2 shows the percentage of the core level associated with each oxidation state as the core level evolves.

Annealing the sample to 550°C to remove the $C_{60}F_{48}$ adlayer causes further changes to the Si2p core level. Figure 7.2 (iv) was acquired on a spot which did not undergo long-term radiation exposure, this Si2p core level corresponds to the C1s core level shown in Fig. 7.1 (iv). The Si2p core level shows that the fluorinated silicon species persist after annealing. Comparing Fig. 7.2 (iv) and (ii), it is seen that the contribution from the +0 species has reduced (45% to 21%), and the +1 species now dominates

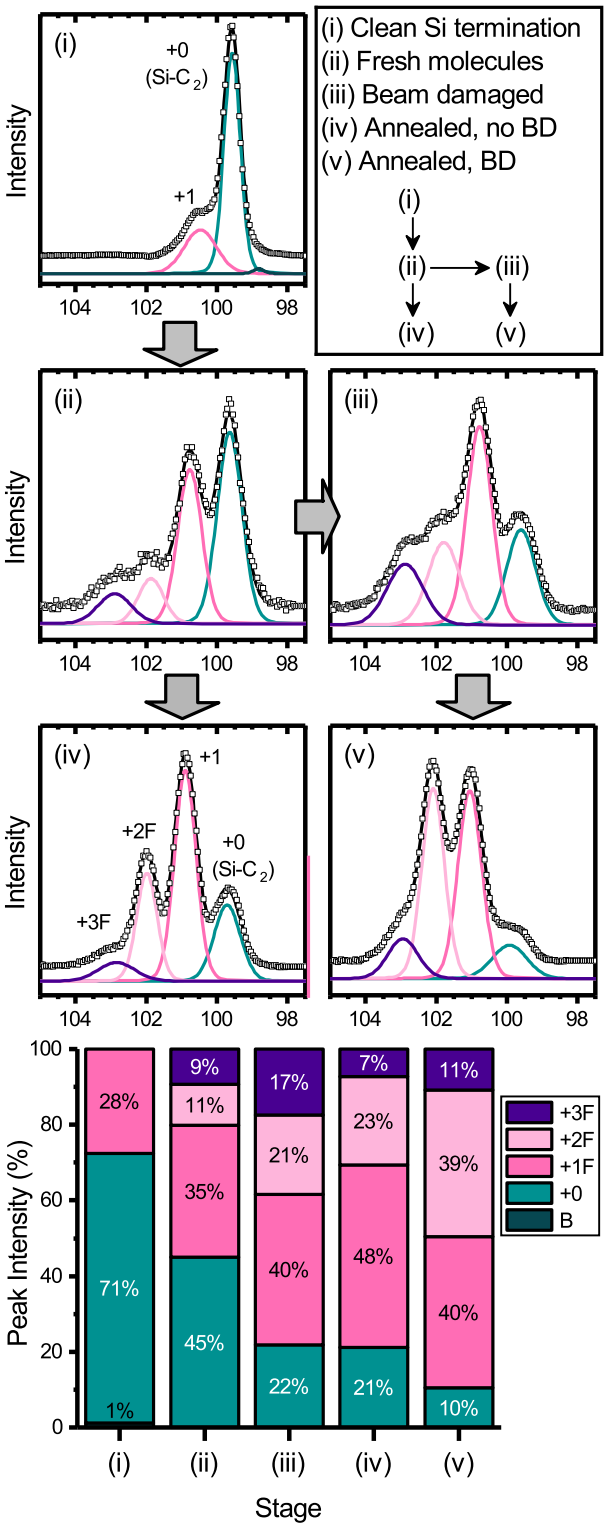


FIGURE 7.2: Evolution in core level appearance from silicon termination, through deposition of $C_{60}F_{48}$, exposure of $C_{60}F_{48}$ to synchrotron radiation, and finally annealing.

the spectrum. While the +2F species has increased from (ii), the proportion of +3F silicon has decreased, and still no +4F species is seen. As silicon tetrafluoride can leave the surface of bulk silicon as a gas,[169] we expect that behaviour to be seen on this surface also, explaining the absence of that species in the silicon core level. The increase of +1 and +2F silicon concurrent with the decrease of +3F silicon suggests that species in the +3F oxidation state may be removed by bonding to a fourth fluorine atom during annealing.

To determine the effect of beam damage prior to annealing, the spectrum shown in Fig. 7.2 (v) was recorded on the same location as (iii), which had been thoroughly exposed. Annealing still results in a decrease in unfluorinated silicon (22% to 10%), this method yielding the lowest proportion of the +0 species. This state represents a nearly equal proportion of +1 and +2F silicon; it also shows a decrease in the proportion of +3F silicon, which was also seen on the non beam-damaged region. This affirms the hypothesis that access to excess fluorine may allow silicon to be removed from the surface through the formation of $SiF_{4(g)}$.

Until this point we have implicitly assumed that the Si2p components developing throughout this experiment are associated with fluorine-silicon bonding, without providing a clear justification, so we now turn to the fitting model we have employed when analysing the Si2p core level of the surface throughout this process. We acknowledge that fluorine is not the only species which may cause the formation of components to high binding energy in the Si2p spectra of the silicon-terminated diamond surface, with published work existing for oxidation of this surface[19], and oxygen is a common vacuum contaminant. Figure 7.3 shows the Si2p core level of as-prepared silicon-terminated diamond (i), the final stage fluorinated silicon-terminated surface of this study (ii), and an oxygen-exposed silicon-terminated diamond surface (iii), as well as the associated survey scans. While it is clear that both fluorination and oxidation create higher binding energy components, the components associated with fluorination have a larger associated chemical shift than those in the oxidised sample. Additionally, the survey scan for the fluorinated surface shows no oxygen-related signals. Combined, these two factors give credence to our assessment that we have fluorinated the silicon-terminated diamond surface, and can quantitatively evaluate the evolution of the process with some certainty. It is unclear from the data we have acquired whether the preferred state of the surface is with one or two fluorine atoms per silicon. Each silicon has, in theory, two dangling bonds which seek to be satisfied,[4] but attaching a fluorine to each may be sterically hindered due to the large size of fluorine and the high packing density such a structure would represent. Counting one fluorine atom per oxidation state increase, the method used for (iv) results in 1.2 fluorine atoms per silicon, while the method used for (v) results in 1.5 F/Si. We note that for both cases there is still a non-negligible proportion of the silicon remaining which has not been terminated by fluorine, and

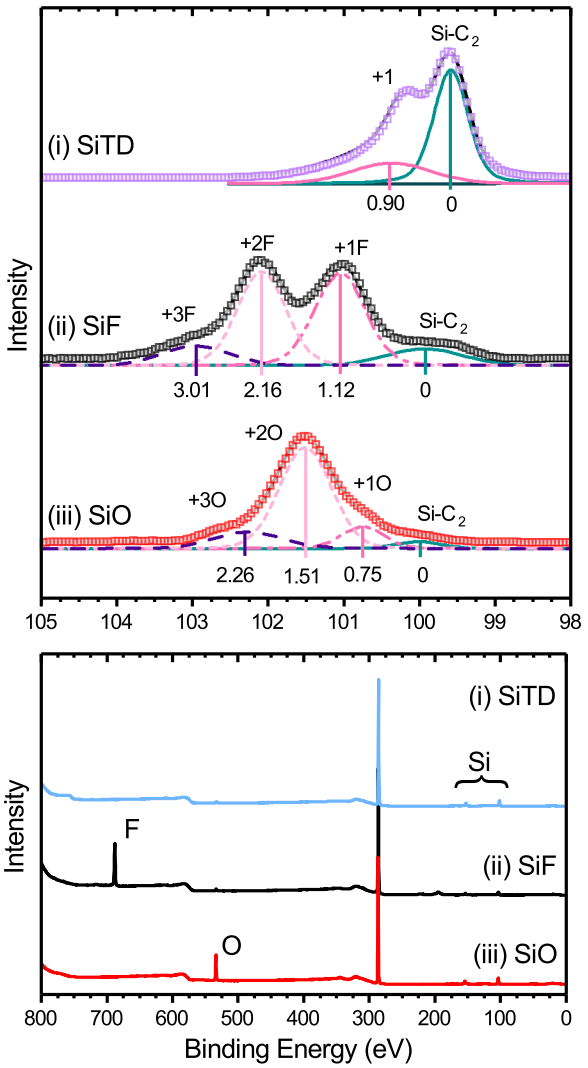


FIGURE 7.3: A comparison of the survey scans and fitting models employed for the Si2p core level of (i) pristine silicon-terminated diamond, (ii) fluorinated silicon-terminated diamond and (iii) oxidised silicon-terminated diamond.

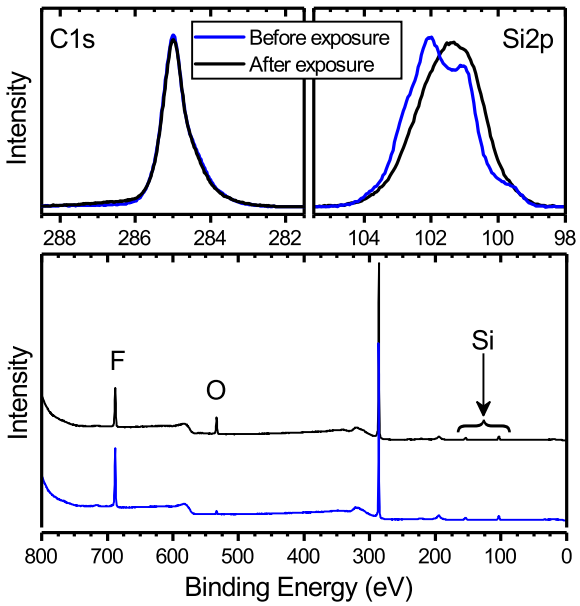


FIGURE 7.4: Atmosphere exposure of the incompletely fluorinated surface results in adsorption of oxygen and broadening of the silicon core level

so further processes may need to be developed in order to achieve a complete fluorine coverage. In both cases, the annealing process increases fluorination and decreases the amount of triply fluorinated silicon. If the goal is to achieve as complete a fluorination as possible, the damage-then-anneal method is preferable. Alternatively, if homogeneity is the goal, then the non beam-damaged method which yields 48% $Si^{+1}$ is superior. The latter method also minimizes the $Si^{+3}$ component of the spectrum, and represent the majority of the sample surface.

Determining the favourable structure will require further study, but we have demonstrated that deposition of $C_{60}F_{48}$ results in fluorine-silicon bonding on the surface, concurrent with the retention of the carbon-silicon bonds which characterize the termination. Both of these bonds also persist after removal of the molecular layer by annealing. That is to say, we have demonstrated the formation of a C-Si-F "bilayer termination". This shows that the silicon termination, in vacuum, retains the desirable property of the bare diamond surface to be tuned by chemical passivation.

### Atmospheric stability of F-SiTD

Having established the ability to modify the silicon-terminated diamond surface with fluorine, we now consider the stability of that fluorinated layer. We have previously demonstrated that 10 minutes of atmosphere exposure is sufficient to cause near-complete oxidation of the silicon terminated surface.[19] In order to determine whether the C−SiF layer is resistant to the removal of fluorine by oxygenation in atmosphere, the sample was removed from vacuum, held in ambient pressure for 10 minutes, and returned to UHV. The results of this treatment may be seen in Figure

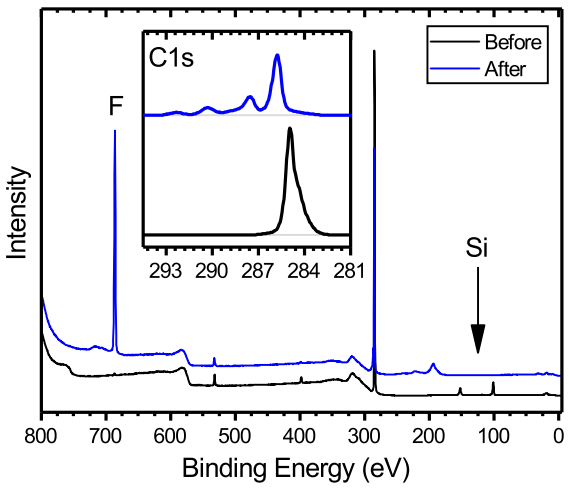


FIGURE 7.5: $SF_6$ plasma treatment of silicon terminated diamond results in the removal of silicon and the formation of fluorinated diamond.

7.4. The exposure to atmosphere causes the adsorption of a large amount of oxygen to the surface *without* apparent loss of fluorine, indicating that the fluorinated silicon is resistant to oxidation. Concurrent with the formation of the oxide component in the survey spectrum, a significant degree of broadening is observed in the silicon core level.

As seen in Figure 7.3, the oxidized and fluorinated silicon components are offset in energy, in their respective spectra. As each peak, additionally, is a doublet, the core level which results from a combination of oxidized and fluorinated silicon does not yield to decomposition in any meaningful way. Since the many components attributed to oxidation and fluorination required for fitting this core level increase the fitting ambiguity to the point that we cannot generate a unique fit, we instead note qualitatively that the silicon core level shows growth in the lower binding energy area of the spectrum, which is consistent with oxygen bonding. As the annealed, non beam-damaged, surface (Fig. 7.2 (iv)) showed an average of 1.2 F atoms per silicon, it is reasonable that the remaining 0.8 bonds per atom may be satisfied by oxygen in the high pressure atmospheric environment,[19, 166] saturating the surface. The retention of fluorine after atmosphere exposure proves that the Group IV termination family represents a diamond surface platform which retains the chemical and electronic tunability of the bare diamond surface. This tunability is a useful property for the development of diamond based functional devices.

**Plasma fluorination of SiTD**

As the fluorination procedure we have demonstrated until this point is fairly complex, it is reasonable to consider if there are other avenues to the same result. Diamond surface fluorination has previously been achieved by exposing the surface to $SF_6$ plasma,[170] a standard processing method in microfabrication. Figure 7.5

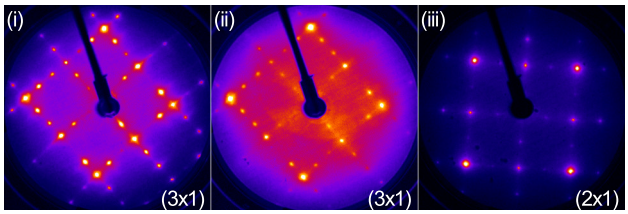


FIGURE 7.6: LEED patterns for (i) the bare silicon termination, showing the characteristic $(3 \times 1)$ reconstruction, (ii) the $C_{60}F_{48}$ fluorinated silicon termination, also $(3 \times 1)$, and (iii) the $SF_6$ plasma treated surface, with a $(2 \times 1)$ reconstruction.

shows x-ray photoelectron spectra acquired on a pristine SiTD surface, and spectra after the same sample has been removed from UHV, exposed to $SF_6$ plasma, and reintroduced to UHV. Before processing, the data reflect what is expected from an as-prepared SiTD surface: a survey spectrum with silicon, carbon and a small proportion of contaminant oxygen, and a C1s spectrum with two components to lower binding energy of the diamond bulk.[4] After plasma treatment, the survey shows that silicon was completely removed from the sample and the growth of a very large F1s peak. The carbon core level also showed several high binding energy components, consistent with various $CF_n$ species. We conclude from this that the plasma treatment removed the silicon monolayer from the sample, not an entirely unexpected result given that $SF_6$ plasma has been observed to etch silicon carbide.[171] This suggests that it may be necessary to rely on milder fluorination methods such as the molecular decomposition approach we have employed here.

As a final matter, we consider the effect fluorination of the SiTD surface has on reconstruction and surface order. Silicon-terminated (100) diamond has been demonstrated to possess a well ordered, two-domain $(3 \times 1)$ surface structure,[4] as shown in Fig 7.6(i). Following the $C_{60}F_{48}$ fluorination treatment, the sample retained its sharp $(3 \times 1)$ LEED pattern with some increase in background signal, but no new spots forming. Retention of the silicon terminated diamond symmetry after adlayer adsorption was also seen in previous studies for the oxidized silicon and germanium terminations.[19, 166] This suggests the fluorine-exposed surface is also highly ordered. Conversely, the sample which was exposed to $SF_6$ plasma treatment demonstrated a $(2 \times 1)$ symmetry pattern, consistent with regular fluorinated diamond, and also with the complete loss of silicon as observed by XPS.

### 7.3.5 Conclusion

We have demonstrated the ability to modify the silicon terminated (100) diamond surface with fluorine, employing decomposition of $C_{60}F_{48}$, which has previously been used to fluorinate diamond[84] and silicon carbide.[168] This is an important demonstration of the tunability of the Group IV termination family. We have achieved a fluorine coverage of at least 1.2 F/Si, and suspect higher coverages may

be possible with further optimisation. This fluorinated surface retains the $3 \times 1$ order of the underlying silicon-terminated surface.

Exposure of the (incompletely) fluorinated surface to atmosphere results in a combination of oxygen and fluorine bonds to the surface silicon, while the underlying carbon remains shielded. The bonded fluorine appears to be resistant to replacement with oxygen, suggesting that a completely fluorinated surface may be robust to atmosphere exposure.

We have also shown that $SF_6$ treatment of the silicon-terminated surface results in removal of the silicon, producing a traditional fluorinated diamond surface. From this we can infer that care may need to be taken when developing processing methods for the silicon-terminated diamond surface, as it is clear that this termination can be removed with plasma processing.

We believe that the unusual electronic structure of the atomic trilayer surface may yield technologically interesting behaviour for the purpose of diamond device fabrication.

## Acknowledgements

This research was undertaken using the Soft X-ray Spectroscopy beamline at the Australian Synchrotron, Victoria, Australia. This work was performed in part at the Melbourne Centre for Nanofabrication (MCN) in the Victorian Node of the Australian National Fabrication Facility (ANFF).This work was supported by the Australian Research Council under the Discovery Project (DP150101673). This work was partly supported by the Research Council of Norway through its Centres of Excellence funding scheme, Project No. 262633, “QuSpin”, and through the Fripro program, Project No. 250985 “FunTopoMat”.

# Chapter 8

# Conclusion

This thesis has presented four studies focused on producing, adapting and exploiting Group IV based diamond (100) surface terminations, analysed by x-ray photoelectron spectroscopy and low energy electron diffraction.

Following the establishment of a unique diamond (100) termination using silicon, this thesis sought to address features which would be desired for use of that termination in real world devices.

## 8.1 Summary

Chapter 4 showed an investigation into the adaptability of the silicon terminated diamond production method. We showed that the same method which produced SiTD could be used for the formation of germanium terminated diamond, involving deposition of an amorpous layer in vacuum and annealing. As they form similar crystal structures and bonding arrangements, we predicted that germanium would bond in the same way as silicon at the diamond surface. Access to an ordered germanium monolayer is desirable because literature-established germanium-sulfur chemistry presents a pathway for attaching biomolecules to diamond *via* a disulfide bond. We found that while the method did cause the formation of a $(3 \times 1)$ reconstruction and Ge-C bonds, it has a sterically limited coverage of 0.63 ML. These results are published in *Journal of Physics: Condensed Matter* 29.14 (2017): 145002.

Chapter 5 showed an example of the functionality of the oxidized silicon termination. By tracking the change in C1s bulk position with XPS, and the Fermi level by contact potential difference measurements, we demonstrated that the oxidized silicon terminated surface could be surface transfer doped using MoC$_8$. Existing surface conductive diamond devices utilize the hydrogen terminated surface, as it is the only termination which has been shown to transfer dope. Showing that a separate system is susceptible to transfer doping is a strong point in favour of the practical viability of the silicon termination in diamond electronic devices. We showed an observable downward shift in the Fermi level position, concurrent with the growth of a charged component in the dopant Mo3d core level, indicating the formation of a hole accumulation layer. This work has been published in *Applied Physics Letters* **110**, 011605 (2017).

Chapter 6 showed a further investigation into the practical viability of the Group IV terminations, through analysing their chemical and thermal stability. We showed that the silicon and germanium terminations are both stable under annealing to at least 1200°C, and quantified the thermal stability of the oxidized silicon and oxidized germanium terminations. In order to be used in standard device fabrication processes, it is necessary for the new terminations we have made to be stable in atmosphere, and able to withstand standard annealing processes. A limitation in the existing well studied diamond surface terminations, oxygen and hydrogen, is that that are removed from the surface at around 500°C and 950°C respectively. If they are to be competitive, our new terminations should also be thermally stable to at least this range. We found that in fact, the GeTD and SiTD surfaces are stable to much higher than 950°C, persisting in the temperature range at which the bare surface graphitizes, indicating that they have a stabilizing effect. The oxidized silicon termination is also stable to above 1200°C, while the germanium termination is limited to low temperature annealing. In combination with the previous study, the oxidized silicon termination appears to be an interesting candidate for further device studies. This work has been published in *Physica Status Solidi A* **2018**, *215*, 1800283.

Chapter 7 showed an investigation into the tunability of the silicon terminated diamond surface. We showed that it is possible to functionalize the silicon termination with fluorine, forming a two layer termination. The appealing property of the diamond surface which was a motivator for the work in this thesis, is the ability to tune the chemical and electronic properties of the surface by a change of the terminating chemical species. For hydrogen and oxygen terminations, this means a change from conductive to insulating in air, and also a change in electron affinity. In this study, we showed that decomposition of $C_{60}F_{48}$ on the SiTD surface, as a way to generate active fluorine atoms, results in silicon-fluorine bonding, and the formation of a fluorinated silicon termination that appears to be resistant to atmospheric oxidation. This result opens up the possibility of a SiTD based analogy to the existing hydrogen-oxygen termination-patterned diamond surface electronic device design. This work has been submitted to Journal of Physics: Condensed Matter (December 2018).

## 8.2 Further Work

Chapter 4 showed that the simple method of in-vacuum deposition onto the hydrogen terminated surface, followed by annealing, was sufficient for the formation of both silicon and germanium bonds. It is worth investigating whether other elements may also be bonded to diamond in this way, as it a method which does not rely on the formation of reactive atomic species by plasma or radical beam methods, and can be performed in an extremely clean UHV environment.

The germanium termination study presented in Chapter 4 tried a range of methods to produce a complete germanium monolayer, and was unsuccessful in doing so. It may be that a complete termination is possible, but doing so would require further study. Similarly, the fluorination study in Chapter 7 did not achieve a complete monolayer fluorination. This may have been due to the procedure which was used and also should be studied further in the future. The surface was also fluorinated on a sample which could not have its work function measured by Kelvin probe, so further work should involve a work function measurement of that system to establish the upper limit of possible electron affinity of silicon terminations.

The study in Chapter 7 proved that silicon terminated diamond can be modified with elements other than oxygen. One process which has not yet been attempted on the silicon termination surface is the formation of a bonded phosphorus layer. The premise of this experiment would be the work of O'Brien *et al.*[172], which showed that phosphine molecules may be attached to silicon dangling bonds in vacuum, and the intrinsic dense array of dangling bonds on the SiTD surface to form a dense layer of bonded phosphorus on top of diamond.

While we have shown a range of properties and functionalities which are achievable within the Group IV termination family, we have yet to fabricate a real-world device using these surfaces. It would be worthwhile to pursue an electronic conductivity study using a four point probe system, to directly determine how the observed band bending in Chapter 5 affects the surface conductivity. If electronic measurements confirm that a conductive hole accumulation layer can be formed, then the question that needs to be addressed is whether the silicon terminations can be effectively patterned. The base silicon termination may be patternable by depositing silicon through a physical mask, causing only exposed areas to be terminated when the sample is subsequently annealed, while the fluorine termination may be patterned upon the base silicon termination by the same method. If it is possible to selectively terminate regions of the surface in this way, then these patterned regions should also undergo conductivity studies.

The silicon terminated surface represents a sharp, ordered heteroatomic interface. It is worth investigating whether this interface remains crystalline and ordered with the deposition of a further thick layer of silicon. With the small size of the diamond lattice, it is difficult to form an atomically sharp interface, since the high density of dangling bonds are not easily satisfied by other semiconductor surfaces.

A crystalline interface between silicon and diamond would be extremely interesting for creating electronic devices, offering access to the established device fabrication processes on silicon, with the high strength and unparalleled thermal conductivity of diamond.

Surface conductive devices are a highly interesting class of diamond electronic devices, which exploit the change in electronic properties caused by changing the chemical termination of the surface. Having shown that the Group IV family of diamond (100) terminations exhibit a range of properties which are potentially useful for device fabrication, the natural next step is to attempt to fabricate and characterise a range of such devices.

# Bibliography


1. O'Donnell, K. M., Martin, T. L. & Allan, N. L. Light Metals on Oxygen-Terminated Diamond (100): Structure and Electronic Properties. *Chemistry of Materials* **27,** 1306–1315. ISSN: 0897-4756 (Feb. 2015).
2. Maier, F, Riedel, M, Mantel, B, Ristein, J & Ley, L. Origin of surface conductivity in diamond. *Physical review letters* **85,** 3472 (2000).
3. Edmonds, M. T. *et al.* Spin–Orbit Interaction in a Two-Dimensional Hole Gas at the Surface of Hydrogenated Diamond. *Nano letters* **15,** 16–20 (2014).
4. Schenk, A. *et al.* Formation of a silicon terminated (100) diamond surface. *Applied Physics Letters* **106,** 191603 (2015).
5. Siegbahn, K. & Nordling, C. ESCA, atomic, molecular and solid state structure studied by means of electron spectroscopy. *Nov. Act. Uppsaliensis* (1967).
6. Einstein, A. On a heuristic point of view about the creation and conversion of light. *Annalen der Physik* **17,** 132–148 (1905).
7. *The Nobel Prize in Physics 1921* 2014. <http://www.nobelprize.org/nobel_prizes/physics/laureates/1921/index.html>.
8. Wiedemann, H. *Synchrotron radiation* (Springer, 2003).
9. *How Diamond Works* <https://www.diamond.ac.uk/Public/How-Diamond-Works.html>.
10. Shaftan, T. *Synchrotron Radiation - Joint CFN and NSLS-II Synchrotron Lecture Series* <https://www.bnl.gov/ps/userguide/lectures/Lecture-2-Shaftan.pdf>.
11. *How does the Australian Synchrotron work?* <http://archive.synchrotron.org.au/index.php/about-us/our-facilities/accelerator-physics/how-does-the-australian-synchrotron-work>.
12. Shabalin, A. *Coherent X-ray diffraction studies of mesoscopic materials* PhD thesis (Feb. 2016). doi:10.13140/RG.2.1.4004.5680.
13. *Insertion Devices* <http://www.esrf.eu/UsersAndScience/Publications/Highlights/2000/machine/XS7.html>.
14. Schlaf, R. *Calibration of Photoemission Spectra and Work Function Determination* <http://rsl.eng.usf.edu/Documents/Tutorials/PEScalibration.pdf>.
15. Shirley, D. A. High-resolution X-ray photoemission spectrum of the valence bands of gold. *Physical Review B* **5,** 4709 (1972).
16. Rietwyk, K. PhD thesis (Oct. 2013).
17. Schenk, A. K. *et al.* High resolution core level spectroscopy of hydrogen-terminated (1 0 0) diamond. *Journal of Physics: Condensed Matter* **28,** 305001 (2016).
18. Schenk, A. *et al.* The surface electronic structure of silicon terminated (100) diamond. *Nanotechnology* **27,** 275201 (2016).

19. Schenk, A. K., Sear, M. J., Tadich, A, Stacey, A & Pakes, C. I. Oxidation of the silicon terminated (1 0 0) diamond surface. *Journal of Physics: Condensed Matter* **29,** 025003 (2016).

20. Graupner, R, Maier, F, Ristein, J, Ley, L & Jung, C. High-resolution surface-sensitive C 1 s core-level spectra of clean and hydrogen-terminated diamond (100) and (111) surfaces. *Physical Review B* **57,** 12397 (1998).

21. Bobrov, K., Mayne, A., Hoffman, A. & Dujardin, G. Atomic-scale desorption of hydrogen from hydrogenated diamond surfaces using the STM. *Surface Science* **528,** 138–143. ISSN: 0039-6028 (Mar. 2003).

22. Stöhr, J. *NEXAFS Spectroscopy* 403. ISBN: 3540544224 (Springer Science & Business Media, 1992).

23. Hüfner, S. *Photoelectron Spectroscopy Principles and Applications* 3rd ed., 978–3–662–09280–4. ISBN: 978-3-662-09280-4. <https://link.springer.com/book/10.1007{\%}2F978-3-662-09280-4> (Springer-Verlag Berlin, 2003).

24. Emtsev, K. *et al.* Electronic properties of clean unreconstructed 6H–SiC(0 0 0 1) surfaces studied by angle resolved photoelectron spectroscopy. *Surface Science* **600,** 3845–3850. ISSN: 0039-6028 (Sept. 2006).

25. Popa, E., Notsu, H., Miwa, T., Tryk, D. A. & Fujishima, A. Selective Electrochemical Detection of Dopamine in the Presence of Ascorbic Acid at Anodized Diamond Thin Film Electrodes. *Electrochemical and Solid-State Letters* **2,** 49. ISSN: 10990062 (Jan. 1999).

26. Notsu, H., Fukazawa, T., Tatsuma, T., Tryk, D. A. & Fujishima, A. Hydroxyl Groups on Boron-Doped Diamond Electrodes and Their Modification with a Silane Coupling Agent. *Electrochemical and Solid-State Letters* **4,** H1. ISSN: 10990062 (Mar. 2001).

27. Actis, P. *et al.* Localized electropolymerization on oxidized boron-doped diamond electrodes modified with pyrrolyl units. *Physical Chemistry Chemical Physics* **8,** 4924. ISSN: 1463-9076 (Oct. 2006).

28. Sque, S. J., Jones, R, Goss, J. P., Briddon, P. R. & Öberg, S. First-principles study of C 60 and C 60 F 36 as transfer dopants for p-type diamond. en. *Journal of Physics: Condensed Matter* **17,** L21–L26. ISSN: 0953-8984 (Jan. 2005).

29. Sque, S. J., Jones, R. & Briddon, P. R. Structure, electronics, and interaction of hydrogen and oxygen on diamond surfaces. *Physical Review B* **73,** 085313. ISSN: 1098-0121 (Feb. 2006).

30. Kawarada, H. Hydrogen-terminated diamond surfaces and interfaces. *Surface Science Reports* **26,** 205–259. ISSN: 0167-5729 (Jan. 1996).

31. Kobashi, K. *Diamond films : chemical vapor deposition for oriented and heteroepitaxial growth* 336. ISBN: 9780080447230 (London, 2005).

32. Maier, F., Ristein, J. & Ley, L. Electron affinity of plasma-hydrogenated and chemically oxidized diamond (100) surfaces. *Physical Review B* **64,** 165411. ISSN: 0163-1829 (Oct. 2001).

33. Schenk, A. *et al.* High resolution core level spectroscopy of hydrogen-terminated (1 0 0) diamond. *Journal of Physics: Condensed Matter* **28,** 305001 (2016).

34. Landstrass, M. I. & Ravi, K. V. Hydrogen passivation of electrically active defects in diamond. *Applied Physics Letters* **55,** 1391–1393. ISSN: 0003-6951 (Oct. 1989).

35. Landstrass, M. I. & Ravi, K. V. Resistivity of chemical vapor deposited diamond films. *Applied Physics Letters* **55,** 975–977. ISSN: 0003-6951 (Sept. 1989).
36. Shirafuji, J. & Sugino, T. Electrical properties of diamond surfaces. *Diamond and Related Materials* **5,** 706–713. ISSN: 0925-9635 (May 1996).
37. Hayashi, K. *et al.* Investigation of the effect of hydrogen on electrical and optical properties in chemical vapor deposited on homoepitaxial diamond films. *Journal of Applied Physics* **81,** 744. ISSN: 0021-8979 (Aug. 1998).
38. Denisenko, A. *et al.* Hypothesis on the conductivity mechanism in hydrogen terminated diamond films. *Diamond and Related Materials* **9,** 1138–1142. ISSN: 0925-9635 (Apr. 2000).
39. Maier, F., Riedel, M., Mantel, B., Ristein, J. & Ley, L. Origin of Surface Conductivity in Diamond. *Physical Review Letters* **85,** 3472–3475. ISSN: 0031-9007 (Oct. 2000).
40. Edmonds, M. *et al.* Surface transfer doping of hydrogen-terminated diamond by C60F48: Energy level scheme and doping efficiency. *The Journal of chemical physics* **136,** 124701 (2012).
41. Qi, D. *et al.* Surface transfer doping of diamond (100) by tetrafluoro-tetracyanoquinodimethane. *Journal of the American Chemical Society* **129,** 8084–8085 (2007).
42. Chen, W., Qi, D., Gao, X. & Wee, A. T. S. Surface transfer doping of semiconductors. *Progress in Surface Science* **84,** 279–321. ISSN: 0079-6816 (Sept. 2009).
43. Crawford, K. G. *et al.* Enhanced surface transfer doping of diamond by $V_2O_5$ with improved thermal stability. *Applied Physics Letters* **108,** 042103 (2016).
44. Russell, S. A. *et al.* Surface transfer doping of diamond by $MoO_3$: A combined spectroscopic and Hall measurement study. *Applied Physics Letters* **103,** 202112 (2013).
45. O'Donnell, K. M. *et al.* Extremely high negative electron affinity of diamond via magnesium adsorption. *Physical Review B* **92,** 035303 (2015).
46. Torrengo, S. *et al.* The role of oxygen in the one step amination process of nanocrystalline diamond surface. *Diamond and Related Materials* **20,** 990–994. ISSN: 0925-9635 (July 2011).
47. Maier, F, Ristein, J & Ley, L. Electron affinity of plasma-hydrogenated and chemically oxidized diamond (100) surfaces. *Physical Review B* **64,** 165411 (2001).
48. Hauf, M. V. *et al.* Chemical control of the charge state of nitrogen-vacancy centers in diamond. *Physical Review B* **83,** 081304. ISSN: 1098-0121 (Feb. 2011).
49. Klauser, F. *et al.* Comparison of different oxidation techniques on single-crystal and nanocrystalline diamond surfaces. *Diamond and Related Materials* **19,** 474–478 (2010).
50. Notsu, H., Yagi, I., Tatsuma, T., Tryk, D. A. & Fujishima, A. Surface carbonyl groups on oxidized diamond electrodes. *Journal of Electroanalytical Chemistry* **492,** 31–37. ISSN: 1572-6657 (Sept. 2000).
51. Martin, T. L. *et al.* Lithium monolayers on single crystal C(100) oxygen-terminated diamond. *MRS Proceedings* **1282,** mrsf10–1282–a06–03. ISSN: 1946-4274 (Jan. 2011).
52. Stacey, A. *et al.* Nitrogen Terminated Diamond. *Advanced Materials Interfaces* **2** (2015).

53. Chandran, M., Shasha, M., Michaelson, S., Akhvlediani, R. & Hoffman, A. Incorporation of nitrogen into polycrystalline diamond surfaces by RF plasma nitridation process at different temperatures: Bonding configuration and thermal stabilty studies by in situ XPS and HREELS. *physica status solidi (a)* **212,** 2487–2495. ISSN: 18626300 (Nov. 2015).

54. Chandran, M., Shasha, M., Michaelson, S. & Hoffman, A. Nitrogen termination of single crystal (100) diamond surface by radio frequency N <sub>2</sub> plasma process: An in-situ x-ray photoemission spectroscopy and secondary electron emission studies. *Applied Physics Letters* **107,** 111602. ISSN: 0003-6951 (Sept. 2015).

55. Denisenko, A., Romanyuk, A., Kibler, L. & Kohn, E. Surface structure and electrochemical characteristics of boron-doped diamond exposed to rf N2-plasma. *Journal of Electroanalytical Chemistry* **657,** 164–171. ISSN: 1572-6657 (July 2011).

56. Attrash, M., Kuntumalla, M. K. & Hoffman, A. Bonding, structural properties and thermal stability of low damage RF (N2) plasma treated diamond (100) surfaces studied by XPS, LEED, and TPD. *Surface Science* **681,** 95–103. ISSN: 0039-6028 (Mar. 2019).

57. Chou, J.-P., Retzker, A. & Gali, A. Nitrogen-Terminated Diamond (111) Surface for Room-Temperature Quantum Sensing and Simulation. *Nano Letters* **17,** 2294–2298. ISSN: 1530-6984 (Apr. 2017).

58. Kuntumalla, M. K., Attrash, M., Li, F. & Hoffman, A. Influence of RF(N2) plasma conditions on the chemical interaction and stability of activated nitrogen with polycrystalline diamond surfaces: A XPS, TPD and HREELS study. *Surface Science* **679,** 37–49. ISSN: 0039-6028 (Jan. 2019).

59. Wei, J. *et al.* Amination of diamond film by ammonia microwave plasma treatment. *Diamond and Related Materials* **54,** 34–38. ISSN: 0925-9635 (Apr. 2015).

60. Suaebah, E. *et al.* Aptamer strategy for ATP detection on nanocrystalline diamond functionalized by a nitrogen and hydrogen radical beam system. *Journal of Applied Physics* **121,** 044506. ISSN: 0021-8979 (Jan. 2017).

61. Szunerits, S. *et al.* Direct amination of hydrogen-terminated boron doped diamond surfaces. *Electrochemistry Communications* **8,** 1185–1190. ISSN: 13882481 (July 2006).

62. Koch, H. *et al.* Plasma amination of ultrananocrystalline diamond/amorphous carbon composite films for the attachment of biomolecules. *Diamond and Related Materials* **20,** 254–258. ISSN: 0925-9635 (Feb. 2011).

63. Zhang, G.-J. *et al.* DNA Micropatterning on Polycrystalline Diamond via One-Step Direct Amination. *Langmuir* **22,** 3728–3734. ISSN: 0743-7463 (Apr. 2006).

64. Simon, N. *et al.* Direct amination of diamond surfaces by electroless treatment in liquid ammonia solution. *Electrochemistry Communications* **42,** 17–20. ISSN: 1388-2481 (May 2014).

65. Todd Strother, *et al.* Photochemical Functionalization of Diamond Films. doi:10.1021/LA0112561. <https://pubs.acs.org/doi/abs/10.1021/la0112561> (2002).

66. May, P. *et al.* The effect of diamond surface termination species upon field emission properties. *Diamond and Related Materials* **7,** 671–676. ISSN: 0925-9635 (Feb. 1998).

67. Miller, J. B. & Brown, D. W. Photochemical Modification of Diamond Surfaces. doi:10.1021/LA9407166. <https://pubs.acs.org/doi/full/10.1021/la9407166> (1996).

68. Cai, J., Retzker, A., Jelezko, F. & Plenio, M. B. A large-scale quantum simulator on a diamond surface at room temperature. *Nature Physics* **9,** 168–173. ISSN: 1745-2473 (Mar. 2013).

69. Cai, J., Retzker, A., Jelezko, F. & Plenio, M. B. A large-scale quantum simulator on a diamond surface at room temperature. *Nature Physics* **9,** 168 (2013).

70. Cui, S. & Hu, E. L. Increased negatively charged nitrogen-vacancy centers in fluorinated diamond. *Applied Physics Letters* **103,** 051603. ISSN: 0003-6951 (July 2013).

71. Karlsson, M., Forsberg, P. & Nikolajeff, F. From Hydrophilic to Superhydrophobic: Fabrication of Micrometer-Sized Nail-Head-Shaped Pillars in Diamond. *Langmuir* **26,** 889–893. ISSN: 0743-7463 (Jan. 2010).

72. Popov, C. *et al.* Surface modification of nanocrystalline diamond/amorphous carbon composite films. *Diamond and Related Materials* **17,** 1229–1234. ISSN: 0925-9635 (July 2008).

73. Schvartzman, M & Wind, S. J. Plasma fluorination of diamond-like carbon surfaces: mechanism and application to nanoimprint lithography. *Nanotechnology* **20,** 145306. ISSN: 0957-4484 (Apr. 2009).

74. Ferro, S. & Battisti, A. D. The 5-V Window of Polarizability of Fluorinated Diamond Electrodes in Aqueous Solutions. doi:10.1021/AC034717R. <https://pubs.acs.org/doi/abs/10.1021/ac034717r> (2003).

75. Sine, G., Ouattara, L., Panizza, M. & Comninellis, C. Electrochemical Behavior of Fluorinated Boron-Doped Diamond. *Electrochemical and Solid-State Letters* **6,** D9. ISSN: 10990062 (Sept. 2003).

76. Ferro, S. & Battisti, A. D. Physicochemical Properties of Fluorinated Diamond Electrodes. doi:10.1021/JP0274280. <https://pubs.acs.org/doi/abs/10.1021/jp0274280> (2003).

77. Durrant, S. F. *et al.* Characterization of diamond fluorinated by glow discharge plasma treatment. *Diamond and Related Materials* **10,** 490–495. ISSN: 0925-9635 (Mar. 2001).

78. Martin, H. B., Argoitia, A., Angus, J. C. & Landau, U. Voltammetry Studies of Single-Crystal and Polycrystalline Diamond Electrodes. *Journal of The Electrochemical Society* **146,** 2959. ISSN: 00134651 (Aug. 1999).

79. Denisenko, A., Romanyuk, A., Pietzka, C., Scharpf, J. & Kohn, E. Electronic surface barrier properties of fluorine-terminated boron-doped diamond in electrolytes. *Surface Science* **605,** 632–637. ISSN: 0039-6028 (Mar. 2011).

80. Kondo, T. *et al.* Characterization and electrochemical properties of CF4 plasma-treated boron-doped diamond surfaces. *Diamond and Related Materials* **17,** 48–54. ISSN: 0925-9635 (Jan. 2008).

81. Jelezko, F & Wrachtrup, J. Single defect centres in diamond: A review. *physica status solidi (a)* **203,** 3207–3225 (2006).

82. Smentkowski, V. S., Yates, J. T., Chen, X. & Goddard, W. A. Fluorination of diamond — C4F9I and CF3I photochemistry on diamond (100). *Surface Science* **370,** 209–231. ISSN: 0039-6028 (Jan. 1997).

83. Rietwyk, K. J. *et al.* Work function and electron affinity of the fluorine-terminated (100) diamond surface. *Applied Physics Letters* **102,** 091604 (2013).
84. Rietwyk, K. J. *et al.* Fluorination of the diamond surface by photoinduced dissociation of C 60 F 48. *Physical Review B* **84,** 035404 (2011).
85. Freedman, A. & Stinespring, C. D. Fluorination of diamond (100) by atomic and molecular beams. *Applied Physics Letters* **57,** 1194–1196. ISSN: 0003-6951 (Sept. 1990).
86. Kealey, C. P., Klapötke, T. M., McComb, D. W., Robertson, M. I. & Winfield, J. M. Fluorination of polycrystalline diamond films and powders. An investigation using FTIR spectroscopy, SEM, energy-filtered TEM, XPS and fluorine-18 radiotracer methods. *Journal of Materials Chemistry* **11,** 879–886. ISSN: 09599428 (Jan. 2001).
87. Shanley, T. W., Martin, A. A., Aharonovich, I. & Toth, M. Localized chemical switching of the charge state of nitrogen-vacancy luminescence centers in diamond. *Applied Physics Letters* **105,** 063103. ISSN: 0003-6951 (Aug. 2014).
88. Tiwari, A. K. *et al.* Calculated electron affinity and stability of halogen-terminated diamond. *Physical Review B* **84,** 245305. ISSN: 1098-0121 (Dec. 2011).
89. Widmann, C. J., Giese, C., Wolfer, M., Kono, S. & Nebel, C. E. F- and Cl-terminations of (100)-oriented single crystalline diamond. *physica status solidi (a)* **211,** 2328–2332. ISSN: 18626300 (Oct. 2014).
90. Freedman, A. Halogenation of diamond (100) and (111) surfaces by atomic beams. *Journal of Applied Physics* **75,** 3112–3120. ISSN: 0021-8979 (Mar. 1994).
91. Himpsel, F. J., Knapp, J. A., VanVechten, J. A. & Eastman, D. E. Quantum photoyield of diamond(111)—A stable negative-affinity emitter. *Phys. Rev. B* **20,** 624–627 (2 1979).
92. O'Donnell, K. M. *et al.* Extremely high negative electron affinity of diamond via magnesium adsorption. *Physical Review B* **92,** 035303. ISSN: 1098-0121 (July 2015).
93. O'Donnell, K. M. *et al.* Diamond Surfaces with Air-Stable Negative Electron Affinity and Giant Electron Yield Enhancement. *Advanced Functional Materials* **23,** 5608–5614. ISSN: 1616301X (Dec. 2013).
94. O'Donnell, K. M., Martin, T. L., Fox, N. A. & Cherns, D. The Li-adsorbed C(100)-(1x1):O Diamond Surface. *MRS Proceedings* **1282,** mrsf10–1282–a05–04. ISSN: 1946-4274 (Jan. 2011).
95. O'Donnell, K. M., Martin, T. L., Fox, N. A. & Cherns, D. Ab initio investigation of lithium on the diamond C(100) surface. *Physical Review B* **82,** 115303. ISSN: 1098-0121 (Sept. 2010).
96. Andrade, H. *et al.* Use of energy-filtered photoelectron emission microscopy and Kelvin probe force microscopy to visualise work function changes on diamond thin films terminated with oxygen and lithium mono-layers for thermionic energy conversion. *International Journal of Nanotechnology* **11,** 796. ISSN: 1475-7435 (2014).
97. Spicer, W. E. Negative affinity 3–5 photocathodes: Their physics and technology. *Applied physics* **12,** 115–130. ISSN: 1432-0630 (Feb. 1977).
98. Loh, K., Foord, J., Egdell, R. & Jackman, R. Tuning the electron affinity of CVD diamond with adsorbed caesium and oxygen layers. *Diamond and Related Materials* **6,** 874–878. ISSN: 0925-9635 (Apr. 1997).

99. Loh, K. P., Xie, X., Yang, S., Pan, J. & Wu, P. A spectroscopic study of the negative electron affinity of cesium oxide-coated diamond (111) and theoretical calculation of the surface density-of-states on oxygenated diamond (111). *Diamond and Related Materials* **11,** 1379–1384. ISSN: 0925-9635 (July 2002).

100. Pickett, W. E. Negative Electron Affinity and Low Work Function Surface: Cesium on Oxygenated Diamond (100). *Physical Review Letters* **73,** 1664–1667. ISSN: 0031-9007 (Sept. 1994).

101. Geis, M. W., Twichell, J. C., Macaulay, J. & Okano, K. Electron field emission from diamond and other carbon materials after H <sub>2</sub> , O <sub>2</sub> , and Cs treatment. *Applied Physics Letters* **67,** 1328–1330. ISSN: 0003-6951 (Aug. 1995).

102. Pollmann, J. & Krüger, P. Reconstruction models of cubic SiC surfaces. *Journal of Physics: Condensed Matter* **16,** S1659–S1703. ISSN: 0953-8984 (May 2004).

103. Soukiassian, P. Cubic silicon carbide surface reconstructions and Si (C) nanostructures at the atomic scale. *Materials Science and Engineering: B* **96,** 115–131. ISSN: 0921-5107 (Nov. 2002).

104. Bermudez, V. Structure and Properties of Cubic Silicon Carbide (100) Surfaces: A Review. *physica status solidi (b)* **202,** 447–473. ISSN: 0370-1972 (July 1997).

105. Hara, S. *et al.* Space fluctuation of empty states on 3C-SiC(001) surface. *Surface Science* **357-358,** 436–440. ISSN: 0039-6028 (June 1996).

106. Hara, S., Misawa, S., Yoshida, S. & Aoyagi, Y. Additional dimer-row structure of 3C-SiC(001) surfaces observed by scanning tunneling microscopy. *Physical Review B* **50,** 4548–4553. ISSN: 0163-1829 (Aug. 1994).

107. Shek, M. Soft X-ray studies of a c(4 × 2)* $\beta$-SiC(100) surface. *Surface Science* **349,** 317–332. ISSN: 0039-6028 (Apr. 1996).

108. Kitamura, J. *et al.* Si-adsorption induced phase transition on the 3C–SiC(001) surface. *Surface Science* **433-435,** 465–469. ISSN: 0039-6028 (Aug. 1999).

109. D'angelo, M. *et al.* Atomic structure determination of the Si-rich $\beta$-SiC(001) 3x2 surface by grazing-incidence x-ray diffraction: A stress-driven reconstruction. *Physical Review B* **68,** 165321. ISSN: 0163-1829 (Oct. 2003).

110. O'Donnell, K. M. *et al.* Diamond Surfaces with Air-Stable Negative Electron Affinity and Giant Electron Yield Enhancement. *Advanced Functional Materials* **23,** 5608–5614 (2013).

111. O'Donnell, K. M. *et al.* Photoelectron emission from lithiated diamond. *physica status solidi (a)* **211,** 2209–2222 (2014).

112. Vermeeren, V., Wenmackers, S., Wagner, P. & Michiels, L. DNA Sensors with Diamond as a Promising Alternative Transducer Material. *Sensors* **9,** 5600 (2009).

113. Pakes, C. I., Garrido, J. A. & Kawarada, H. Diamond surface conductivity: Properties, devices, and sensors. *MRS Bulletin* **39,** 542–548. ISSN: 1938-1425 (2014).

114. Sakai, T. *et al.* Ozone-treated channel diamond field-effect transistors. *Diamond and Related Materials* **12,** 1971–1975. ISSN: 0925-9635 (2003).

115. Akhgar, G. *et al.* Strong and Tunable Spin-Orbit Coupling in a Two-Dimensional Hole Gas in Ionic-Liquid Gated Diamond Devices. *Nano letters* (2016).

116. Schenk, A. K. *et al.* The surface electronic structure of silicon terminated (100) diamond. *Nanotechnology* **27,** 275201 (2016).

117. Cordero, B. *et al.* Covalent radii revisited. *Dalton Transactions,* 2832–2838 (2008).

118. Lyman, P. *et al.* Structure of a passivated Ge surface prepared from aqueous solution. *Surface science* **462,** L594–L598 (2000).

119. Cowie, B., Tadich, A & Thomsen, L. *The current performance of the wide range (90–2500 eV) soft x-ray beamline at the Australian Synchrotron* in *SRI 2009, 10TH INTERNATIONAL CONFERENCE ON RADIATION INSTRUMENTATION* **1234** (2010), 307–310.

120. Lee, G., Cho, E.-J., Park, Y, Cho, S & Lee, H.-G. Surface reactivity of the alkali-metal-induced Ge (111)-3× 1 surface under ultrahigh vacuum. *Surface science* **501,** L177–L183 (2002).

121. Kinsky, J, Graupner, R, Stammler, M & Ley, L. Surface vibrations on clean, deuterated, and hydrogenated single crystal diamond (100) surfaces studied by high-resolution electron energy loss spectroscopy. *Diamond and related materials* **11,** 365–370 (2002).

122. Petrini, D. & Larsson, K. Origin of the reactivity on the nonterminated (100),(110), and (111) diamond surfaces: an electronic structure DFT study. *The Journal of Physical Chemistry C* **112,** 14367–14376 (2008).

123. Petrini, D. & Larsson, K. A theoretical study of the energetic stability and geometry of hydrogen-and oxygen-terminated diamond (100) surfaces. *The Journal of Physical Chemistry C* **111,** 795–801 (2007).

124. Gao, K., Seyller, T. & Ley, L. How the solid state matrix affects the chemical shift of core-level binding energies: A novel method to take the induction effect into account. *Solid state communications* **139,** 370–375 (2006).

125. Pehrsson, P. E., Mercer, T. W. & Chaney, J. A. Thermal oxidation of the hydrogenated diamond (100) surface. *Surface science* **497,** 13–28 (2002).

126. Shpilman, Z. *et al.* A near edge X-ray absorption fine structure study of oxidized single crystal and polycrystalline diamond surfaces. *Diamond and Related Materials* **45,** 20 –27. ISSN: 0925-9635 (2014).

127. Zhou, X., Ishida, M., Imanishi, A. & Nakato, Y. Roles of charge polarization and steric hindrance in determining the chemical reactivity of surface Si-H and Si-Si bonds at H-terminated Si (100) and-(111). *The Journal of Physical Chemistry B* **105,** 156–163 (2001).

128. Tice, J. B. *Synthesis and Fundamental Studies of Novel Main Group IV and Azidoarsenic CVD Precursors* (ProQuest, 2008).

129. Needels, M, Payne, M. & Joannopoulos, J. High-order reconstructions of the Ge (100) surface. *Physical Review B* **38,** 5543 (1988).

130. Sussmann, R. S. *CVD diamond for electronic devices and sensors* (John Wiley & Sons, 2009).

131. Tordjman, M., Saguy, C., Bolker, A. & Kalish, R. Superior surface transfer doping of diamond with MoO3. *Advanced Materials Interfaces* **1** (2014).

132. Verona, C *et al.* Comparative investigation of surface transfer doping of hydrogen terminated diamond by high electron affinity insulators. *Journal of Applied Physics* **120,** 025104 (2016).

133. Schenk, A. K., Sear, M. J., Tadich, A, Stacey, A & Pakes, C. I. Oxidation of the silicon terminated (1 0 0) diamond surface. *Journal of Physics: Condensed Matter* **29,** 025003 (2016).

134. Edmonds, M. T. *et al.* Air-stable electron depletion of bi2se3 using molybdenum trioxide into the topological regime. *ACS nano* **8,** 6400–6406 (2014).

135. Langley, D. *et al.* Surface transfer doping of diamond with a molecular heterojunction. *Applied Physics Letters* **100,** 032103 (2012).

136. Hunger, R. *et al.* Chemical and electronic characterization of methyl-terminated Si (111) surfaces by high-resolution synchrotron photoelectron spectroscopy. *Physical Review B* **72,** 045317 (2005).

137. Greiner, M. T., Chai, L., Helander, M. G., Tang, W.-M. & Lu, Z.-H. Transition metal oxide work functions: the influence of cation oxidation state and oxygen vacancies. *Advanced Functional Materials* **22,** 4557–4568 (2012).

138. Xue, K, Ho, H. & Xu, J. Local study of thickness-dependent electronic properties of ultrathin silicon oxide near SiO2/Si interface. *Journal of Physics D: Applied Physics* **40,** 2886 (2007).

139. Kröger, M. *et al.* P-type doping of organic wide band gap materials by transition metal oxides: A case-study on Molybdenum trioxide. *Organic Electronics* **10,** 932–938 (2009).

140. Schirhagl, R., Chang, K., Loretz, M. & Degen, C. L. Nitrogen-vacancy centers in diamond: nanoscale sensors for physics and biology. *Annual review of physical chemistry* **65,** 83–105 (2014).

141. Loretz, M, Pezzagna, S, Meijer, J & Degen, C. Nanoscale nuclear magnetic resonance with a 1.9-nm-deep nitrogen-vacancy sensor. *Applied Physics Letters* **104,** 033102 (2014).

142. Balasubramanian, G., Lazariev, A., Arumugam, S. R. & Duan, D.-w. Nitrogen-vacancy color center in diamond—emerging nanoscale applications in bioimaging and biosensing. *Current opinion in chemical biology* **20,** 69–77 (2014).

143. Wu, Y., Jelezko, F., Plenio, M. B. & Weil, T. Diamond quantum devices in biology. *Angewandte Chemie International Edition* **55,** 6586–6598 (2016).

144. Yang, W. & Hamers, R. J. Fabrication and characterization of a biologically sensitive field-effect transistor using a nanocrystalline diamond thin film. *Applied Physics Letters* **85,** 3626–3628 (2004).

145. Xu, N. & Huq, S. E. Novel cold cathode materials and applications. *Materials Science and Engineering: R: Reports* **48,** 47–189 (2005).

146. Okano, K., Koizumi, S., Silva, S. R. P. & Amaratunga, G. A. Low-threshold cold cathodes made of nitrogen-doped chemical-vapour-deposited diamond. *Nature* **381,** 140 (1996).

147. Geis, M. *et al.* Diamond cold cathode. *IEEE Electron Device Letters* **12,** 456–459 (1991).

148. Akhgar, G. *et al.* G-factor and well width variations for the two-dimensional hole gas in surface conducting diamond. *Applied Physics Letters* **112,** 042102 (2018).

149. Zheng, J., Xie, X., Wee, A. & Loh, K. P. Oxygen-induced surface state on diamond (100). *Diamond and related materials* **10,** 500–505 (2001).

150. Chandran, M., Shasha, M., Michaelson, S. & Hoffman, A. Nitrogen termination of single crystal (100) diamond surface by radio frequency N2 plasma process: An in-situ x-ray photoemission spectroscopy and secondary electron emission studies. *Applied Physics Letters* **107,** 111602 (2015).

151. Coffinier, Y. *et al.* Covalent linking of peptides onto oxygen-terminated boron-doped diamond surfaces. *Diamond and related materials* **16,** 892–898 (2007).

152. Raymakers, J. *et al.* Expanding the Scope of Diamond Surface Chemistry: Stille and Sonogashira Cross-Coupling Reactions. *The Journal of Physical Chemistry C* **121,** 23446–23454 (2017).

153. Sear, M. J. *et al.* Germanium terminated (1 0 0) diamond. *Journal of Physics: Condensed Matter* **29,** 145002 (2017).

154. Sear, M. J., Schenk, A. K., Tadich, A., Stacey, A. & Pakes, C. I. P-type surface transfer doping of oxidised silicon terminated (100) diamond. *Applied Physics Letters* **110,** 011605 (2017).

155. Buriak, J. M. Organometallic chemistry on silicon and germanium surfaces. *Chemical reviews* **102,** 1271–1308 (2002).

156. Bent, S. F. Organic functionalization of group IV semiconductor surfaces: principles, examples, applications, and prospects. *Surface science* **500,** 879–903 (2002).

157. Prabhakaran, K & Ogino, T. Oxidation of Ge (100) and Ge (111) surfaces: an UPS and XPS study. *Surface Science* **325,** 263–271 (1995).

158. Kuhr, H. & Ranke, W. Orientation dependent adsorption of oxygen on a cylindrical Ge sample. *Surface science* **201,** 408–418 (1988).

159. Kuhr, H. & Ranke, W. H2O adsorption on a cylindrical germanium sample. *Surface science* **187,** 98–111 (1987).

160. Schmeisser, D *et al.* Surface oxidation states of germanium. *Surface science* **172,** 455–465 (1986).

161. Streit, D. C. & Allen, F. G. Thermal and Si-beam assisted desorption of SiO2from silicon in ultrahigh vacuum. *Journal of Applied Physics* **61,** 2894–2897 (Apr. 1987).

162. Frantsuzov, A. & Makrushin, I. Growth of an oxide film on a clean silicon surface and the kinetics of its evaporation. *Thin Solid Films* **32,** 247–249 (Mar. 1976).

163. Naydenov, B. *et al.* Increasing the coherence time of single electron spins in diamond by high temperature annealing. *Applied Physics Letters* **97,** 242511 (2010).

164. Prins, J. F. Improved activation of boron-dopant atoms implanted into diamond. *Nuclear Instruments and Methods in Physics Research Section B: Beam Interactions with Materials and Atoms* **35,** 484–487 (1988).

165. Prins, J. F. Annealing effects when activating dopant atoms in ion-implanted diamond layers. *Nuclear Instruments and Methods in Physics Research Section B: Beam Interactions with Materials and Atoms* **59,** 1387–1390 (1991).

166. Sear, M. J., Schenk, A. K., Tadich, A., Stacey, A. & Pakes, C. I. Thermal Stability and Oxidation of Group IV Terminated (100) Diamond Surfaces. *physica status solidi (a)* **215,** 1800283 (2018).

167. Rietwyk, K. J. *et al.* Work function and electron affinity of the fluorine-terminated (100) diamond surface. *Applied Physics Letters* **102,** 091604. ISSN: 0003-6951 (Mar. 2013).

168. Wong, S. L. *et al.* Quasi-free-standing epitaxial graphene on SiC (0001) by fluorine intercalation from a molecular source. *ACS nano* **5,** 7662–7668 (2011).

169. Chuang, T. Electron spectroscopy study of silicon surfaces exposed to XeF2 and the chemisorption of SiF4 on silicon. *Journal of Applied Physics* **51,** 2614–2619 (1980).

170. Osterkamp, C. *et al.* Stabilizing shallow color centers in diamond created by nitrogen delta-doping using SF6 plasma treatment. *Applied Physics Letters* **106,** 113109 (2015).

171. Khan, F. & Adesida, I. High rate etching of SiC using inductively coupled plasma reactive ion etching in SF 6-based gas mixtures. *Applied physics letters* **75,** 2268–2270 (1999).

172. O'Brien, J. L. *et al.* Towards the fabrication of phosphorus qubits for a silicon quantum computer. *Phys. Rev. B* **64,** 161401 (16 Sept. 2001).